USGS
science for a changing world

Evaluation of 2-D Shear-Wave Velocity Models and V_{S30} at Six Strong-Motion Recording Stations in Southern California using Multichannel Analysis of Surface Waves and Refraction Tomography

Open-File Report 2024–1016

U.S. Department of the Interior
U.S. Geological Survey

Cover. U.S. Geological Survey scientists and volunteers preparing to acquire active-source seismic data at Southern California Edison substation in La Habra, California.

Evaluation of 2-D Shear-Wave Velocity Models and V_{S30} at Six Strong-Motion Recording Stations in Southern California using Multichannel Analysis of Surface Waves and Refraction Tomography

By Joanne H. Chan, Rufus D. Catchings, Mark R. Goldman, Coyn J. Criley, and Robert R. Sickler

Open-File Report 2024–1016

U.S. Department of the Interior
U.S. Geological Survey

U.S. Geological Survey, Reston, Virginia: 2024

Suggested citation:
Chan, J.H., Catchings, R.D., Goldman, M.R., Criley, C.J., and Sickler, R.R., 2024, Evaluation of 2-D shear-wave velocity models and V_{S30} at six strong-motion recording stations in southern California using multichannel analysis of surface waves and refraction tomography: U.S. Geological Survey Open-File Report 2024–1016, 58 p., https://doi.org/10.3133/ofr20241016.

Associated data for this publication:
Chan, J.H., Catchings, R.D., Goldman, M.R, Criley, C.J., and Sickler, R.R., 2021, High-resolution seismic data acquired at six Southern California seismic network (SCSN) recording stations in 2017: U.S. Geological Survey data release, https://doi.org/10.5066/P990O55F.

ISSN 2331-1258 (online)

Acknowledgments

We thank Roderick dela Cruz of Southern California Edison for field site access. We thank Keith Galvin, Koichi Hayashi, Dan Langermann, Tony Martin, Devin McPhillips, Ian Richardson, David Saucedo-Green, Luther Strayer, Nathan Suits, and Alan Yong for assistance in the field.

Contents

Figures

Tables

Conversion Factors

International System of Units to U.S. customary units

Multiply	By	To obtain
	Length	
centimeter (cm)	0.3937	inch (in.)
millimeter (mm)	0.03937	inch (in.)
meter (m)	3.281	foot (ft)
kilometer (km)	0.6214	mile (mi)
	Flow rate	
meter per second (m/s)	3.281	foot per second (ft/s)
	Mass	
kilogram (kg)	2.205	pound avoirdupois (lb)

U.S. customary units to International System of Units

Multiply	By	To obtain
	Length	
inch (in.)	2.54	centimeter (cm)
inch (in.)	25.4	millimeter (mm)
foot (ft)	0.3048	meter (m)
mile (mi)	1.609	kilometer (km)
	Flow rate	
foot per second (ft/s)	0.3048	meter per second (m/s)
	Mass	
pound, avoirdupois (lb)	0.4536	kilogram (kg)

Abbreviations

1-D	one-dimensional
2-D	two-dimensional
AWD	accelerated weight-drop
CMPCC	common midpoint cross-correlation
GMPEs	ground-motion prediction equations
Hz	hertz
MASW	multichannel analysis of surface waves
MAS_LW	MASW using Love-waves
MAS_RW	MASW using Rayleigh-waves
SCE	Southern California Edison
SCSN	Southern California seismic network
V_P	P-wave or compressional-wave velocity
V_S	S-wave or shear-wave velocity
V_{S30}	time-averaged shear-wave velocity in the upper 30 meters of the subsurface

Evaluation of 2-D Shear-Wave Velocity Models and V_{S30} at Six Strong-Motion Recording Stations in Southern California using Multichannel Analysis of Surface Waves and Refraction Tomography

By Joanne H. Chan, Rufus D. Catchings, Mark R. Goldman, Coyn J. Criley, and Robert R. Sickler

Abstract

To better understand the potential for amplified ground shaking at sites that house critical infrastructure, the U.S. Geological Survey (USGS) evaluated shear-wave velocities (V_S) at six strong-motion recording stations in Southern California Edison facilities in southern California. We calculated V_{S30} (time-averaged shear-wave velocity in the upper 30 meters [m]), which is a parameter used in ground-motion prediction equations (GMPEs) to account for site amplification (Building Safety Seismic Council, 2003; Holtzer and others, 2005; Baltay and Boatwright, 2015). Previous site-characterization studies using multiple methods in Alameda, Napa, and Sonoma Counties, Calif., and in British Columbia (Catchings and others, 2017, 2019; Chan and others, 2018a, 2018b) show that some sites have significant lateral variability; thus, a single measurement of V_{S30} nearest to the strong-motion recording station may not accurately account for the actual subsurface velocity variations. In the summer of 2017, we recorded body and surface waves along linear profiles (118–174 m long) using active-source seismic methods (226-kilogram [kg] accelerated weight-drop and 3.5-kg sledgehammer impacts) near strong-motion recording stations. We used S-wave refraction tomography and a multichannel analysis of surface waves (MASW) method (using common midpoint cross-correlation; CMPCC) to evaluate two-dimensional (2-D) V_S from body and surface waves, respectively. We evaluated V_S from both Rayleigh- and Love-waves.

Seismic Survey

Date Acquisition

We acquired high-resolution P- and S-wave seismic data (Chan and others, 2021) along linear profiles near strong-motion recording stations located near Southern California Edison substations (figs. 1–7). We generated P-wave data using one of three types of active sources: a 226-kilogram (kg) vertical accelerated weight-drop (AWD), a 3.5-kg sledgehammer and steel plate combination, or a 2.7-kg hammer and steel plate combination. Active-source S-waves were generated using a combination of a 45-degree (°)-angle AWD and by horizontally striking an aluminum block with a 3.5-kg sledgehammer (table 1). We co-located P-wave sources (roughly 1-m offset) and 40-hertz (Hz), Sercel™ L-40A vertical-component geophones every 2 or 4 m to record P-wave data. After acquisition of P-wave data along each profile, we replaced the vertical-component geophones with 4.5-Hz, Sercel™ L-28-LBH horizontal-component geophones and co-located S-wave sources (roughly 1-m offset) with the geophones to record S-wave data. Two 60-channel, Geometrics StrataView RX-60™ seismographs were connected to the geophones via refraction cables to record the P- and S-wave data.

Profile LA17-1—Olinda (SCSN OLI)

Profile LA17-1-OLI was oriented west to east on an elevated dirt path, adjacent to the Southern California Edison (SCE) Olinda substation (fig. 2). The strong-motion recording station (SCSN OLI) was in the southwest corner of the substation, approximately 65 m from the nearest geophone of the seismic profile. We deployed 82 P- and S-wave geophones at 2-m intervals along the profile and co-located P-wave (226-kg vertical AWD) and S-wave (3.5-kg sledgehammer) sources. We also used a 45°-angle AWD S-wave source approximately every 20 m along the profile and a 2.7-kg hammer and steel plate P-wave source approximately every 24 m along the profile.

Profile LA17-1b—Olinda (SCSN OLI)

Profile LA17-1b-OLI was oriented south to north, adjacent to the SCE Olinda substation (fig. 2). The strong-motion recording station (SCSN OLI) was approximately 15 m from the closest geophone of the seismic profile. We deployed 30 P-wave geophones at 4-m spacing along the profile and co-located P-wave (226-kg AWD) seismic sources. S-wave (body waves) data were not acquired along profile LA17-1b-OLI due to time limitations.

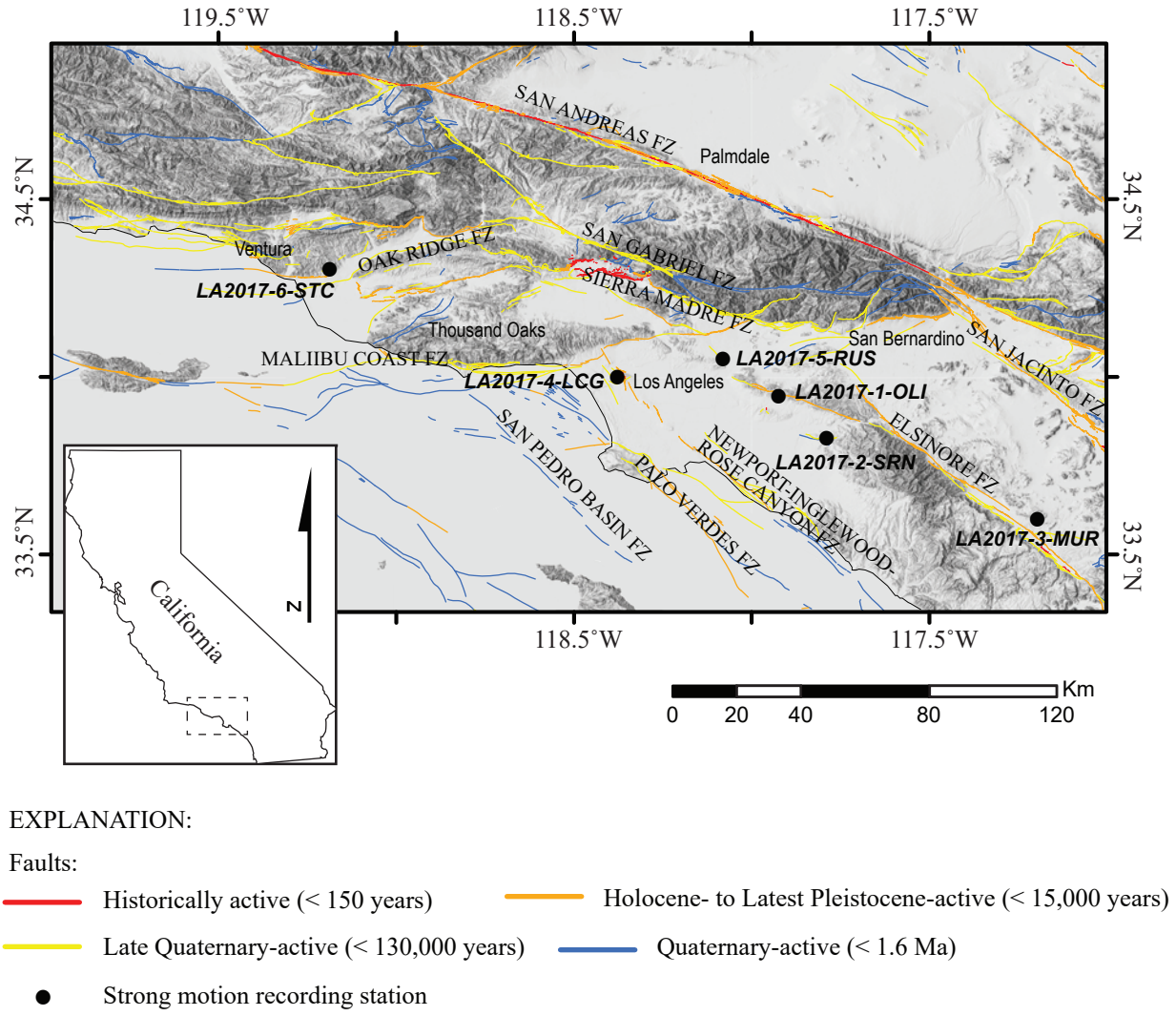

Figure 1. Shaded relief map of southern California showing Quaternary-active faults (lines) and the approximate locations (black circles) of the six strong-motion recording stations and our seismic surveys. Quaternary fault data was acquired from the U.S. Geological Survey Quaternary Fault and Fold Database of the United States (https://usgs.maps.arcgis.com/apps/webappviewer/index.html?id=5a6038b3a1684561a9b0aadf88412fcf, U.S. Geological Survey Earthquake Hazards Program, 2020).

Table 1. Total number of traces used for P- and S-wave inversion to develop seismic velocity models (Hole, 1992).

[Each column shows the number of traces generated by different seismic sources for each of the 7 profiles (Chan and others, 2021). kg, kilograms; °, degrees; AWD, accelerated weight-drop; NA, not applicable]

Seismic source	LA17-1-OLI	LA17-1b-OLI	LA17-2-SRN	LA17-3-MUR	LA17-4-LCG	LA17-5-RUS	LA17-6-STC
P-wave (226-kg AWD)	6,724	840	7,480	3,600	1,860	3,600	3,600
P-wave (2.7-kg hammer)[1]	656	NA	528	420	NA	NA	420
S-wave (45° AWD)	738	NA	880	420	NA	NA	NA
S-wave (3.5-kg sledgehammer)	6,724	NA	7,744	3,600	3,600	3,600	3,600

[1]Seismic data generated by 2.7-kg hammer are not used to create velocity models.

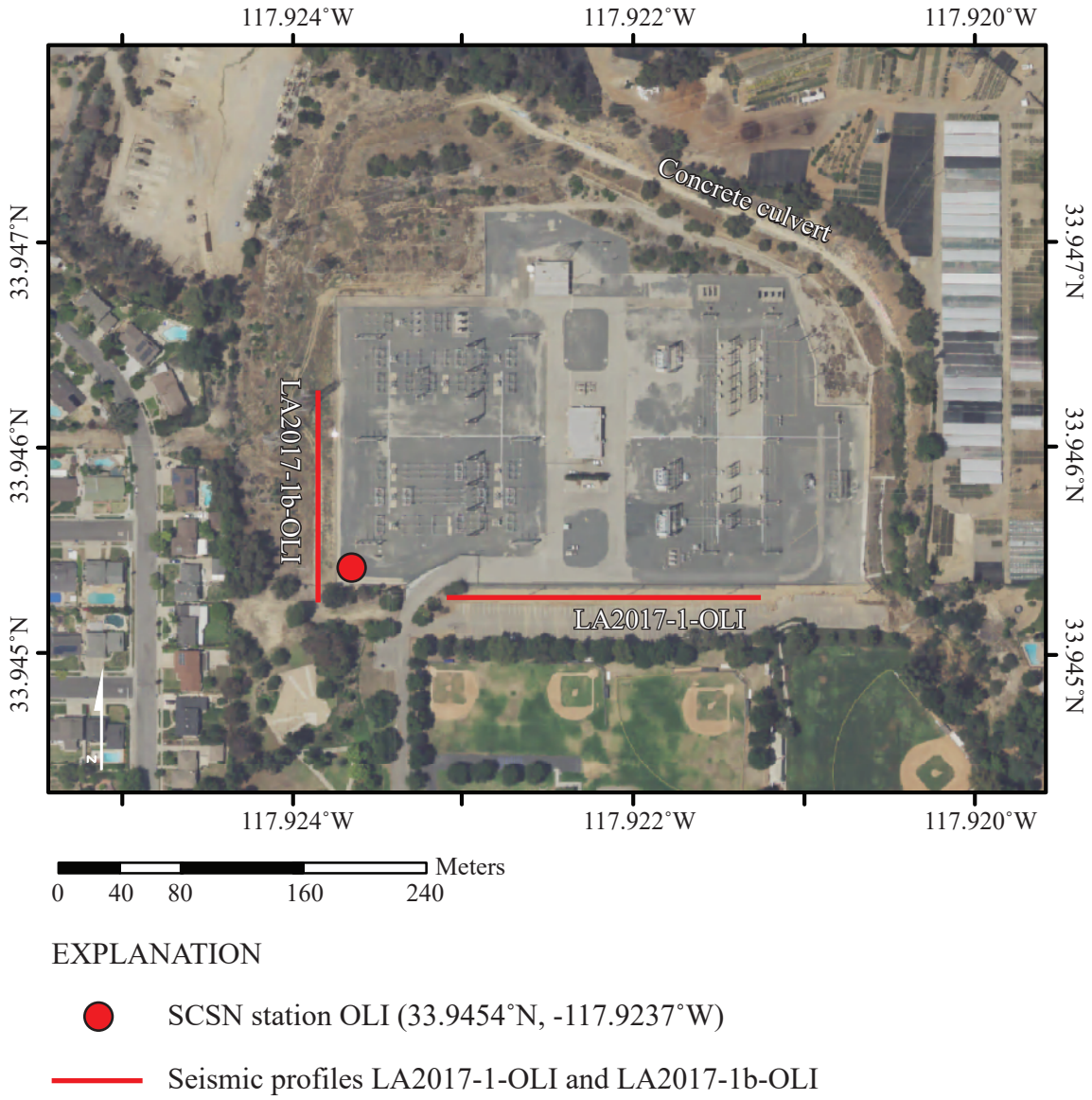

Figure 2. Orthoimage showing seismic profiles LA17-1-OLI and LA17-1b-OLI (red lines) adjacent to Southern California Edison substation in La Habra, Calif. Strong-motion recording station SCSN OLI is in the southwest corner of the substation (red circle). The concrete culvert visible in the upper right-hand corner of the image shows the water drainage rerouted away from the substation. (SCSN, Southern California seismic network). Orthoimage was acquired from The National Map-Orthoimagery (https://apps.nationalmap.gov/viewer/, U.S. Geological Survey National Geospatial Program, 2009).

Profile LA17-2—Serrano (SCSN SRN)

Profile LA17-2-SRN was oriented southwest to northeast inside the SCE Serrano substation (fig. 3). The strong-motion recording station (SCSN SRN) was approximately 200 m southeast of the closest geophone of the seismic profile. We deployed 88 P- and S-wave wave geophones along the profile, with 2-m spacing between geophones. We co-located P-wave (226-kg AWD) and S-wave (3.5-kg sledgehammer) sources with the geophones (1-m offset), including a 45°-angle AWD S-wave source approximately every 20 m along the profile and a 2.7-kg hammer and steel plate P-wave source approximately every 36 m along the profile.

Profile LA17-3—Murrieta (SCSN MUR)

Profile LA17-3-MUR was oriented southwest to northeast, adjacent to the SCE Murrieta substation (fig. 4). The strong-motion recording station (SCSN MUR) was located approximately 40 m southwest of the nearest geophone of the seismic profile. We deployed 60 P- and S-wave geophones at 2-m spacing along the profile and co-located P-wave (226-kg AWD) and S-wave (3.5-kg sledgehammer) sources. We also generated S-wave sources using the 45°-angle AWD source and a 2.7-kg hammer and steel plate P-wave source approximately every 20 m along the profile.

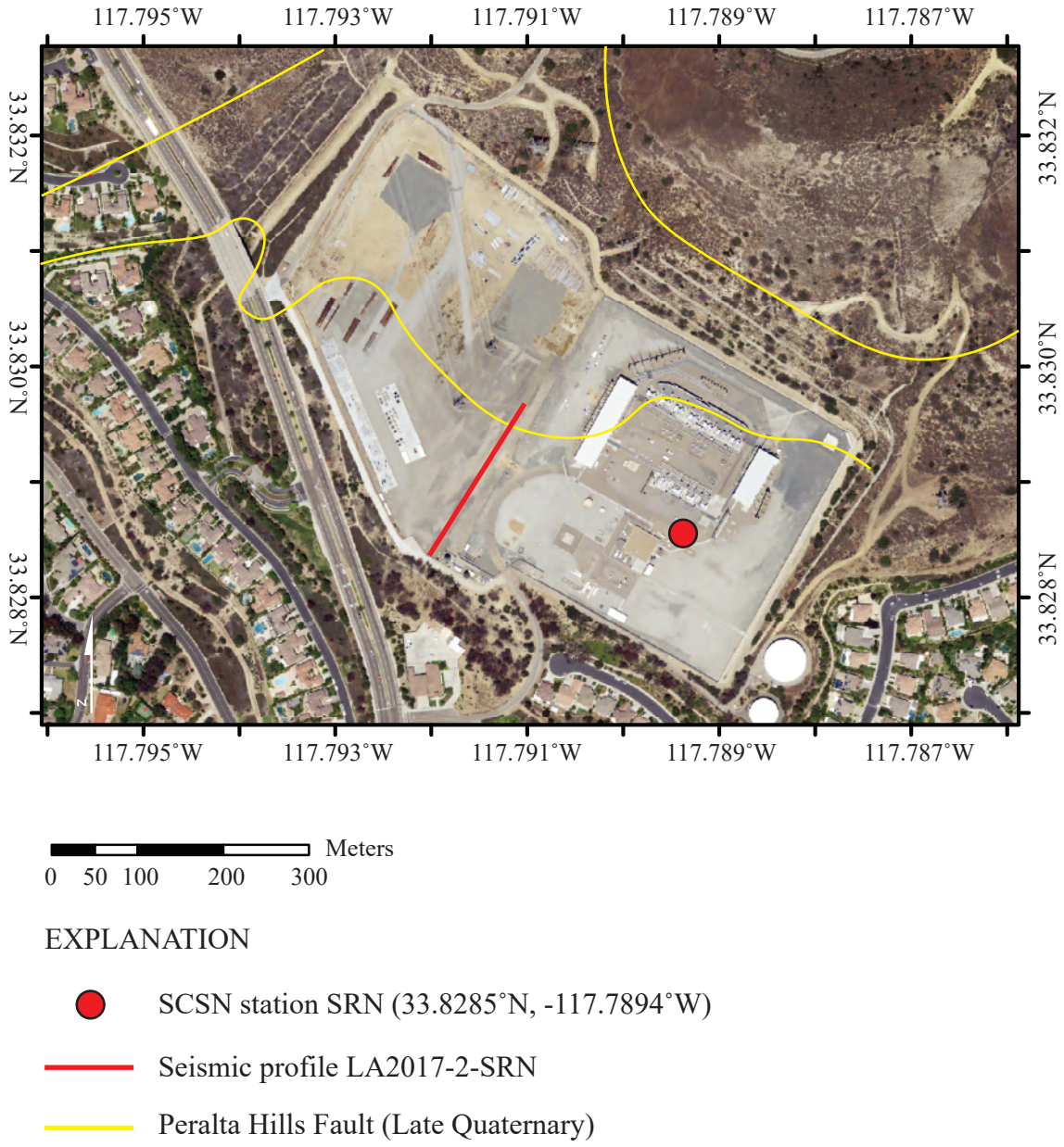

Figure 3. Orthoimage showing seismic profile LA17-2-SRN (red line) inside a Southern California Edison substation in Orange, Calif. Strong-motion recording station SCSN SRN is in the southeastern area of the substation (red circle). The late Quaternary Peralta Hills Fault (yellow lines) is mapped crossing the substation and our seismic profile (SCSN, Southern California seismic network). Orthoimage was acquired from The National Map-Orthoimagery (https://apps.nationalmap.gov/viewer/, U.S. Geological Survey National Geospatial Program, 2009).

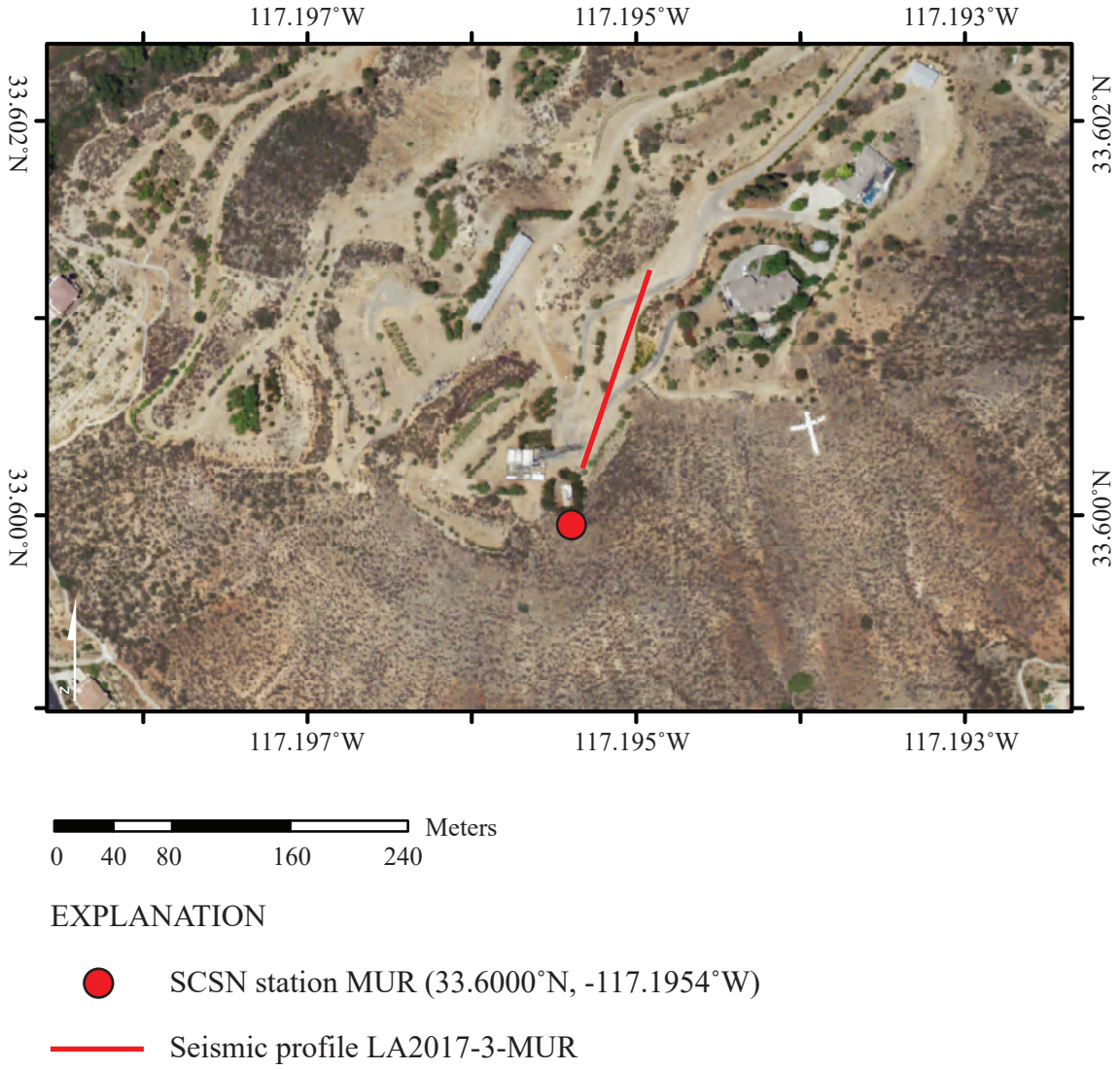

Figure 4. Orthoimage showing seismic profile LA17-3-MUR (red line) adjacent to Southern California Edison substation in Murrieta, Calif. Strong-motion recording station SCSN MUR is in the southeast area of the substation (red circle); (SCSN, Southern California seismic network). Orthoimage was acquired from The National Map-Orthoimagery (https://apps.nationalmap.gov/viewer/, U.S. Geological Survey National Geospatial Program, 2009).

Profile LA17-4—La Cienega (SCSN LCG)

Profile LA17-4-LCG was oriented southeast to northwest, adjacent to the SCE La Cienega substation (fig. 5). The strong-motion recording station (SCSN LCG) was approximately 130 m northwest of the closest geophone of the seismic profile. We deployed 60 P- and S-wave geophones at 2-m spacing along the profile, with co-located S-wave (3.5-kg sledgehammer) seismic sources. P-wave (226-kg AWD) sources were located at every other geophone (4 m spacing) along the profile. We did not use the 45°-angle AWD S-wave or the 2.7-kg hammer and steel plate P-wave sources along this profile due to time limitations.

Profile LA17-5—Rush (SCSN RUS)

Profile LA17-5-RUS was oriented southeast to northwest, adjacent to the SCE Rush substation (fig. 6). The strong-motion recording station (SCSN RUS) was approximately 90 m southwest of the nearest geophone of the seismic profile. We deployed 60 P- and S-wave geophones at 2-m spacing along the profile and co-located P-wave (226-kg AWD) and S-wave (3.5-kg sledgehammer) sources. We did not use the 45°-angle AWD S-wave or the 2.7-kg hammer and steel plate P-wave sources here due to time limitations.

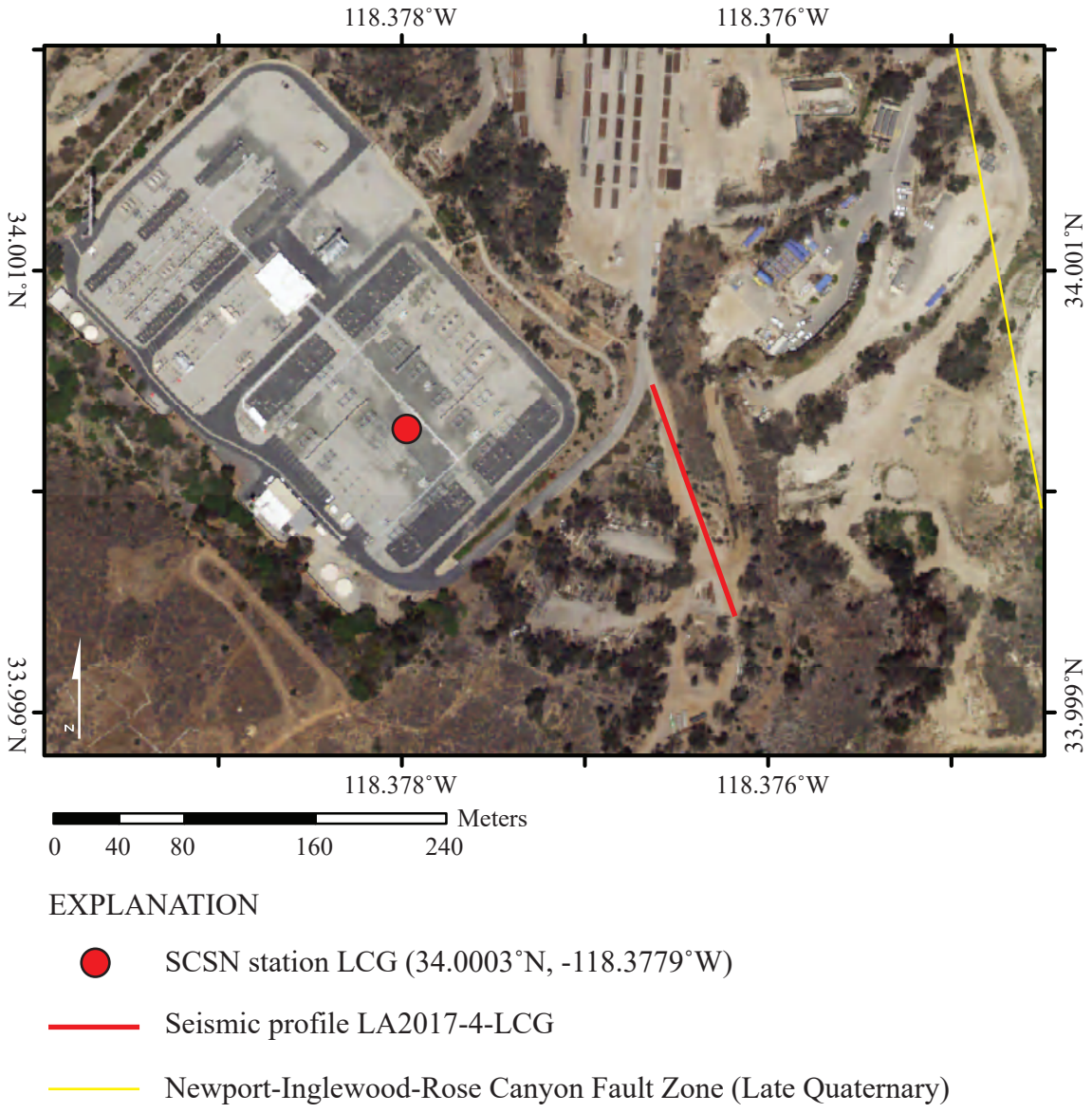

Figure 5. Orthoimage showing seismic profile LA17-4-LCG (red line) east of Southern California Edison substation in Ladera Heights, Calif. Strong-motion recording station SCSN LCG is in the eastern area of the substation (red circle). Late Quaternary Newport-Inglewood-Rose Canyon Fault Zone (yellow line) is mapped less than 200 meters northeast of our seismic profile. (SCSN, Southern California seismic network). Orthoimage was acquired from The National Map-Orthoimagery (https://apps.nationalmap.gov/viewer/, U.S. Geological Survey National Geospatial Program, 2009).

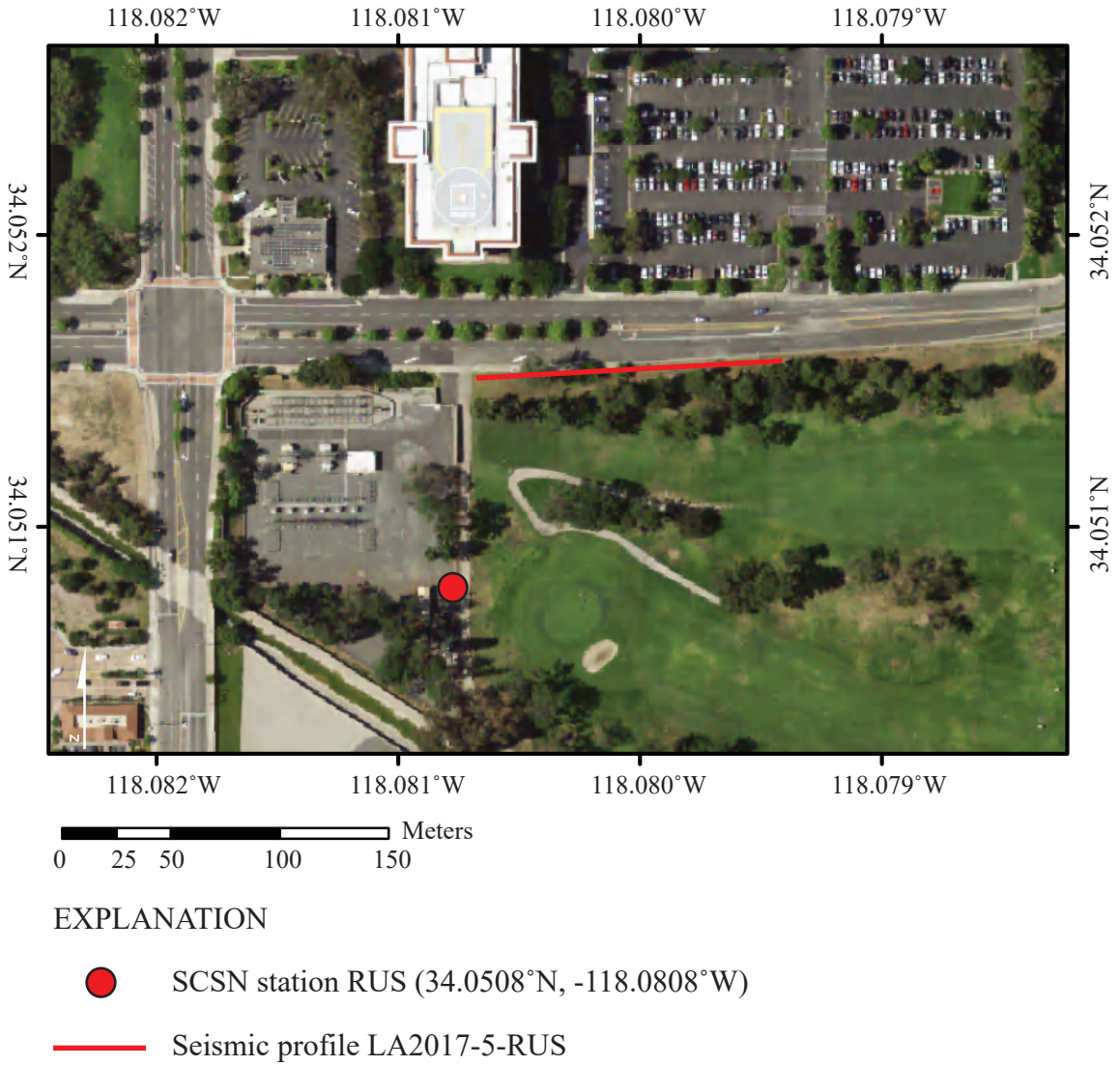

Figure 6. Orthoimage showing seismic profile LA17-5-RUS (red line) northeast of a Southern California Edison substation in Rosemead, Calif. Strong-motion recording station SCSN RUS is in the southeast corner of the substation (red circle); (SCSN, Southern California seismic network). Orthoimage was acquired from The National Map-Orthoimagery (https://apps.nationalmap.gov/viewer/, U.S. Geological Survey National Geospatial Program, 2009).

Profile LA17-6—Santa Clara (SCSN STC)

Profile LA17-6-STC was oriented southeast to northwest, adjacent to the SCE Santa Clara substation (fig. 7). The strong-motion recording station (SCSN STC) was in the northwest corner of the substation, approximately 250 m northwest of the seismic profile. We deployed 60 P- and S-wave geophones at 2-m spacing along the profile and co-located P-wave (226-kg AWD) and S-wave (3.5-kg sledgehammer) sources. We did not use the 45°-angle AWD S-wave or the 2.7-kg hammer and steel plate P-wave sources at this site due to time limitations.

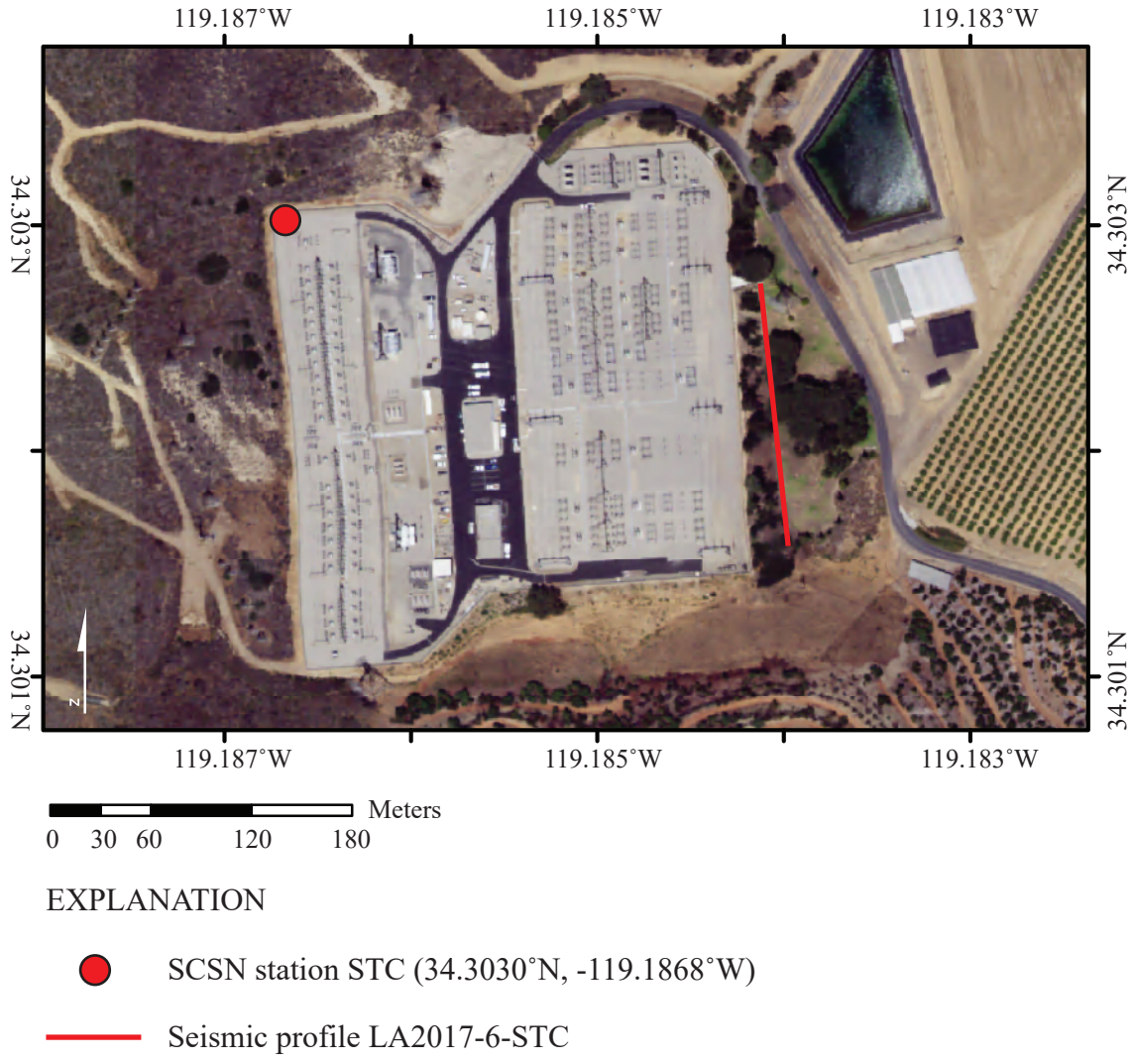

Figure 7. Orthoimage showing seismic profile LA17-6-STC (red line) east of Southern California Edison substation in Ventura, Calif. Strong-motion recording station SCSN STC is in northwest corner of the substation (red circle); (SCSN, Southern California seismic network). Orthoimage was acquired from The National Map-Orthoimagery (https://apps.nationalmap.gov/viewer/, U.S. Geological Survey National Geospatial Program, 2009).

Seismic-Imaging Methods

We used an acquisition geometry that allowed us to develop 2-D P- and S-wave refraction tomography models, tomographic-based V_P/V_S and Poisson's ratio models (all based on body waves), and V_S models based on Rayleigh and Love waves using the multichannel analysis of surface waves (MASW) method.

Refraction-Tomography Modeling

We used refraction tomography to model subsurface P- and S-wave velocities along all profiles. We first processed the seismic data (Chan and others, 2021) by grouping the recorded seismic traces into shot gathers and adding the survey geometry. We removed traces without recorded signals and corrected the timing of each shot gather to match the timing of each P- and S-wave source. First arrivals from P- and S-wave shot gathers were inverted (table 1) to develop seismic-velocity models using the algorithm of Hole (1992). We developed P- and S-wave starting models based on one-dimensional (1-D) modeling of the shot gathers, and we parameterized our initial 2-D models into vertical and horizontal grids with each grid space at 2-m based on shot and geophone spacing. The total number of traces ranged between 420 and 7,743 for each seismic profile (table 1), and, generally, the large number of first arrivals used for each profile allows for a well-determined velocity model.

Multichannel Analysis of Surface Waves (MASW)

Our data-acquisition method allows us to use Rayleigh- and Love-waves to develop 2-D S-wave velocity models from vertical- and horizontal-component data, respectively, using the MASW method. The MASW method utilizes the dispersive nature of surface waves to estimate V_S velocities in the shallow subsurface (Park and others, 1999; Xia and others, 1999). The MASW technique is often used on surface waves in geotechnical site investigations and shallow subsurface studies (Pujol, 2003; Ivanov and others, 2003, 2008, 2013; Miller and others, 1999; Park and others, 1999, 2007; Zeng and others, 2012; Park, 2013; Xia and others, 2000; Yong and others, 2013). We used the common midpoint cross-correlation (CMPCC) method, developed by Hayashi and Hikima (2003) and Hayashi and Suzuki (2004), to construct phase velocity (dispersion) curves from all receivers along each profile. In our analysis, we grouped cross-correlated pairs of seismic traces with common midpoints and converted the CMPCC gathers from time-distance waveform data to images of phase velocity-frequency through an integral transformation. We examined and manually adjusted the fundamental mode dispersion curve picks before inverting the selected picks using a non-linear, least-squares approach. Our starting models (table 2) extended to between 40 and 50 m depth, consisted of 15 layers, and were inverted using up to 10 iterations. The starting model depths were based on one-half to one-third of the length of each seismic profile, whereas other parameters were based on starting models from prior studies with similar underlying geology and topography. Finally, the multiple 1-D V_S models along each profile were combined to make 2-D V_S models.

V_{S30} Calculations

We evaluated the time-averaged V_S in the upper 30 m of the subsurface (V_{S30}) from (a) our tomographic *Vs* models, (b) our MASW Rayleigh-wave models (MAS_RW), and (c) our MASW Love-wave models (MAS_LW). V_{S30} is frequently used to evaluate soil properties (Holtzer and others, 2005) and to account for site amplification in ground-motion models (Baltay and Boatwright, 2015) and in ground-motion prediction equations (GMPEs). V_{S30} is also used to determine site classification, which is an important consideration for establishing building codes for seismic safety (Building Seismic Safety Council, 2003). We calculated V_{S30} at every 1 m along all profiles for areas of our models with V_S values to at least 30 m depth. For parts of our model where V_S was not measured to depths of at least 30 m, we calculated V_{SZ} (V_S as a function of depth) using interpolated shear-wave velocities to 30 m depth. From our models, we evaluated lateral variations in V_{S30} across the seismic profiles, and we compared V_{S30} that were calculated using the multiple modeling methods (Catchings and others, 2017; 2019, Chan and others, 2018a; 2018b).

Velocity Models and Dispersion Curves

In the following sections, we present the various velocity models that we developed using the techniques described above. Appendix 1 shows Rayleigh- and Love-wave dispersion curves nearest to the strong-motion recording stations along each seismic profile. Appendix 2 shows Rayleigh- and Love-wave dispersion curve picks along the entire lengths of the profiles. Appendix 3 shows 1-D

Table 2. Inversion parameters of multichannel analysis of surface waves initial models.

[m, meters]

Seismic profile	Depth (m)	Number of layers	Layer thickness		Number of inversions
			Gradient	Bottom layer multiplier	
LA17-1-OLI	50	15	0.5	3	10
LA17-1b-OLI	40	15	0.5	3	10
LA17-2-SRN	50	15	0.5	3	10
LA17-3-MUR	50	15	0.5	3	10
LA17-4-LCG	50	15	0.5	3	10
LA17-5-RUS	50	15	0.5	3	10
LA17-6-STC	50	15	0.5	3	10

velocity-depth profiles nearest to the strong-motion recording stations along each seismic profile. We did not analyze seismic data generated by the 2.7-kg hammer because the source provided no additional seismic information to the refraction tomography and MASW methods.

Profile LA17-1—Olinda (SCSN OLI)

P-wave Refraction Tomography (V_P) Model

Along the Olinda LA17-1-OLI seismic profile, P-wave velocities (V_P) range from approximately 375 meters per second (m/s) near the surface to approximately 1,050 m/s at 40 m depth (fig. 8). Below about 5 m depth, velocity contours and gradients are generally sub-parallel to the surface, and there are slightly higher velocities in the western part of the seismic profile. The strong-motion recording station (SCSN OLI) was located approximately 65 m west of our seismic profile and was nearest to distance meter 0.

S-wave Refraction Tomography (V_S) Model

Determined from refraction tomography, V_S values range from approximately 200 near the surface to approximately 1,100 m/s at 60 m depth (fig. 9). Similar to the P-wave refraction model, V_S gradients are generally sub-parallel to the surface in the western part of the profile, with slightly higher velocities in the upper 20 m of the subsurface to the west. We calculated the range of V_{S30} across the profile to range from 290 to 362 m/s, with a V_{S30} of 320 m/s nearest to the strong-motion recording station (SCSN OLI) at distance meter 0 (table 3). To determine V_{S30} at meter 0, velocities near the center of the profile at 30 m depth are assumed to extend horizontally to meter 0.

MAS_RW 2-D S-wave Velocity Model

A Rayleigh-wave dispersion curve shown in appendix 1 (fig. 1.1*A*) was developed for the location (meter 0) along our seismic profile nearest to the SCSN OLI strong-motion recording station. Fundamental mode dispersion curve picks (red circles) are between phase velocities of approximately 250 and 2,300 m/s and frequencies between 2 and 17 Hz. Rayleigh-wave fundamental mode dispersion curve picks across the entire length of the profile (fig. 2.1*A*) generally coincide with phase velocities between approximately 200 and 2,500 m/s and frequencies between 3 and 20 Hz. The Rayleigh-wave 1-D depth-velocity model (fig. 3.1*A*) nearest to the strong-motion recording station shows a weak positive gradient in V_S in the upper 30 m of the subsurface and stronger positive gradient in *Vs* below 30 m depth. We calculated (a) V_{S30} to be 371 nearest to the SCSN OLI strong-motion recording station, with (b) V_{S30} ranging from 237 to 371 m/s, and (c) an average V_{S30} of 291 m/s across the profile (table 3).

We developed a V_S model for the LA17-1-OLI seismic profile by evaluating Rayleigh-waves with the MASW technique. Our 2-D V_S model (fig. 10*A*) shows V_S ranges from approximately 150 m/s near the surface to 650 m/s at 40 m depth. V_S is slightly higher at depth in the western half of the seismic profile, with channel-like velocity structure at depth near distance meter 130.

MAS_LW 2-D S-wave Velocity Model—3.5-kg Sledgehammer Source

The Love-wave dispersion curve shown in appendix 1 (fig. 1.1*B*) was developed for the location along our seismic profile nearest to the SCSN OLI strong-motion recording station (meter 0). Fundamental mode dispersion curve picks (red circles) are between phase velocities of approximately 250 and 2,300 m/s and frequencies between 2 and 26 Hz; we do not observe higher mode dispersion curves. The Love-wave fundamental mode dispersion curve picks across the entire length of the profile (fig. 2.1*B*) generally coincide with phase velocities between approximately 200 and 2,500 m/s at frequencies between 2 and 25 Hz. The Love-wave 1-D depth-velocity profile (fig. 3.1*B*) nearest to the strong-motion recording station shows a gradual increase in V_S below approximately 10 m depth. We calculated (a) V_{S30} to be 494 m/s nearest to the SCSN OLI strong-motion recording station, with (b) V_{S30} ranging from 241 to 494 m/s, as calculated for each meter along the profile. The average V_{S30} across the entire profile is 289 m/s. (table 3).

Our 2-D MAS_LW V_S model along the LA17-1-OLI seismic profile (fig. 10*B*) indicates V_S ranges from approximately 150 m/s near the surface to approximately 650 m/s at 40 m depth. Modeled velocities are slightly higher at depth in the western half of the seismic profile, with a channel-like velocity structure near distance meter 130.

MAS_LW 2-D S-wave Velocity Model—45°-Angle Weight-Drop Source

A Love-wave dispersion curve shown in appendix 1 (fig. 1.1*C*) was developed for the location (meter 0) along our seismic profile that was nearest to the SCSN OLI strong-motion recording station. Fundamental mode dispersion curve picks (red circles) coincide with phase velocities between approximately 250 and 2,300 m/s at frequencies between 2 and 24 Hz; we do not observe higher mode dispersion curves. The Love-wave fundamental mode dispersion curve picks across the entire length of the profile (fig. 2.1*C*) generally coincide with phase velocities between approximately 200 and 2,000 m/s at frequencies between 2 and 25 Hz. The Love-wave 1-D velocity-depth model (fig. 3.1*C*) nearest to the strong-motion recording station shows gradual positive gradient in V_S below approximately 10 m depth. We calculated (a) V_{S30} to be 410 m/s nearest to the SCSN OLI strong-motion recording station, with (b) V_{S30} ranging from 258 to 410 m/s (as measured at each meter along the profile), and (c) an average V_{S30} of 309 m/s along the entire profile (table 3).

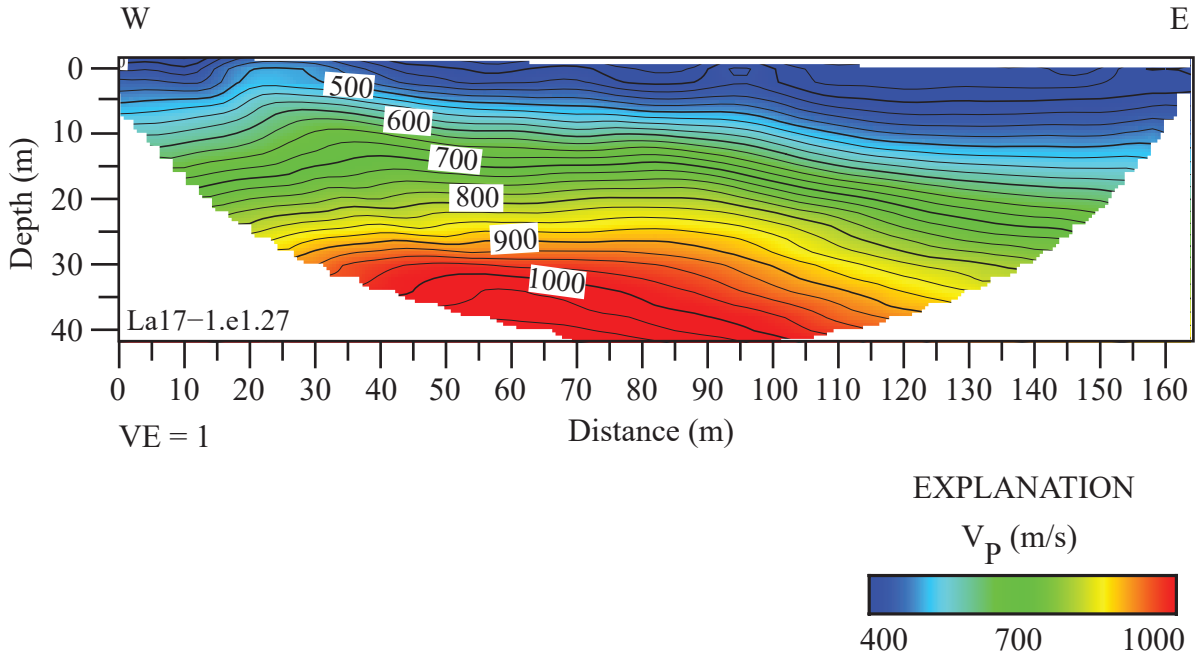

Figure 8. P-wave refraction tomography model for profile LA17-1-OLI. P-wave velocities range from approximately 375 meters per second (m/s) in the near surface to 1,050 m/s at 40 m depth. P-wave velocities are higher near the west end of the seismic profile and at depth. (W, west; E, east; VE, vertical exaggeration; V_P, P-wave velocity.)

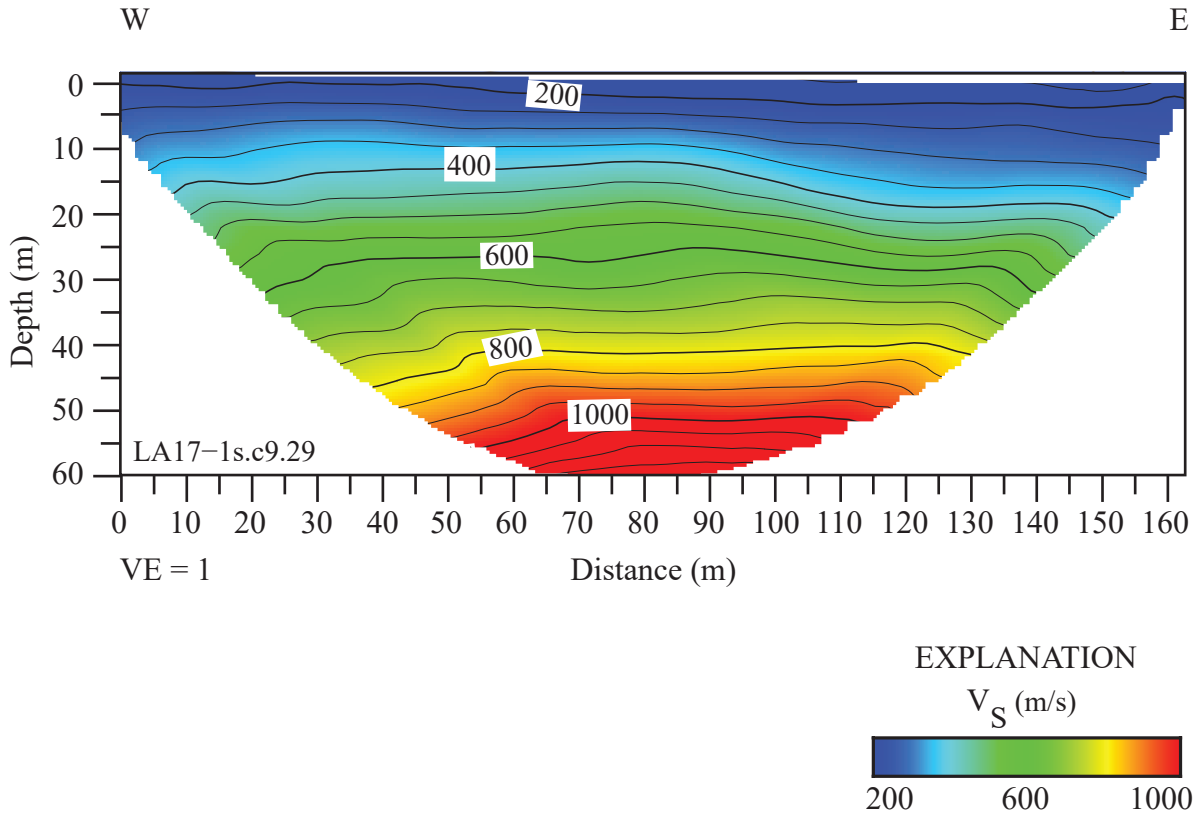

Figure 9. S-wave refraction tomography model for profile LA17-1-OLI. S-wave velocities range from approximately 200 meters per second (m/s) near the surface to approximately 1100 m/s at 60 meters (m) depth. S-wave velocities are slightly higher near the western half of the seismic profile. (W, west; E, east; VE, vertical exaggeration; V_S, S-wave velocity.)

Table 3. V_{S30} values for seven seismic profiles near strong-motion recording stations located at Southern California Edison substations.

[m/s, meters per second; NA, not applicable; 2-D, two dimensional; kg, kilograms; AWD, accelerated weight-drop]

Model	LA17-1-OLI SCSN OLI	LA17-1b-OLI SCSN OLI	LA17-2-SRN SCSN SRN	LA17-3-MUR SCSN MUR	LA17-4-LCG SCSN LCG	LA17-5-RUS SCSN RUS	LA17-6-STC SCSN STC
Range of V_{S30} along seismic profile (m/s)							
S-wave refraction tomography	290–362	NA	470–588	497–769	518–774	393–490	372–504
2-D MAS_RW (226-kg AWD)	237–371	281–362	344–429	557–651	357–425	310–330	269–318
2-D MAS_LW (3.5-kg sledgehammer)	241–494	NA	415–475	318–508	513–645	288–351	302–331
2-D MAS_LW (45° AWD)	258–410	NA	435–486	318–543	NA	NA	NA
Average V_{S30} (m/s) across profile							
S-wave refraction tomography	334	NA	542	685	660	448	443
2-D MAS_RW (226-kg AWD)	291	309	383	592	374	310	294
2-D MAS_LW (3.5-kg sledgehammer)	289	NA	444	463	555	308	320
2-D MAS_LW (45° AWD)	309	NA	462	491	NA	NA	NA
Approximate V_{S30} nearest to strong-motion recording station (m/s)							
S-wave refraction tomography	320	NA	537	497	595	468	377
2-D MAS_RW (226-kg AWD)	371	330	379	613	425	305	311
2-D MAS_LW (3.5-kg sledgehammer)	494	NA	432	318	645	351	330
2-D MAS_LW (45° AWD)	410	NA	443	318	NA	NA	NA

Our 2-D MAS_LW V_S model along the LA17-1-OLI seismic profile (fig. 10*C*) shows that V_S ranges from approximately 150 m/s near the surface to approximately 650 m/s at 40 m depth. Modeled V_S is slightly higher at depth in the western half of the seismic profile, with a channel-like velocity structure near distance meter 130.

Profile LA17-1b—Olinda (SCSN OLI)

P-wave Refraction Tomography (V_P) Model

V_P ranges from approximately 500 m/s near the surface to approximately 1,800 m/s at 45 m depth (fig. 11). Velocity contours are generally sub-parallel, and there are slightly higher velocities in the southern half of the seismic profile. The strong-motion recording station (SCSN OLI) is approximately 10 m east of our seismic profile and nearest to distance meter 16. The 1,500 m/s contour, which has been shown to coincide with the top of groundwater in other studies (Catchings and others, 2001, 2006, 2013, 2014, 2017), is located at approximately 30–40 m depth.

MAS_RW 2-D S-wave Velocity Model

An MAS_RW Rayleigh-wave dispersion curve shown in appendix 1 (fig. 1.1*D*) was developed for the location (meter 16) along our seismic profile that was nearest to the SCSN OLI strong-motion recording station. Fundamental mode dispersion curve picks (red circles) coincide with phase velocities between approximately 250 and 1,400 m/s and frequencies between 3 and 12 Hz. Rayleigh-wave fundamental mode dispersion curve picks across the entire length of the profile (fig. 2.1*D*) generally coincide with phase velocities between approximately 200 and 1,500 m/s at frequencies between 3 and 21 Hz. The Rayleigh-wave 1-D velocity-depth model (fig. 3.1*D*) for the geophone nearest to the strong-motion recording station shows a gradual positive gradient in V_S below approximately 8 m depth. We calculated (a) V_{S30} to be

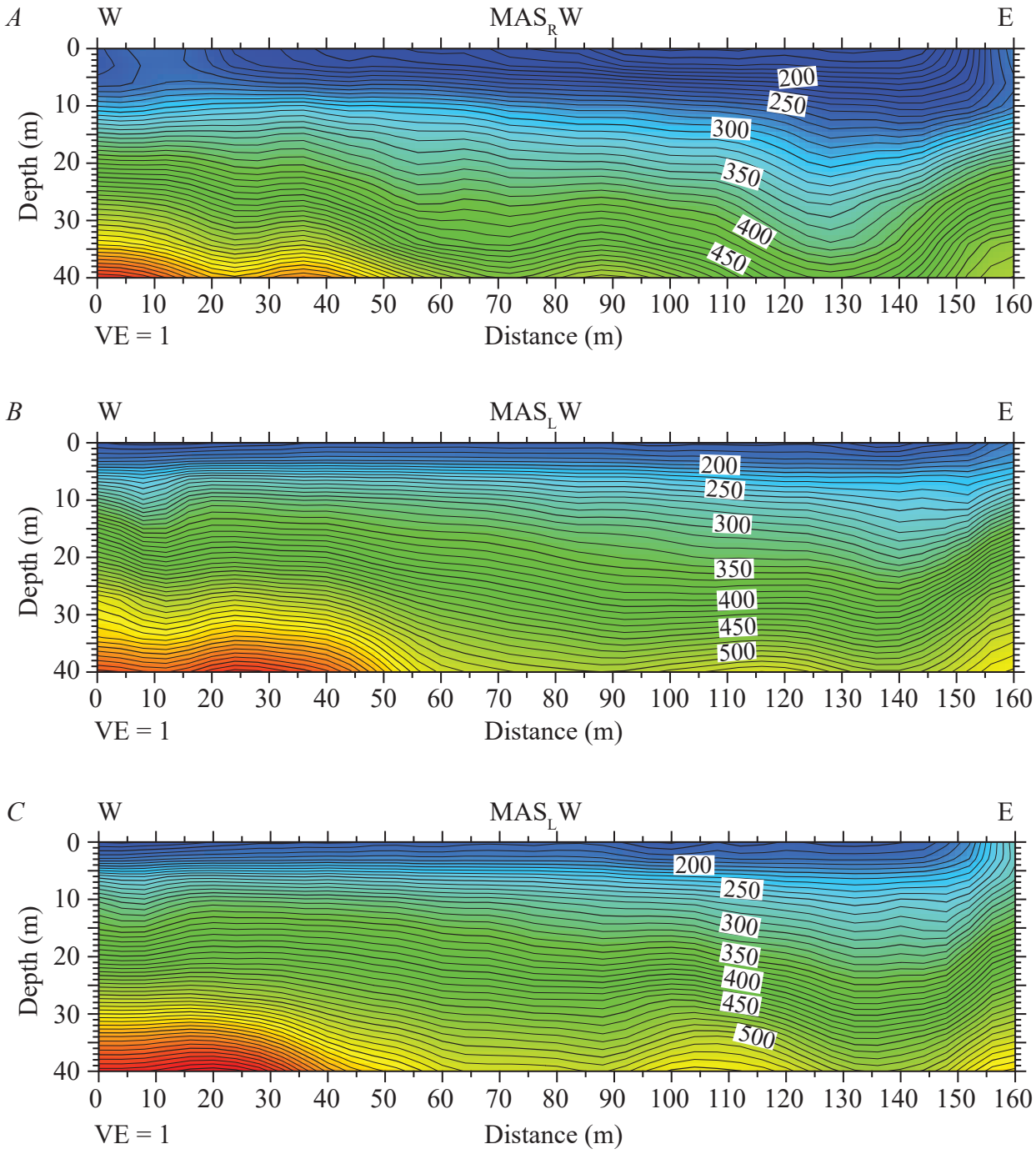

Figure 10. Two-dimensional MAS_RW and MAS_LW shear-wave velocity models for profile LA17-1-0LI. *A*, S-wave velocities for our MAS_RW model range from approximately 150 meters per second (m/s) near the surface to approximately 650 m/s at 40 meters (m) depth. *B*, MAS_LW model developed from data generated by a 3.5-kilogram-sledgehammer and aluminum shear-wave block source. S-wave velocities range from approximately 150 m/s near the surface to approximately 650 m/s at 40 m depth. *C*, MAS_LW model developed from data generated by a 45°-angle accelerated weight-drop and aluminum shear-wave block source. S-wave velocities range from approximately 150 m/s near the surface to approximately 650 m/s at 40 m depth. All three multichannel analysis of surface waves models show slightly higher S-wave velocities in the western third of the seismic profile and a channel-like velocity structure near distance meter 130. (W, west; E, east; VE, vertical exaggeration; V_S, S-wave velocity.)

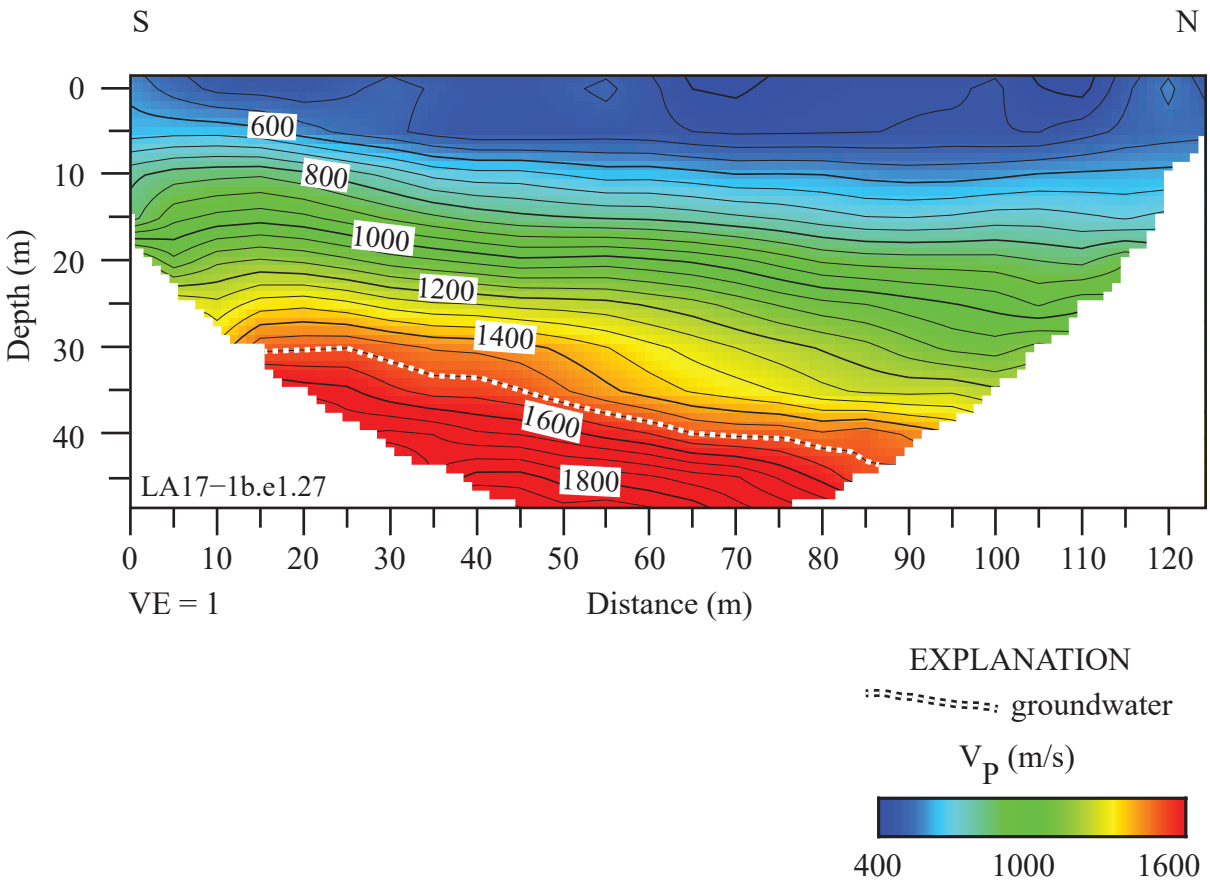

Figure 11. P-wave refraction tomography model for profile LA17-1b-OLI. P-wave velocities range from approximately 500 meters per second (m/s) near the surface to approximately 1,800 m/s at approximately 45 meters (m) depth. P-wave velocities are higher near the south end of the seismic profile at depth. Prior studies suggest the top of groundwater (white dashed line) coincides with 1,500 m/s P-wave velocity contour. (S, south; N, north; VE, vertical exaggeration; V_P, P-wave velocity.)

336 m/s nearest to the SCSN OLI strong-motion recording station, with (b) a range of V_{S30} between 281 and 362 m/s (measured at each meter along the profile), and (c) an average V_{S30} of 309 m/s for the entire profile (table 3).

Our 2-D MAS$_R$W V_S model along the LA17-1b-OLI seismic profile (fig. 12) indicates that V_S ranges from approximately 200 m/s near the surface to approximately 550 m/s at 40 m depth. Model velocity contours are generally sub-parallel, and V_S is slightly higher at depth in the southern third (between distance meters 0 and 40) of the seismic profile. We observe high-velocity contours in the upper south corner of the model, which we interpret as artifacts due to lack of S-wave data in that area.

Profile LA17-2—Serrano (SCSN SRN)

P-wave Refraction Tomography (V_P) Model

V_P ranges between approximately 700 m/s near the surface to approximately 2,000 m/s at 50 m depth (fig. 13). V_P is lower near both the southwest and northeast ends of the seismic profile. The SCSN SRN strong-motion recording station was approximately 200 m southeast of our seismic profile and nearest to distance meter 124. The 1,500 m/s velocity contour (top of groundwater) varies between about 35 and 45 m beneath the surface.

S-wave Refraction Tomography (V_S) Model

V_S determined from refraction tomography ranges from approximately 400 m/s near the surface to approximately 900 m/s at 40 m depth (fig. 14). V_S is lower near the northeast end of the seismic profile between distance meters 100 and 170. We calculated (a) V_{S30} along the profile to range between 470 and 588 m/s (measured at each meter along the profile), with (b) a V_{S30} of 537 m/s nearest (meter 124) to the SCSN SRN strong-motion recording station (table 3).

MAS$_R$W 2-D S-wave Velocity Model

We present an MAS$_R$W (Rayleigh-wave) dispersion curve (fig. 1.2*A*) for the location (meter 124) along our seismic profile nearest to the SCSN SRN strong-motion recording

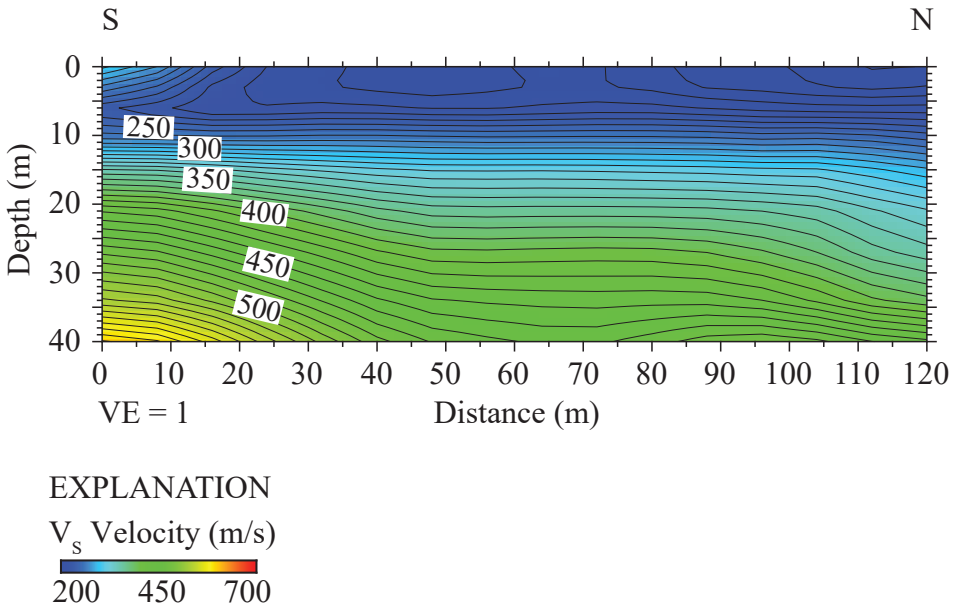

Figure 12. Two-dimensional MAS_RW shear-wave velocity model for profile LA17-1b-OLI. S-wave velocities for our MAS_RW model range from approximately 200 meters per second (m/s) near the surface to approximately 550 m/s at 40 meters (m) depth. (S, south; N, north; VE, vertical exaggeration; V_S, S-wave velocity.)

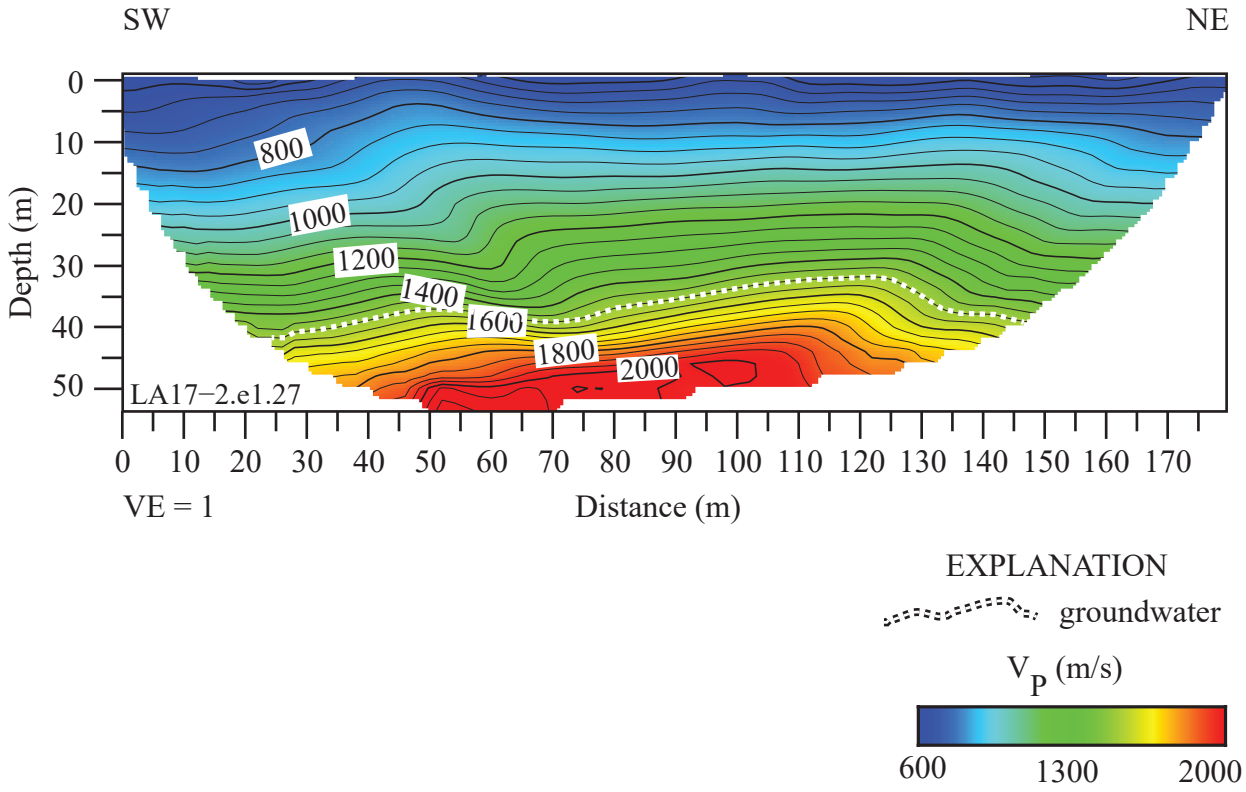

Figure 13. P-wave refraction tomography model for profile LA17-2-SRN. P-wave velocities range from approximately 700 meters per second (m/s) near the surface to approximately 2,000 m/s at approximately 45 meters (m) depth. Top of groundwater is shown as a dashed line. (SW, southwest; NE, northeast; VE, vertical exaggeration; V_P, P-wave velocity.)

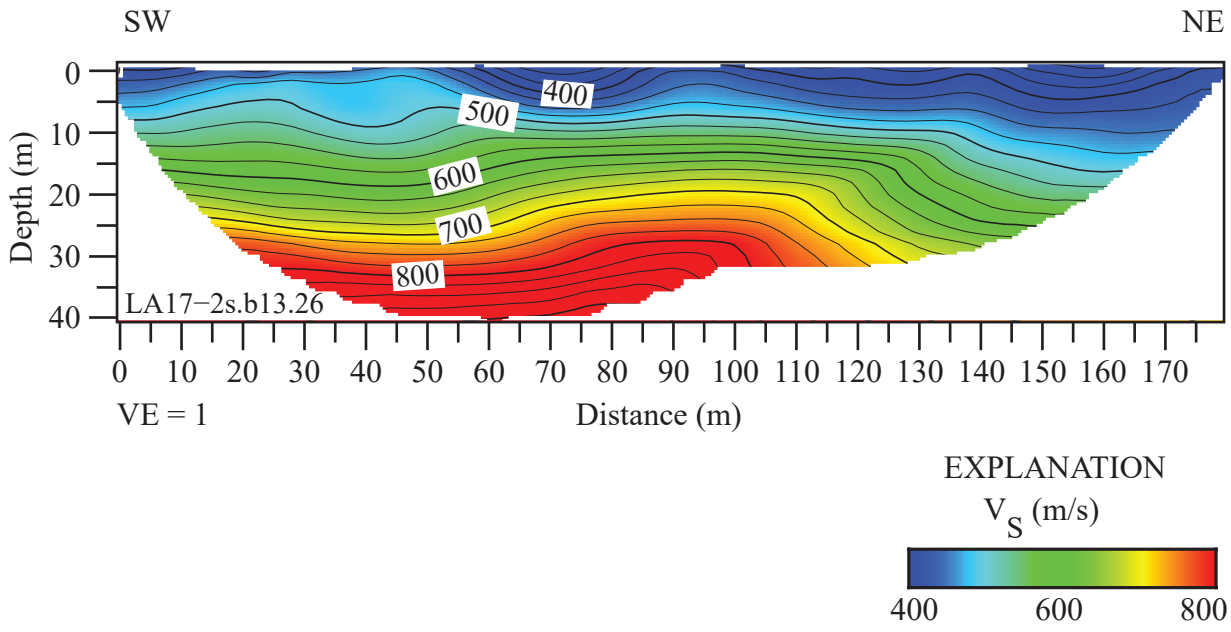

Figure 14. S-wave refraction tomography model for profile LA17-2-SRN. S-wave velocities range from approximately 400 meters per second (m/s) near the surface to approximately 900 m/s at approximately 40 meters (m) depth. S-wave velocities are lower near the northeast end of the seismic profile. (SW, southwest; NE, northeast; VE, vertical exaggeration; V_S, S-wave velocity.)

station. Fundamental mode dispersion curve picks (red circles) coincide with phase velocities between approximately 250 and 1,000 m/s at frequencies between 4 and 22 Hz. Rayleigh-wave fundamental mode dispersion curve picks along the entire length of the profile (fig. 2.2*A*) generally coincide with phase velocities between approximately 250 and 2,500 m/s at frequencies between 2 and 40 Hz. Our Rayleigh-wave 1-D depth-velocity profile (fig. 3.2*A*) at the geophone nearest to the strong-motion recording station shows a positive gradient in V_S below approximately 2 m depth. We calculated (a) V_{S30} to be 379 m/s nearest to the SCSN SRN strong-motion recording station, with (b) V_{S30} ranging between 344 and 429 m/s (measured at each meter along the profile), and (c) an average V_{S30} of 383 m/s along the entire profile (table 3).

We developed a V_S model for the LA17-2-SRN seismic profile by evaluating Rayleigh-waves with the MASW technique. Our 2-D MAS_RW V_S model for the LA17-2-SRN seismic profile (fig. 15*A*) indicates V_S ranges from approximately 300 m/s near the surface to approximately 900 m/s at 50 m depth. Our model shows undulating velocity contours below approximately 20 m depth along the entire seismic profile.

MAS_LW 2-D S-wave Velocity Model—3.5-kg Sledgehammer Source

The MAS_LW (Love-wave) dispersion curve shown in figure 1.2*B* was developed for the location (meter 124) along our seismic profile nearest to the SCSN SRN strong-motion recording station. Fundamental mode dispersion curve picks (red circles) coincide with phase velocities between approximately 250 and 1,200 m/s at frequencies between 2 and 30 Hz. The Love-wave fundamental mode dispersion curve picks along the entire length of the profile (fig. 2.2*B*) generally coincide with phase velocities between approximately 250 and 2,500 m/s at frequencies between 1 and 40 Hz. Our Love-wave 1-D velocity depth model (fig. 3.2*B*) for the location nearest to the strong-motion recording station shows a gradual increase in V_S between approximately 2 and 20 m depth, then a gradual decrease in V_S between approximately 20 and 40 m depth. We calculated (a) V_{S30} to be 432 m/s nearest to the SCSN SRN strong-motion recording station, with (b) the V_{S30} ranging from approximately 415 to approximately 475 m/s (measured at each meter along the profile), and (c) V_{S30} averaging 444 m/s along the entire profile (table 3).

Our 2-D MAS_LW V_S model along the LA17-2-SRN seismic profile (fig. 15*B*) shows V_S ranges from approximately 350 m/s near the surface to approximately 850 m/s at 50 m depth. Our model shows undulating velocity contours, which suggest complex geologic structures, such as bedrock, at depth.

MAS_LW 2-D S-wave Velocity Model—45°-Angle Weight-Drop Source

An MAS_LW (Love-wave) dispersion curve shown in figure 1.2*C* was developed for the location (meter 124) of our seismic profile that was nearest to the SCSN SRN strong-motion recording station. Fundamental mode dispersion curve picks (red circles) are between phase velocities approximately 250 and 1,100 m/s at frequencies between 2 and 30 Hz. Love-wave fundamental mode dispersion curve picks across the entire length of the profile (fig. 2.2*C*) are generally at phase velocities between

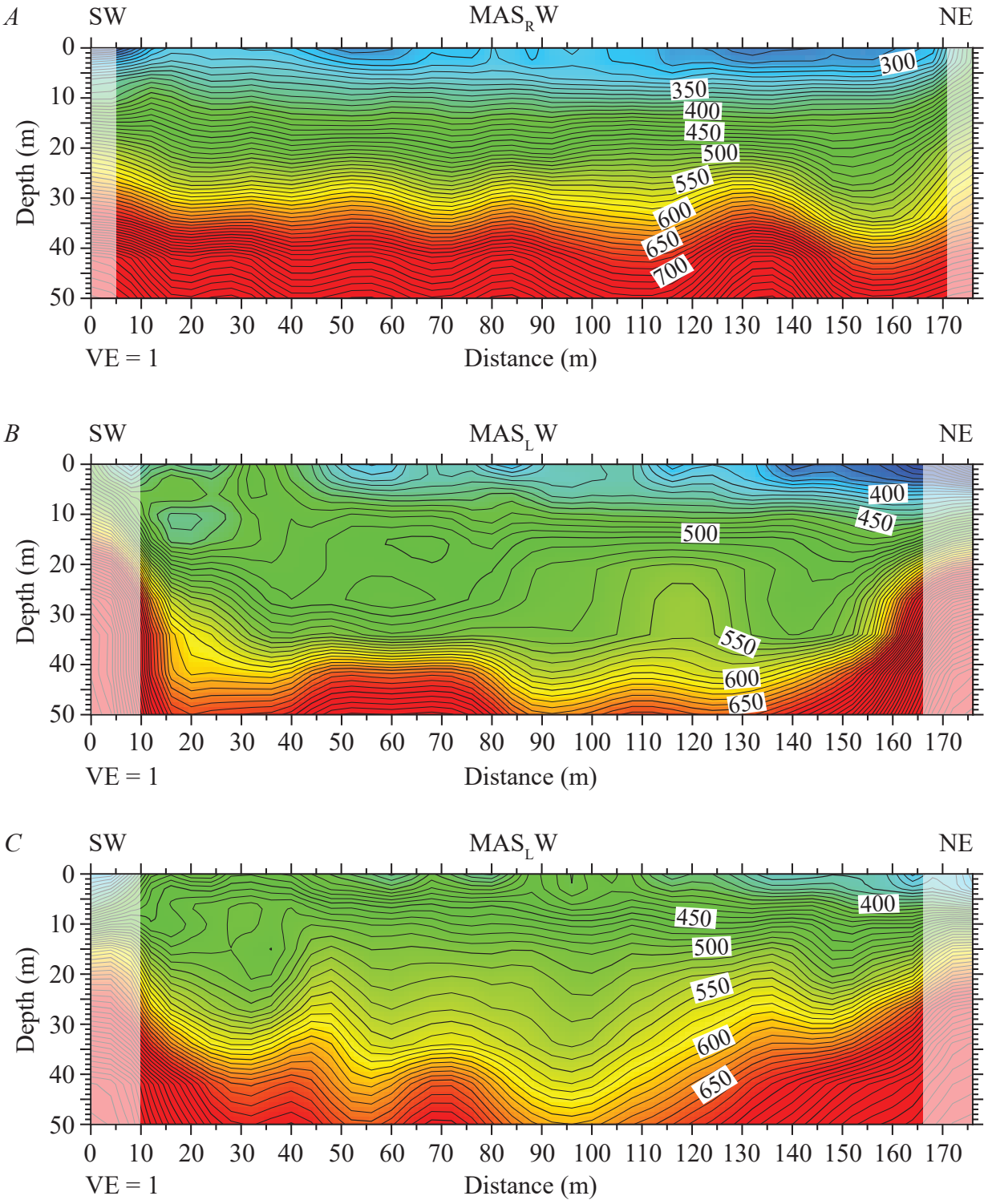

Figure 15. Two-dimensional MAS_RW and MAS_LW shear-wave velocity models for profile LA17-2-SRN. *A*, S-wave velocities for our MAS_RW model range from approximately 300 meters per second (m/s) near the surface to approximately 900 m/s at 50 meters (m) depth. *B*, MAS_LW model developed from data generated by 3.5-kilogram sledgehammer and aluminum shear-wave block sources. S-wave velocities range from approximately 350 m/s near the surface to approximately 850 m/s at 50 m depth. *C*, MAS_LW model developed from data generated by 45°-angle accelerated weight-drop and aluminum shear-wave block sources. S-wave velocities range from approximately 350 m/s near the surface to 800 m/s at 50 m depth. All three multichannel analysis of surface waves models show undulating velocity contours along the entire profile. Shaded areas represent regions with few data points. (SW, southwest; NE, northeast; VE, vertical exaggeration; V_S, S-wave velocity.)

approximately 250 and 1,600 m/s at frequencies between 2 and 40 Hz. Our Love-wave 1-D velocity-depth model (fig. 3.2*C*) for the location nearest to the strong-motion recording station shows a gradual increase in V_S below approximately 2 m depth. We calculated (a) V_{S30} to be 443 m/s nearest to the SCSN SRN strong-motion recording station, with (b) V_{S30} ranging between 435 and 486 m/s (measured at each meter along the profile) and (c) V_{S30} averaging 462 m/s along the profile (table 3).

Our 2-D $MASW_L$ V_S model along the seismic profile LA17-2-SRN (fig. 15*C*) indicates V_S ranges between approximately 350 m/s at the near surface to 800 m/s at 50 m depth. Our model shows undulating velocity contours, which suggest complex structures at depth.

Profile LA17-3—Murrieta (SCSN MUR)

P-wave Refraction Tomography (V_P) Model

Along the SCSN MUR seismic profile, V_P ranges between approximately 500 m/s near the surface and approximately 3,500 m/s at 30 m depth (fig. 16). V_P is lower near the southwest end of the seismic profile, between distance meters 0 and 70. The SCSN MUR strong-motion recording station is approximately 40 m southwest of our seismic profile and nearest to distance meter 0. The 1,500 m/s velocity contour (top of groundwater) varies between about 10 and 25 m beneath the surface, and the top of groundwater appears shallower in the northeastern half of the profile (distance meter 50 to 120).

S-wave Refraction Tomography (V_S) Model

V_S along the SCSN MUR seismic profile, as determined from refraction tomography, ranges between approximately 400 m/s near the surface and approximately 1,800 m/s at 30 m depth (fig. 17). Similar to the V_P model, V_S is lower near the southwest end of the seismic profile between distance meters 0 and 70. On the basis of our V_S tomography model, we calculated V_{S30} along the profile, which ranges between 497 and 769 m/s (measured at each meter along the profile), and the V_{S30} nearest to the SCSN MUR strong-motion station (distance meter 0) is 497 m/s (table 3).

$MASW_R$ 2-D S-wave Velocity Model

We present a Rayleigh-wave dispersion curve (fig. 1.3*A*) for the location (meter 0 of our seismic profile) nearest to the SCSN MUR strong-motion recording station. Fundamental mode dispersion curve picks (red circles) range between phase velocities of approximately 250 and 1,500 m/s at

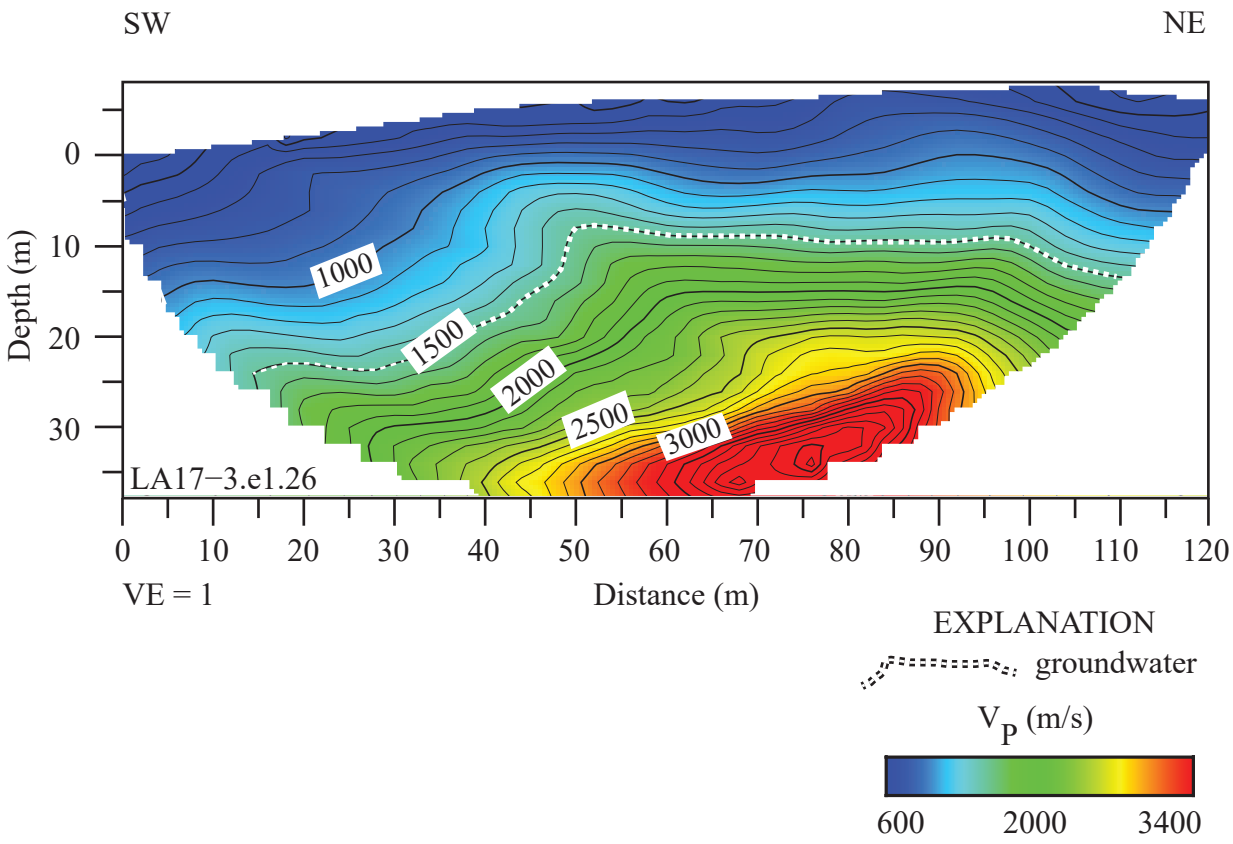

Figure 16. P-wave refraction tomography model for profile LA17-3-MUR (station SCSN MUR). P-wave velocities range between approximately 500 meters per second (m/s) near the surface and 3,500 m/s at approximately 30 meters (m) depth. Top of groundwater is shown as a dashed line. (SW, southwest; NE, northeast; VE, vertical exaggeration; V_P, P-wave velocity.)

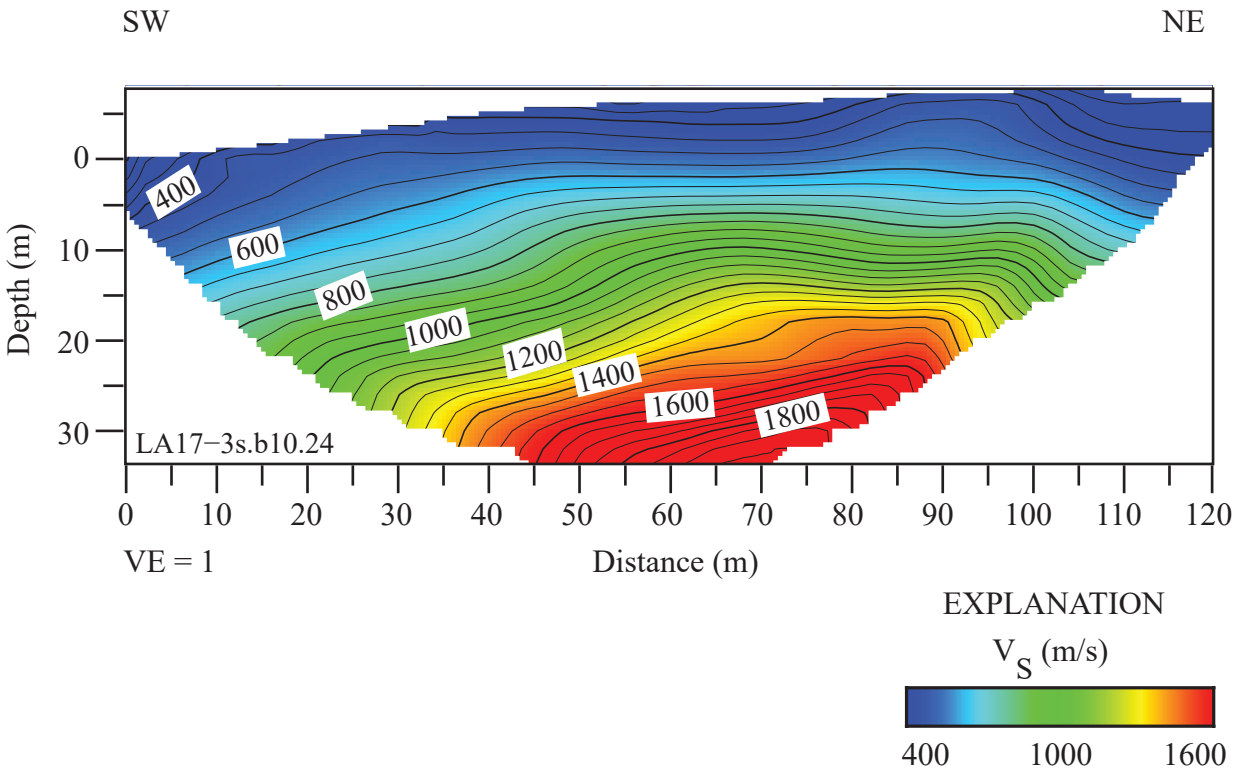

Figure 17. S-wave refraction tomography model for profile LA17-3-MUR (SCSN MUR). S-wave velocities range between approximately 400 meters per second (m/s) near the surface and 1,800 m/s at approximately 30 meters (m) depth. V_S is lower along the southwestern half of the seismic profile. (SW, southwest; NE, northeast; VE, vertical exaggeration; V_S, S-wave velocity.)

frequencies between 4 and 20 Hz. Rayleigh-wave fundamental mode dispersion curve picks along the length of the profile (fig. 2.3*A*) range between phase velocities of approximately 100 and 2,600 m/s at frequencies between 4 and 45 Hz. Our derived Rayleigh-wave 1-D velocity model (fig. 3.3*A*) for the area of the SCSN MUR seismic profile nearest to the strong-motion recording station includes a positive gradient between approximately 8 and approximately 18 m depth and below approximately 36 m depth. From the Rayleigh-wave data, we calculated (a) V_{S30} to be 613 m/s nearest to the SCSN MUR strong-motion recording station, with (b) a range of V_{S30} between 557 and 651 m/s along the profile (calculated at each meter along the profile), and (c) an average V_{S30} of 592 m/s for the entire profile (table 3).

We developed a V_S model for the LA17-3-MUR seismic profile by evaluating Rayleigh-waves with the MASW technique. Our 2-D MAS_RW V_S model for the SCSN MUR seismic profile (fig. 18*A*) suggests V_S ranges between approximately 300 m/s near the surface and approximately 1400 m/s at 40 m depth. Our model shows undulating velocity contours below approximately 8 m depth and channel-like structures centered near distance meters 40 and 80 along the profile. V_S is higher near the northeast end of the profile below approximately 5 m depth.

MAS_LW 2-D S-wave Velocity Model—3.5-kg Sledgehammer Source

We present a Love-wave dispersion curve (fig. 1.3*B*) for the location (meter 0 of our seismic profile) nearest to the SCSN MUR strong-motion recording station. Fundamental mode dispersion curve picks (red circles) range between phase velocities approximately 250 and 1,500 m/s and frequencies between 4 and 32 Hz. Love-wave fundamental mode dispersion curve picks for sites along the length of the profile (fig. 2.3*B*) generally coincide with phase velocities between approximately 200 and 1,500 m/s and frequencies between 3 and 33 Hz. Our Love-wave 1-D velocity model (fig. 3.3*B*) for the site (meter 0) nearest to the strong-motion recording station indicates a positive V_S gradient at all depths. From the Love-wave data, we calculated (a) V_{S30} to be 318 m/s nearest to the SCSN MUR strong-motion recording station, with (b) a range of V_{S30} between 318 and 508 m/s (calculated at every meter along the profile), and (c) an average V_{S30} of 463 m/s for the entire profile (table 3).

We developed a 2-D MAS_LW V_S model for the seismic profile LA17-3-MUR (fig. 18*B*) near the SCSN MUR strong-motion station. Our model indicates V_S ranges between approximately 300 m/s near the surface and approximately 900 m/s at 40 m depth. Our model shows undulating velocity

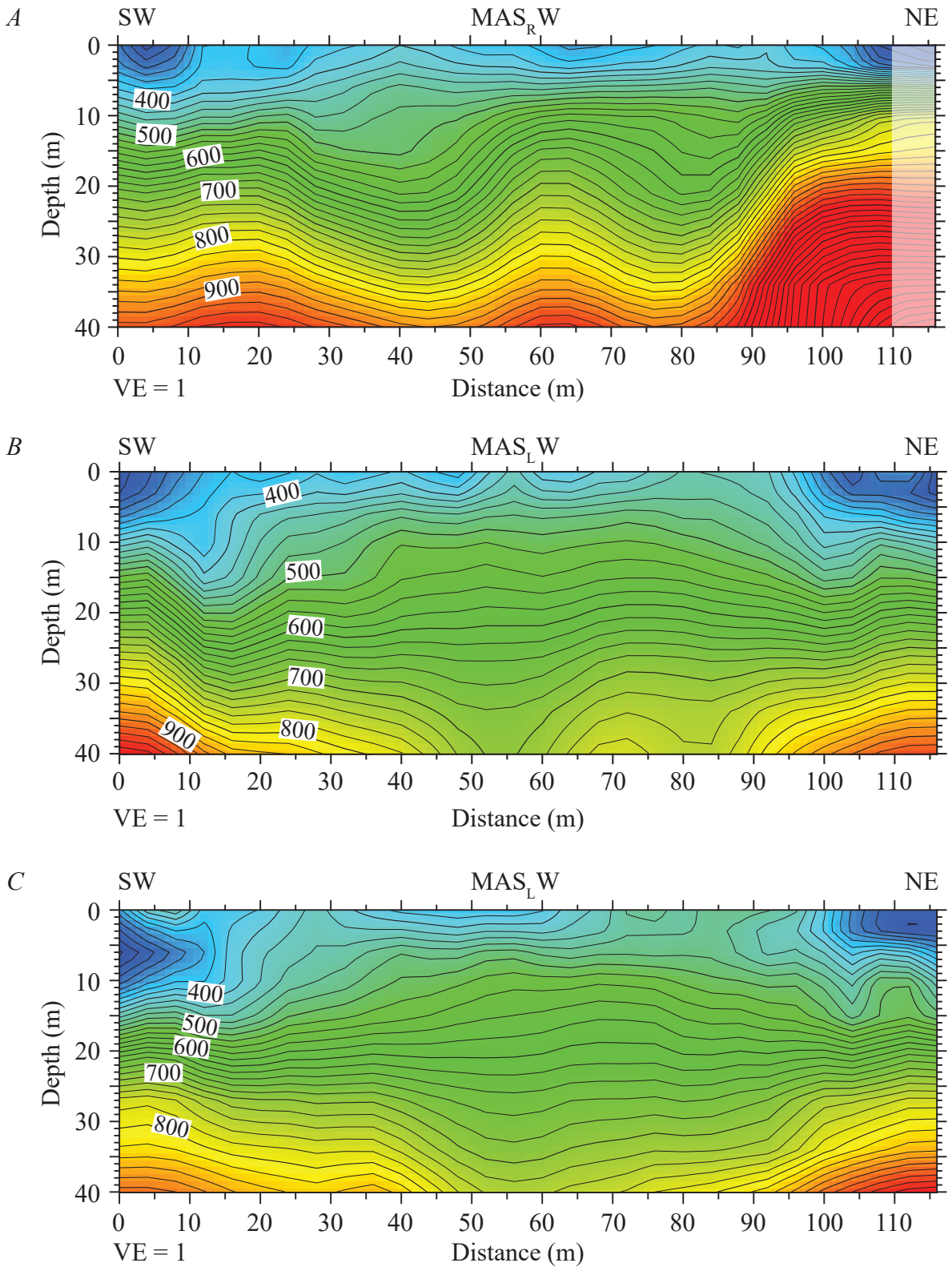

Figure 18. Two-dimensional MAS$_R$W and MAS$_L$W V_S models for profile LA17-3-MUR near the SCSN MUR strong-motion recording station. *A*, V_S for MAS$_R$W model ranges between approximately 300 meters per second (m/s) near the surface and approximately 1,400 m/s at 40 meters (m) depth. Gray box between distance meters 110 and 115 represents an area of low confidence due to unclear dispersion curves. *B*, MAS$_L$W V_S model derived from data generated by the 3.5-kilogram sledgehammer and aluminum block source. V_S ranges between approximately 300 m/s near the surface and 900 m/s at 40 m depth. *C*, MAS$_L$W V_S model derived from data generated by the 45°-angle accelerated weight-drop and aluminum block source. V_S ranges between approximately 300 m/s near the surface and 900 m/s at 40 m depth. All three multichannel analysis of surface waves models show undulating velocity contours across the profile. (SW, southwest; NE, northeast; VE, vertical exaggeration; V_S, S-wave velocity.)

contours along much of the profile, with V_S values higher below approximately 25 m near the northeast and southwest ends of the profile.

MAS$_L$W 2-D S-wave Velocity Model—45°-Angle Weight-Drop Source

We present a Love-wave dispersion curve (fig. 1.3*C*) for the location (meter 0) on our seismic profile nearest to the SCSN MUR strong-motion recording station. Fundamental mode dispersion curve picks (red circles) range between phase velocities of approximately 250 and 1,500 m/s and frequencies between 4 and 32 Hz. Love-wave fundamental mode dispersion curve picks across the length of the profile (fig. 2.3*C*) are generally at phase velocities between approximately 200 and 2,500 m/s and frequencies between 3 and 30 Hz. The Love-wave 1-D depth-velocity profile (fig. 3.3*C*) nearest to the strong-motion recording station shows a gradual increase in V_S at all depths. We calculated (a) V_{S30} to be 318 m/s nearest to the SCSN MUR strong-motion recording station, (b) V_{S30} at each meter along the profile to range between 318 and 543 m/s, and (c) the average V_{S30} along the entire profile to be 491 m/s (table 3).

Our 2-D MAS$_L$W V_S model along the LA17-3-MUR seismic profile (fig. 18*C*) shows V_S ranges between approximately 300 m/s near the surface and approximately 900 m/s at 40 m depth. Our model shows undulating velocity contours throughout much of the profile, and V_S is higher below approximately 25 m at both the northeast and southwest ends of the profile.

Profile LA17-4—La Cienega (SCSN LCG)

P-wave Refraction Tomography (V_P) Model

Along the LA17-4-LCG seismic profile near the SCSN LCG, V_P ranges between approximately 700 m/s near the surface and approximately 2,200 m/s at 25 m depth (fig. 19). V_P is relatively higher below approximately 10 m depth at distance meters between approximately 25 and 55. The SCSN LCG strong-motion recording station is approximately 120 m northwest of our seismic profile and nearest to distance meter 120 of the profile. The 1,500 m/s velocity contour (top of groundwater) varies between about 10 to 20 m beneath the surface.

S-wave Refraction Tomography (V_S) Model

Our V_S refraction tomography model along the LA17-4-LCG seismic profile indicates that V_S ranges between approximately 400 m/s near the surface and approximately 1,100 m/s at 30 m depth (fig. 20). V_S is relatively higher between distance meters approximately 20 and 60, with undulating velocity contours in the

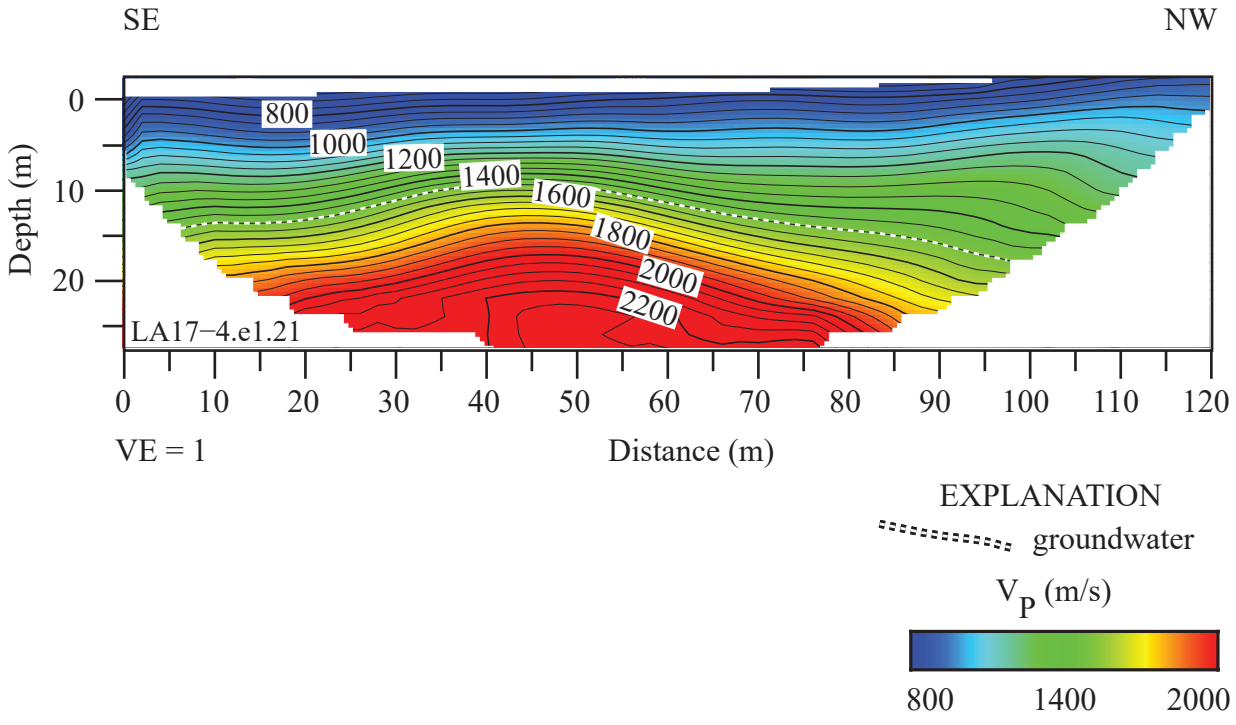

Figure 19. P-wave refraction tomography model for profile LA17-4-LCG. P-wave velocities (V_P) range between approximately 700 m/s near the surface and 2,200 m/s at approximately 25 m depth. V_P is lower in the northwest and southeast ends of the seismic profile. Top of groundwater is shown as a dashed line. (SE, southeast; NW, northwest; VE, vertical exaggeration; V_P, P-wave velocity.)

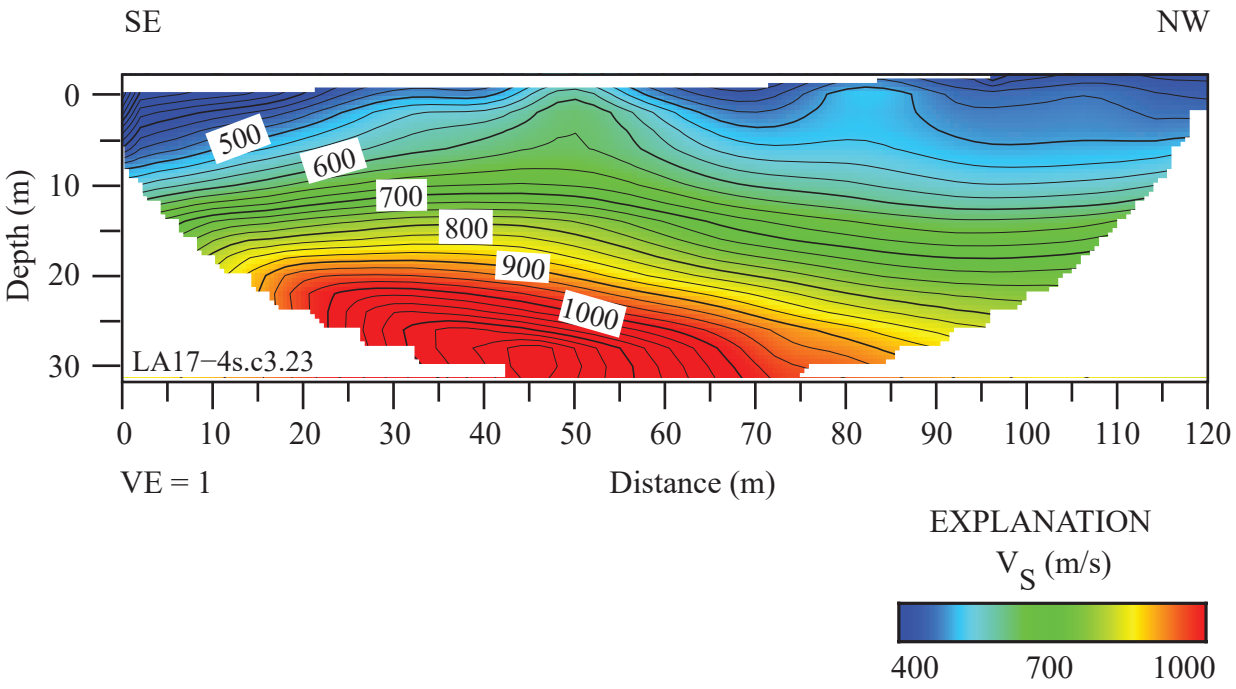

Figure 20. S-wave refraction tomography velocity model for profile LA17-4-LCG. V_S ranges between approximately 400 meters per second (m/s) in the near surface and 1,100 m/s at approximately 30 meters (m) depth. V_S is lower near the northwest and southeast ends of the seismic profile. (SE, southeast; NW, northwest; VE, vertical exaggeration; V_S, S-wave velocity.)

upper approximately 10 m of the subsurface. We calculated V_{S30} along the profile to be between 518 and 774 m/s. Calculated V_{S30} nearest to the SCSN LCG strong-motion station (at distance meter 120 of our seismic profile) is 595 m/s (table 3).

MAS_RW 2-D S-wave Velocity Model

We present a Rayleigh-wave dispersion curve (fig. 1.4*A*) for the location (meter 120) on our seismic profile that is nearest to the SCSN LCG strong-motion recording station. Fundamental mode dispersion curve picks (red circles) are between phase velocities of approximately 250 and 1,600 m/s and frequencies between 2 and 56 Hz. Rayleigh-wave fundamental mode dispersion curve picks for the entire length of the profile (fig. 2.4*A*) are generally at phase velocities between approximately 250 and 1,500 m/s and frequencies between 2 and 56 Hz. Our Rayleigh-wave 1-D depth-velocity profile (fig. 3.4*A*) for our geophone that was nearest to the SCSN LCG strong-motion recording station shows a gradual increase in V_S below approximately 12 m depth. We calculated (a) V_{S30} to be 425 m/s nearest to the SCSN LCG strong-motion recording station, (b) V_{S30} at each meter along the profile to range between 357 and 425 m/s, and (c) the average V_{S30} across the entire profile to be 374 m/s (table 3).

We developed a V_S model for the LA17-4-LCG seismic profile by evaluating Rayleigh-waves with the MASW technique. Our 2-D MAS_RW V_S model along the LA17-4-LCG seismic profile (fig. 21*A*) shows V_S ranges between approximately 300 m/s near the surface and approximately 650 m/s at 40 m depth. Our model shows a channel-like structure (V_S less than 400 m/s) centered at distance meter 90, extending to approximately 35 m depth. V_S is generally between approximately 300 and 400 m/s in the upper 35 m of the subsurface and increases to approximately 650 m/s at depths between 35 and 40 m. V_S is higher at the southeast end of the profile at depths below approximately 20 m.

MAS_LW 2-D S-wave Velocity Model—3.5-kg Sledgehammer Source

We show a Love-wave dispersion curve (fig. 1.4*B*) for the location (meter 120) along our seismic profile that was nearest to the SCSN LCG strong-motion recording station. Fundamental mode dispersion curve picks (red circles) correlate phase velocities between approximately 250 and 1,600 m/s and frequencies between 2 and 56 Hz. Love-wave fundamental mode dispersion curve picks along the entire length of the profile (fig. 2.4*B*) generally coincide with phase velocities between approximately 150 and 1,600 m/s and frequencies between 2 and 70 Hz. A Love-wave 1-D depth-velocity profile (fig. 3.4*B*) for the part of seismic profile nearest to the SCSN LCG strong-motion recording station shows a gradual increase in V_S between 2 and 40 m depth. We calculated (a) V_{S30} to be 645 m/s nearest to the SCSN LCG strong-motion recording station, (b) V_{S30} at each meter along the profile to be between 513 and 645 m/s, and (c) the average V_{S30} along the entire profile to be 555 m/s (table 3).

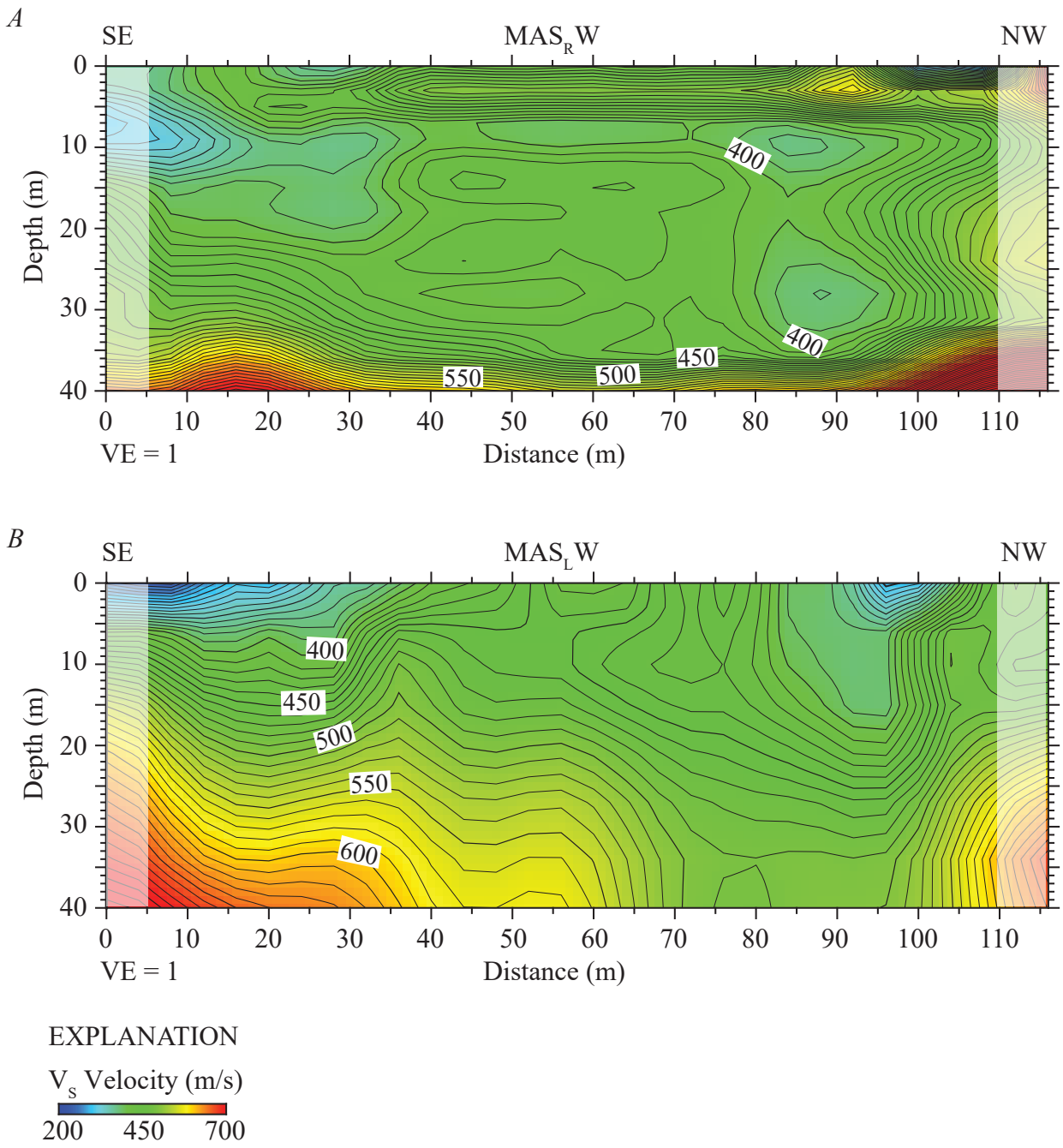

Figure 21. Two-dimensional MAS$_R$W- and MAS$_L$W-derived shear-wave velocity models for profile LA17-4-LCG. *A*, MAS$_R$W-based V_S ranges between approximately 300 meters per second (m/s) near the surface and approximately 650 m/s at approximately 40 meters (m) depth. *B*, MAS$_L$W data were generated using a 3.5-kilogram sledgehammer and aluminum block. V_S ranges between approximately 300 m/s near the surface and 650 m/s at 40 m depth. Both MASW-based models show undulating and complex velocity contours along the entire profile. Shaded areas represent regions with few data points. (SE, southeast; NW, northwest; VE, vertical exaggeration; V_S, S-wave velocity.)

We developed a 2-D MAS$_L$W V_S model along the LA17-4-LCG seismic profile (fig. 21*B*) using Love-waves. Our model shows V_S ranges between approximately 300 m/s near the surface and approximately 650 m/s at 40 m depth. Our model shows undulating velocity contours throughout much of the profile and a channel-like velocity structure (V_S less than 500 m/s) centered at distance meter 90, which extends past the maximum depth of our model at 40 m. V_S is relatively high below approximately 20 m near both the southeast and northwest ends of the profile.

Profile LA17-5—Rush (SCSN RUS)

P-wave Refraction Tomography (V_P) Model

We developed a V_P model along the LA17-5-RUS seismic profile near the SCSN RUS strong-motion recording station. Along our profile, V_P ranges between approximately 300 m/s near the surface and approximately 1,700 m/s at 20 m depth (fig. 22). Velocity contours are generally sub-horizontal in the upper approximately 13 m of the subsurface, and V_P is generally higher between distance meters 0 and 50 along the profile. The SCSN RUS strong-motion recording station is approximately 87 m southwest of our seismic profile and nearest to distance meter 0 of the profile. The 1,500 m/s velocity contour (top of groundwater) appears at two discreet locations at depths below approximately 15, which may suggest a perched water table.

S-wave Refraction Tomography (V_S) Model

We developed a S-wave refraction tomography model along the LA17-5-RUS seismic profile using first-arrival S-waves. Our refraction tomography derived V_S values range between approximately 300 near the surface and approximately 550 m/s at 25 m depth (fig. 23). V_S is relatively higher between distance meters approximately 25 and 60, and a minor basin-like velocity structure is apparent between distance meters approximately 60 and 120. We calculated V_{S30} at every meter along the profile to range between 393 and 490 m/s. V_{S30} nearest to the SCSN RUS strong-motion station (distance meter 0 of our seismic profile) is calculated to be 468 m/s (table 3).

MAS$_R$W 2-D S-wave Velocity Model

We developed a V_S model for the LA17-5-RUS seismic profile by evaluating Rayleigh-waves with the MASW technique. We show a Rayleigh-wave dispersion curve (fig. 1.5*A*) for the location (meter 0 of our seismic profile) nearest to the SCSN RUS strong-motion recording station. Fundamental mode dispersion curve picks (red circles) correlate with phase velocities between approximately 200 and 800 m/s and frequencies between 2 and 32 Hz. Rayleigh-wave fundamental mode dispersion curve picks for the entire length of the profile (fig. 2.5*A*) correlate with phase velocities between approximately 200 and 1,300 m/s and frequencies between 2 and 60 Hz. A Rayleigh-wave 1-D depth-velocity profile (fig. 3.5*A*) nearest to the SCSN LCG strong-motion recording station shows a gradual increase in V_S at all depths. We calculated (a) V_{S30} to be 305 m/s nearest to the SCSN LCG strong-motion recording station, (b) V_{S30} at each meter along the profile to be between 310 and 330 m/s, and (c) the average V_{S30} along the entire profile to be 310 m/s (table 3).

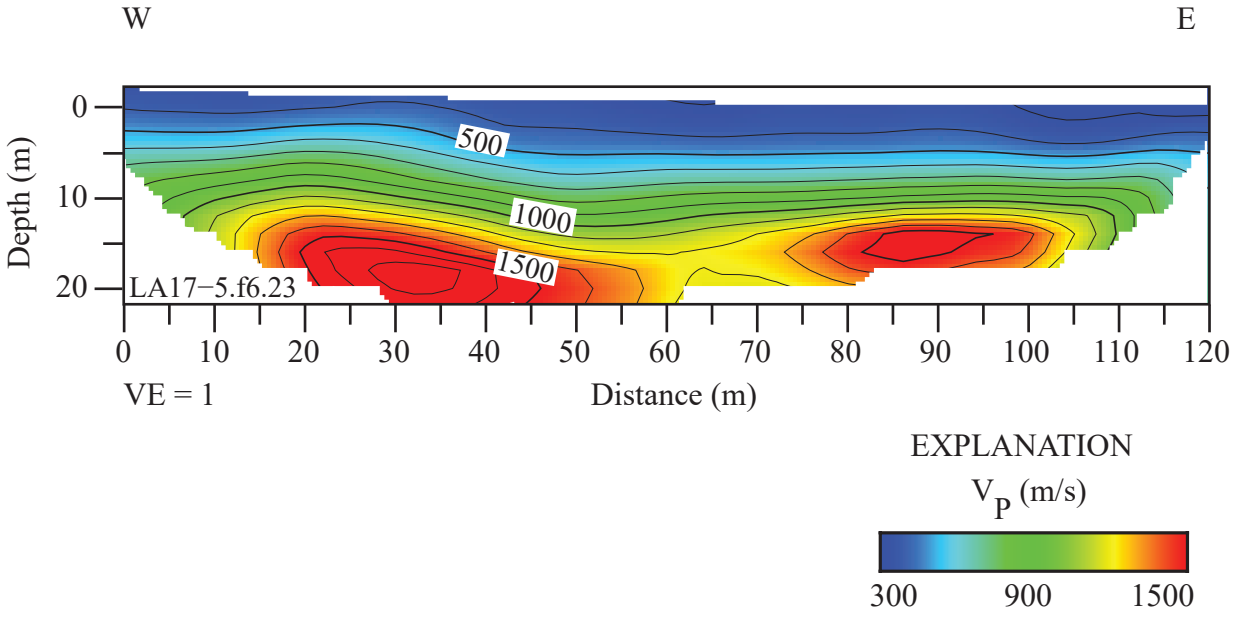

Figure 22. P-wave refraction tomography velocity model for the LA17-5-RUS profile. V_P ranges between approximately 300 meters per second (m/s) near the surface and 1,700 m/s at approximately 20 meters (m) depth. V_P is relatively higher near the western half of the profile at all depths. (W, west; E, east; VE, vertical exaggeration; V_P, P-wave velocity.)

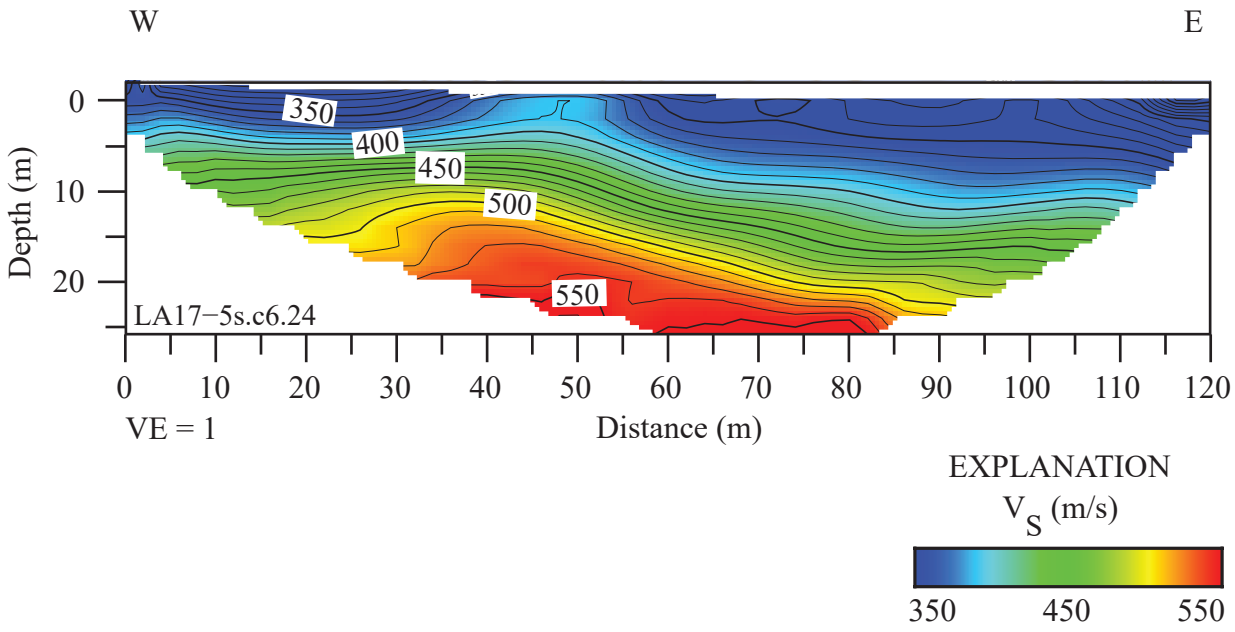

Figure 23. S-wave refraction tomography model for the LA17-5-RUS profile. V_S ranges between approximately 300 meters per second (m/s) near the surface and 550 m/s at approximately 25 meters (m) depth. Higher values of V_S occur at shallower depths between distance meters approximately 25 and 60 m of the profile. V_S is generally higher in the west end of the seismic profile. (W, west; E, east; VE, vertical exaggeration; V_S, S-wave velocity.)

We also developed a 2-D MAS_RW V_S model along the seismic profile LA17-5-RUS (fig. 24*A*) using Rayleigh-waves. Our model shows V_S ranges between approximately 200 m/s near the surface and approximately 650 m/s at 40 m depth. Our model shows V_S ranges between 200 and 350 m/s in the upper 25 m of the subsurface with a higher gradient below approximately 25 m depth. V_S is higher at both the west and east ends of the profile at depths below approximately 10 m.

MAS_LW 2-D S-wave Velocity Model—3.5-kg Sledgehammer Source

We developed a Love-wave dispersion curve (fig. 1.5*B*) for the location (meter 0 on our seismic profile) nearest to the SCSN RUS strong-motion recording station. Fundamental mode dispersion curve picks (red circles) correlate with phase velocities between approximately 150 and 800 m/s and frequencies between 2 and 24 Hz. Love-wave fundamental mode dispersion curve picks along the entire profile (fig. 2.5*B*) correlate with phase velocities between approximately 150 and 1,200 m/s and frequencies between 2 and 40 Hz. The Love-wave 1-D depth-velocity profile (fig. 3.5*B*) nearest to the SCSN RUS strong-motion recording station shows a gradual increase in V_S below approximately 2 m depth. We calculated (a) V_{S30} to be 351 m/s nearest to the SCSN RUS strong-motion recording station, (b) V_{S30} at each meter along the profile to be between 288 and 351 m/s, and (c) the average V_{S30} across the entire profile to be 308 m/s (table 3).

We developed a 2-D MAS_LW V_S model along the LA17-5-RUS seismic profile (fig. 24*B*). Our model shows V_S ranges between approximately 250 m/s near the surface and approximately 800 m/s at 40 m depth. Our model shows V_S ranges between 200 and 350 in the upper 20 m of the subsurface, with a relatively higher gradient below 20 m depth. V_S is generally higher at both west and east ends of the seismic profile at depths below approximately 10 m.

Profile LA17-6—Santa Clara (SCSN STC)

P-wave Refraction Tomography (V_P) Model

We developed a refraction tomography P-wave velocity model from first arrival refractions. In our model, V_P ranges between approximately 350 m/s near the surface and approximately 1400 m/s at 45 m depth (fig. 25). Velocity contours are generally sub-horizontal along the entire seismic profile at all depths in the upper 45 m of the subsurface. The SCSN STC strong-motion recording station was located approximately 240 m northwest of our seismic profile and nearest to distance meter 120 of our profile.

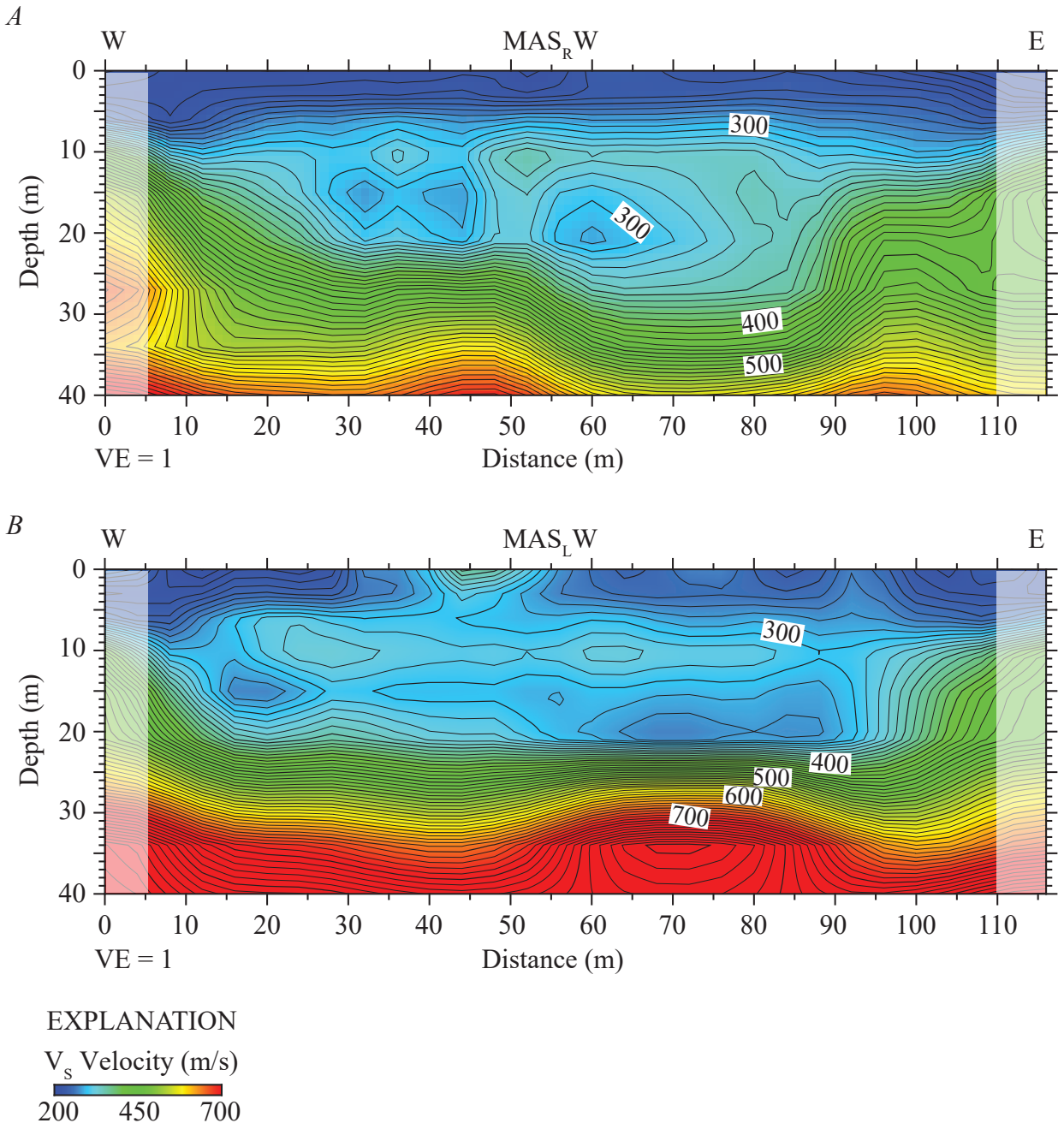

Figure 24. Two-dimensional MAS$_R$W and MAS$_L$W shear-wave velocity models for profile LA17-5-RUS. *A*, Our MAS$_R$W-derived V_S ranges between approximately 200 meters per second (m/s) near the surface and approximately 650 m/s at approximately 40 meters (m) depth. *B*, Two-dimensional MAS$_L$W model (derived from a 3.5-kg sledgehammer and aluminum block source) indicates V_S ranges between approximately 250 m/s near the surface and approximately 800 m/s at 40 m depth. Both MASW-based models show V_S to be between 250 and 400 m/s in the upper 20 m of the subsurface, with higher V_S gradients below 20 m. Shaded areas represent regions with few data points. (W, west; E, east; VE, vertical exaggeration; V_S, S-wave velocity.)

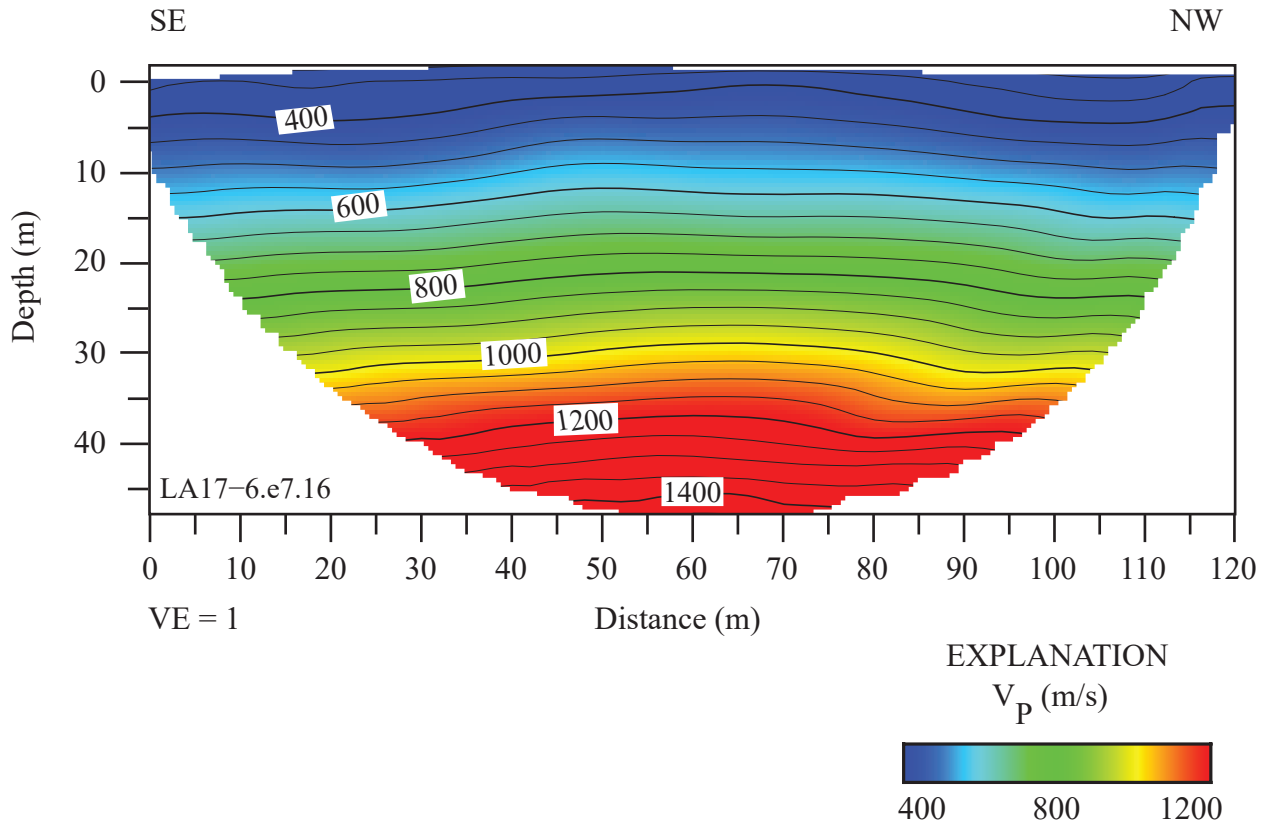

Figure 25. P-wave refraction tomography model for profile LA17-6-STC. P-wave velocities range between approximately 350 meters per second (m/s) near the surface and 1,400 m/s at approximately 45 meters (m) depth. (SE, southeast; NW, northwest; VE, vertical exaggeration; V_P, P-wave velocity.)

S-wave Refraction Tomography (V_S) Model

We developed an S-wave refraction tomography model from first-arrival shear-waves. Our model shows that V_S ranges between approximately 300 m/s near the surface and approximately 700 m/s at 25 m depth (fig. 26). V_S contours are generally sub-parallel between distance meters 0 and approximately 65 along the profile. We calculated V_{S30} at every meter along the profile to be between 372 and 504 m/s and calculated V_{S30} nearest to the SCSN STC strong-motion station (near distance meter 120 of our seismic profile) to be 377 m/s (table 3).

MAS$_R$W 2-D S-wave Velocity Model

We developed a Rayleigh-wave dispersion curve (fig. 1.6*A*) for the location nearest to the SCSN STC strong-motion recording station (meter 120 of our seismic profile). Fundamental mode dispersion curve picks (red circles) correlate with phase velocities between approximately 200 and 500 m/s and frequencies between 4 and 60 Hz. Rayleigh-wave fundamental mode dispersion curve picks along the entire length of the profile (fig. 2.6*A*) generally correlate at phase velocities between approximately 150 and 1,400 m/s and frequencies between 2 and 70 Hz. The Rayleigh-wave 1-D depth-velocity profile (fig. 3.6*A*) nearest to the SCSN STC strong-motion recording station indicates a gradual increase in V_S below approximately 8 m depth. We calculated (a) V_{S30} to be 311 m/s nearest to the SCSN STC strong-motion recording station, (b) V_{S30} at each meter along the profile to range between 269 and 318 m/s, and (c) the average V_{S30} along the entire profile to be 294 m/s (table 3).

We developed a V_S model for the LA17-6-STC seismic profile by evaluating Rayleigh-waves with the MASW technique. Our 2-D MAS$_R$W V_S model along the seismic profile

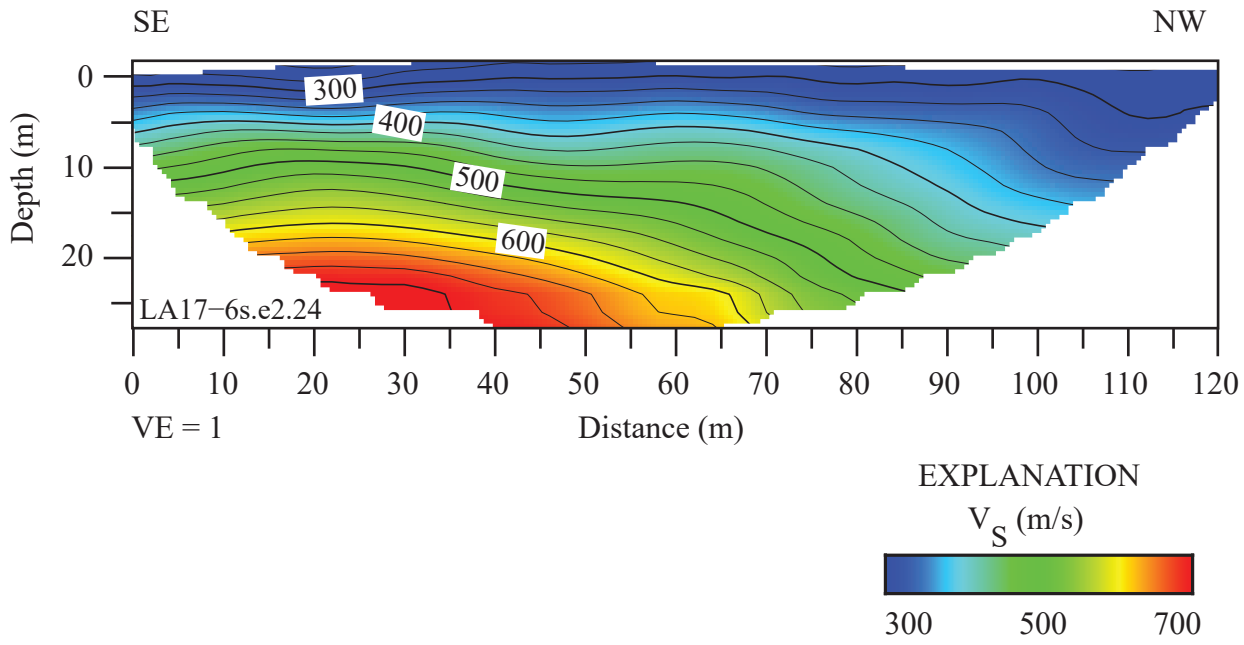

Figure 26. S-wave refraction tomography model for the LA17-6-STC seismic profile. V_S ranges between approximately 300 meters per second (m/s) near the surface and 700 m/s at approximately 25 meters (m) depth. V_S is generally lower near the northwest half of the seismic profile. (SE, southeast; NW, northwest; VE, vertical exaggeration; V_S, S-wave velocity.)

LA17-6-STC (fig. 27*A*) shows V_S ranges between approximately 180 m/s near the surface and approximately 550 m/s at 40 m depth. Our V_S model shows a channel-like velocity structure below approximately 10 m depth between distance meters approximately 40 and 80. A smaller channel-like velocity structure is also observed between distance meters 90 and 105. V_S is higher near both the southeast and northwest ends of the profile at depths below approximately 12 m.

MAS_LW 2-D S-wave Velocity Model—3.5-kg Sledgehammer Source

We present a Love-wave dispersion curve (fig. 1.6*B*) for the location (meter 120 of our seismic profile) nearest to the SCSN STC strong-motion recording station. Fundamental mode dispersion curve picks (red circles) correlate with phase velocities between approximately 200 and 600 m/s and frequencies between 3 and 55 Hz. Love-wave fundamental mode dispersion curve picks along the entire length of the profile (fig. 2.6*B*) generally correlate with phase velocities between approximately 150 and 1,300 m/s and frequencies between 2 and 80 Hz. Our Love-wave 1-D depth-velocity profile (fig. 3.6*B*) nearest to the SCSN STC strong-motion recording station shows a gradual increase in V_S between approximately 2 and 40 m depth. We calculated (a) V_{S30} to be 330 m/s nearest to the SCSN STC strong-motion recording station, (b) V_{S30} at each meter along the profile to be between 302 and 331 m/s, and (c) the average V_{S30} across the entire profile to be 320 m/s (table 3).

We developed a 2-D MAS_LW V_S model along the seismic profile LA17-6-STC (fig. 27*B*). Our model shows V_S ranges between approximately 200 m/s near the surface and approximately 450 m/s at 40 m depth. Our V_S MAS_LW-derived model shows a channel-like velocity structure below approximately 10 m depth between distance meters approximately 45 and 95. V_S is generally higher near both the southeast and northwest ends of the seismic profile at depths below approximately 10 m.

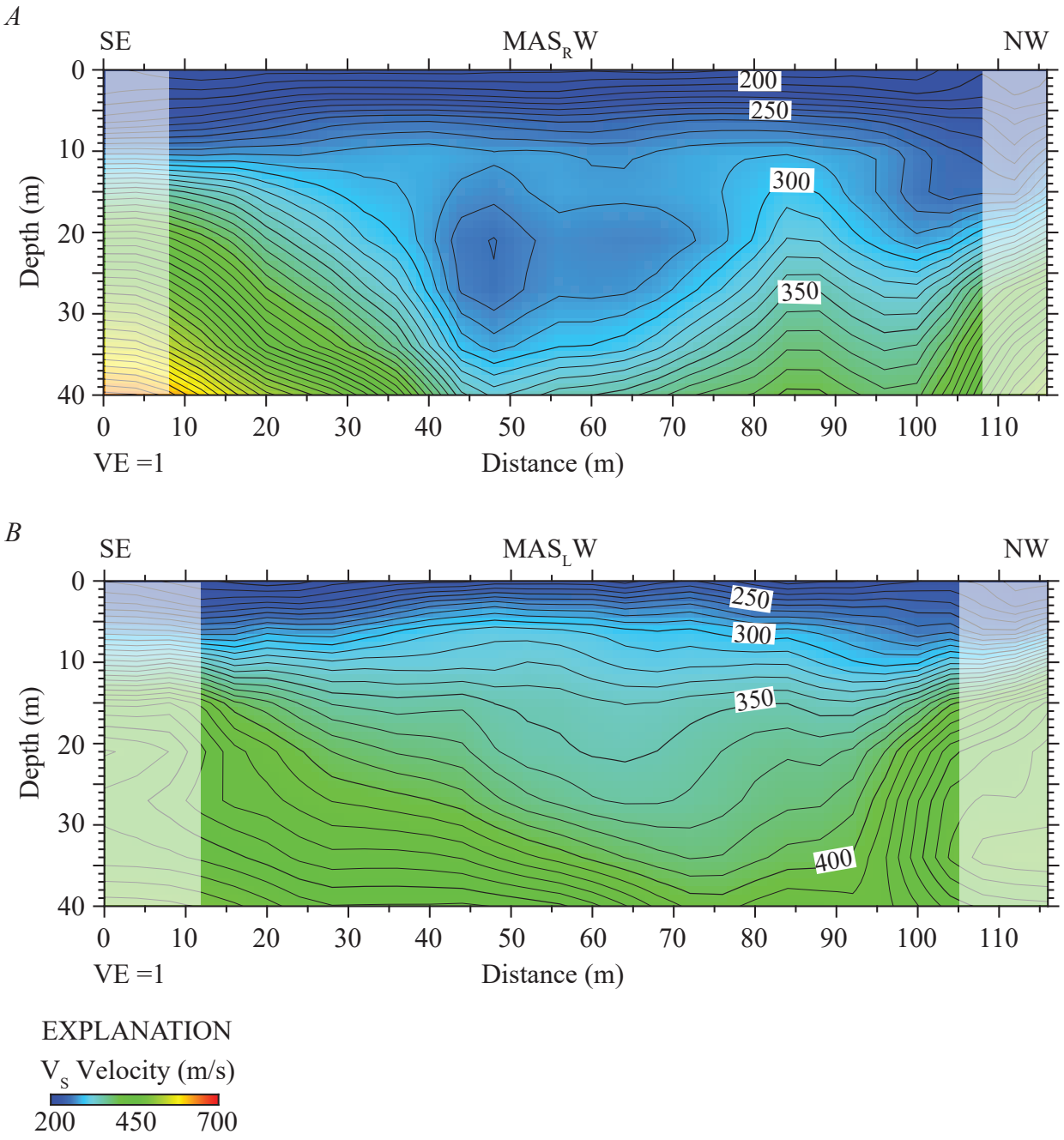

Figure 27. Two-dimensional MAS$_R$W- and MAS$_L$W-derived V_S models for profile LA17-6-STC. *A*, Our MAS$_R$W model indicates V_S ranges between approximately 180 meters per second (m/s) near the surface and approximately 550 m/s at approximately 40 meters (m) depth. *B*, Our MAS$_L$W model was derived from data generated by 3.5-kilogram sledgehammer and aluminum block source. V_S, derived from the MAS$_L$W data, ranges between approximately 200 m/s near the surface and approximately 450 m/s at 40 m depth. Both multichannel analysis of surface waves models show channel-like velocity structures near the middle of the profile, between distance meters approximately 40 and approximately 90. Shaded areas represent regions with few data points. (SE, southeast; NW, northwest; VE, vertical exaggeration; V_S, S-wave velocity.)

V_P/V_S Ratios

The ratio of P-wave velocities to S-wave velocities (V_P/V_S) can provide information about the physical state and lithology of subsurface materials (Tatham, 1982; Castagna and others, 1985). We derived V_P/V_S models for each of the six seismic profiles (appendix 4) in this report by dividing V_P by the V_S at each node of the refraction tomography models. V_P/V_S ratios range between 1 and 3 in all six seismic profiles. V_P/V_S ratios along the LA17-1-OLI seismic profile range between approximately 1.3 and 2.6, with the highest V_P/V_S ratios (more than 2) occurring in the upper 5 m of the subsurface (fig. 4.1). V_P/V_S ratios along the LA17-2-SRN seismic profile range between approximately 1.2 and 2, with the highest V_P/V_S ratios (approximately 2) forming a southwest-dipping feature between distance meters 110 and 170, which coincides with the approximate mapped trace of the Peralta Hills Fault (fig. 4.2). V_P/V_S ratios along the LA17-3-MUR seismic profile range between 1 and 2, with the highest ratios (approximately 2) occurring at depths below approximately 25 m between distance meters 65 and 95 and occurring at discrete locations at varying depths between distance meters 45 and 105 (fig. 4.3). V_P/V_S ratios along the LA17-4-LCG seismic profile range between 1.4 and 2.6, with the highest ratios (more than 2) occurring near the south end of the profile in the upper 10 m of the subsurface and at depths below approximately 10 m between distance meters 40 and 115 (fig. 4.4). V_P/V_S ratios along the LA17-5-RUS seismic profile range between 1 and 3.5, with the highest ratios occurring at depths below approximately 15 m (fig. 4.5). Finally, V_P/V_S ratios along the LA17-6-STC seismic profile range between 1 and 1.6, with the highest ratios (approximately 1.6) occurring at depths below approximately 15 to 20 meters between distance meters 70 and 100 (fig. 4.6).

Poisson's Ratios

Poisson's ratios provide information about water-saturation levels and clay content of the soil in subsurface materials (Castagna and others, 1985; Catchings and others, 2006), whereby relatively high Poisson's ratios above 0.44 (determined from tomographic seismic data) typically coincide with the top of groundwater (Catchings and others, 2006; 2014). We developed Poisson's ratio models from refraction tomographic V_P and V_S models using the calculation determined by Thomsen (1990). These models are presented in appendix 5 of this report.

Poisson's ratios along the LA17-1-OLI seismic profile range between approximately 0.02 and 0.4. The highest Poisson's ratios (approximately 0.4) occur in the upper meter of the subsurface, which may suggest near-surface saturated materials or materials with high clay content on the berm (fig. 5.1). Poisson's ratios along the LA17-2-SRN seismic profile range between approximately 0.025 and 0.325. The highest Poisson's ratios (more than 0.3) occur below approximately 5 m depth between distance meters 110 and 155 (fig. 5.2). Whereas Poisson's ratios along the profile are inconsistent with saturated materials, the highest Poisson's ratios coincide with a mapped trace of the Peralta Hills Fault, which indicates fluid accumulation along the fault. Poisson's ratios along the LA17-3-MUR seismic profile range between approximately 0.1 and 0.325, with highest Poisson's ratios (more than 0.3) occurring at discreet locations and varying depths along the profile (fig. 5.3). Poisson's ratios along the LA17-4-LCG seismic profile range between approximately 0.05 and 0.375, with highest Poisson's ratios (more than 0.35) occurring below approximately 5 m depth between distance meters 25 and 120 and extending to the surface between distance meters 0 and 10 (fig. 5.4). Poisson's ratios along the LA17-5-RUS seismic profile range between 0.05 and 0.45, with highest ratios (more than 0.45) occurring in a near-horizontal zone at approximately 15 m depth, which suggest the presence of saturated materials or clay (fig. 5.5). Poisson's ratios along the LA17-6-STC seismic profile range between approximately 0.05 and 0.22. The highest ratios (more than 0.2) occur below approximately 20 m depth between distance meters 70 and 100 (fig. 5.6).

Summary

The USGS evaluated V_S at six strong-motion recording stations in Southern California Edison substations to better understand the potential for amplified ground shaking during an earthquake. Prior site-characterization studies in California show some sites exhibit considerable lateral variability in shear-wave velocities due to complex geologic structures at depth. We used refraction tomography and MASW methods to evaluate the 2-D V_S from body and surface waves data recorded along linear profiles generated by active-source seismic methods. We calculated V_{S30} at every meter along the linear profiles and compared results between the different methods of analysis.

V_S and V_{S30} Comparisons

Profile LA17-1—Olinda (SCSN OLI)

S-wave refraction tomography, MAS_RW, and MAS_LW models all show slightly higher V_S in the west side of the LA17-1-OLI profile, whereas the surface-wave models show a channel-like velocity structure centered near distance meter 130 near the east end of the profile. Orthoimagery (fig. 2) indicates a stream (culvert) may have been rerouted around the eastern portion of the substation. The average V_{S30} values for the profile (table 3), calculated from S-wave refraction tomography, MAS_RW, and MAS_LW (sledgehammer and 45°-angle AWD methods), are 334 meters per second (m/s), 291 m/s, 289 m/s, and 309 m/s, respectively. The various methods show only a 45 m/s difference in V_{S30} values. At the point on the seismic profile nearest to the strong-motion recording station, V_{S30} values, calculated from S-wave refraction tomography, MAS_RW, and MAS_LW (sledgehammer and 45°-angle AWD) methods, are 320 m/s, 371 m/s, 494 m/s, and 410 m/s, respectively. The various methods show up to a 174 m/s difference (table 3) in V_{S30} values for the location of the profile nearest to the strong-motion recording

station, with the greatest difference occurring between V_{S30} derived from the S-wave refraction tomography and MAS_LW methods. Calculated using surface wave methods, the average V_{S30} along the seismic profile nearest to the strong-motion recording station are up to 205 m/s higher than the average V_{S30} for the entire seismic profile, suggesting significant lateral V_S variability across the recording site.

Profile LA17-1b—Olinda (SCSN OLI)

Our MAS_RW-derived V_S model shows slightly higher V_S at the southern part of the LA17-1b-OLI profile between distance meters 0 and 45 (fig. 12). The average V_S calculated for the entire profile is 309 m/s, whereas V_S calculated at the point nearest to the recording station is 330 m/s. V_{S30} calculated at every meter along the profile in the north-south direction is smaller in range than those calculated for the west-to-east direction (table 3), which suggests variation in V_S is smaller in the north-to-south direction.

Profile LA17-2—Serrano (SCSN SRN)

S-wave refraction tomography, MAS_RW, and MAS_LW models all show undulating velocity contours, which suggest complex geologic structures at depth (figs. 14 and 15). The Peralta Hills Fault has been mapped as crossing the substation and our seismic profile at approximately distance meters 160–165; our V_P/V_S and Poisson's ratios are highest at the same general location, which corroborates the mapped trace of the fault (figs. 4.2 and 5.2). The average V_{S30} for the profile (table 3), calculated from S-wave refraction tomography, MAS_RW, and MAS_LW (sledgehammer and 45°-angle AWD) methods, are 542 m/s, 383 m/s, 444 m/s, and 462 m/s, respectively (a range of 159 m/s). $V_{S30,}$ calculated from S-wave refraction tomography, MAS_RW, and MAS_LW (sledgehammer and 45°-angle AWD) methods at the point on the seismic profile nearest to the strong-motion recording station, are 537 m/s, 379 m/s, 432 m/s, and 443 m/s, respectively (a range of 158 m/s). The difference between the average V_{S30} values calculated for the entire seismic profile and V_{S30} calculated at the point nearest to the strong-motion recording station is minor (difference up to 19 m/s). Overall, the difference between minimum and maximum V_{S30} values along the seismic profile ranges between 51 and 118 m/s, with V_{S30} calculated from the S-wave refraction tomography method having the largest range and higher values than those calculated using surface wave methods. We attribute the differences observed among the different models to the surface wave methods' difficulty in resolving complex bedrock structures at shallow depths.

Profile LA17-3—Murrieta (SCSN MUR)

S-wave refraction tomography and MAS_RW models both show higher V_S in the northeast end of the LA17-3-MUR profile, between distance meters 40 and 100 (S-wave refraction tomography) and between distance meters 85 and 110 (MAS_RW). Surface-wave models show more significant undulating velocity contours, which may suggest complex geologic structures in the subsurface; however, there is significant topographic variation along the profile, which causes difficulty for the 1-D surface-wave methods. The average V_{S30} values for the profile, calculated from S-wave refraction tomography, MAS_RW, and MAS_LW (sledgehammer and 45°-angle AWD) methods, are 685 m/s, 592 m/s, 463 m/s, and 491 m/s, respectively. V_{S30} values (table 3), calculated from S-wave refraction tomography, MAS_RW, and MAS_LW (sledgehammer and 45°-angle AWD) methods at the point on the seismic profile nearest to the strong-motion recording station, are 497 m/s, 613 m/s, 318 m/s, and 318 m/s, respectively. The average V_{S30} calculated for the seismic profile varies by as much as 188 m/s from V_{S30} calculated nearest to the strong-motion recording station, which suggests lateral V_S variability due to complex geological structures and a change in surface topography. Overall, the difference between minimum and maximum V_{S30} values across the seismic profiles among different methods range between 94 and 272 m/s, with V_{S30} values calculated from the S-wave refraction tomography method having the largest range. This quality of the S-wave refraction tomography method is generally consistent across the different sites in this study.

Profile LA17-4—La Cienega (SCSN LCG)

S-wave refraction tomography and MAS_RW-based models for the LA17-4-LCG profile indicate relatively higher V_S at depths below approximately 15 meters (m) at distance meters between 0 and 45 (S-wave refraction tomography) and at distance meters between 8 and 25 (MAS_RW). However, our MAS_LW-based model shows a channel-like structure, whereas both S-wave refraction tomography and MAS_RW models show higher V_S at depth. Undulating velocity contours seen in all three models may suggest complex geological structures at depth (figs. 20 and 21). The Newport-Inglewood-Rose Canyon Fault Zone has been mapped (fig. 5) less than 200 m northeast of our seismic profile, further suggesting structural complexity at this location. The average V_{S30} values for the profile (table 3), calculated from S-wave refraction tomography, MAS_RW, and MAS_LW methods, are 660 m/s, 374 m/s, and 555 m/s, respectively. $V_{S30,}$ calculated from S-wave refraction tomography, MAS_RW, and MAS_LW methods at the point on the seismic profile nearest to the strong-motion recording station are 595 m/s, 425 m/s, and 645 m/s, respectively. The average V_{S30} calculated for the seismic profile varies by as much as 90 m/s from V_{S30} calculated nearest to the strong-motion recording station, which suggests lateral V_S variability due to complex geological structures at depth. Overall, the difference between minimum and maximum V_{S30} along the seismic profile ranges between 69 and 256 m/s, with V_{S30} calculated from the S-wave refraction tomography method having the largest range. In general, V_s determined from the S-wave refraction tomography method is higher than V_S determined from surface-wave methods at this location.

Profile LA17-5—Rush (SCSN RUS)

Our S-wave refraction tomography model shows higher V_S in the western part of the seismic profile between distance meters 0 and approximately 50, whereas our surface-wave models show higher V_S in both the west and east ends of the profile (figs. 23 and 24). The surface-wave models show V_S is generally less than 350 m/s in the upper approximately 20 m of the subsurface between distance meters 25 and 90 ($MAS_R W$) and between distance meters 10 and 100 ($MAS_L W$), with high V_S gradients from approximately 20 m depth to the bottom of the models at 40 m. The average V_{S30} values for the profile (table 3), calculated from S-wave refraction tomography, $MAS_R W$, and $MAS_L W$ methods, are 448 m/s, 310 m/s, and 308 m/s, respectively. V_{S30} measurements, calculated from the S-wave refraction tomography, $MAS_R W$, and $MAS_L W$ methods at the point on the seismic profile nearest to the strong-motion recording station, are 468 m/s, 305 m/s, and 351 m/s, respectively. The average V_{S30} calculated from the seismic profile varies as much as 43 m/s from V_{S30} calculated nearest to the strong-motion recording station. Overall, the difference between minimum and maximum V_{S30} along the seismic profile ranges between 20 and 97 m/s, with V_{S30} calculated from S-wave refraction tomography having the largest range.

Profile LA17-6—Santa Clara (SCSN STC)

Our S-wave refraction tomography, $MAS_R W$, and $MAS_L W$ models all show higher V_S in the southeastern part of the seismic profile; however, our surface-wave models show channel-like velocity structures between distance meters 40 and 100 (figs. 26 and 27). The average V_{S30} values for the profile (table 3), calculated from S-wave refraction tomography, $MAS_R W$, and $MAS_L W$ methods, are 443 m/s, 294 m/s, and 320 m/s, respectively. V_{S30}, calculated from S-wave refraction tomography, $MAS_R W$, and $MAS_L W$ methods at the point on the seismic profile nearest to the strong-motion recording station, are 377 m/s, 311 m/s, and 330 m/s, respectively. Overall, the difference between minimum and maximum V_{S30} along the seismic profile ranges between 29 and 132 m/s, with V_{S30} calculated from S-wave refraction tomography having the largest and highest ranges relative to those calculated from surface-wave methods.

Method Comparison

We find varying magnitudes of differences in V_{S30} among all methods (refraction tomography, Rayleigh-wave $MAS_R W$, and Love-wave $MAS_L W$) when the site contains surface topography, shallow bedrock, and (or) complex geologic structures at depth. Our prior studies (Chan and others, 2018a; 2018b) indicate 2-D S-wave refraction tomography is better at resolving complex sites, while both body- and surface wave methods perform similarly at sites without topography and (or) bedrock. Furthermore, we expect varying V_S in our surface wave models due to non-uniqueness of inversion results and the challenges of wave propagation in weathered bedrock (Garofalo and others, 2016a; 2016b; Ladak and others, 2021).

References Cited

Baltay, A.S., and Boatwright, J., 2015, Ground-motion observations of the 2014 south Napa earthquake: Seismological Research Letters, v. 86, no. 2A, p. 355–360, https://doi.org/10.1785/0220140232.

Building Seismic Safety Council, 2003, NEHRP recommended provisions for seismic regulations for new buildings and other structures, part I—Provisions: Washington, D.C., Federal Emergency Management Agency, FEMA 450.

Castagna, J.P., Batzle, M.L., and Eastwood, R.L., 1985, Relationships between compressional-wave and shear-wave velocities in clastic silicate rocks: Geophysics, v. 50, no. 4, p. 571–581, https://doi.org/10.1190/1.1441933.

Catchings, R.D., Addo, K.O., Goldman, M.R., Chan, J.H., Sickler, R.R., and Criley, C.J., 2019, Two-dimensional seismic velocities and structural variations at three British Columbia Hydro and Power Authority (BC Hydro) dam sites, Vancouver Island, British Columbia, Canada: U.S. Geological Survey Open-File Report 2019–1015, 137 p., https://doi.org/10.3133/ofr20191015.

Catchings, R.D., Borchers, J.W., Goldman, M.R., Gandhok, G., Ponce, D.A., and Steedman, C.E., 2006, Subsurface structure of the East Bay plain ground-water basin—San Francisco Bay to the Hayward Fault, Alameda County, California: U.S. Geological Survey Open-File Report 2006–1084, 61 p., https://doi.org/10.3133/ofr20061084.

Catchings, R.D., Gandhok, G., Goldman, M.R., Okaya, D., 2001, Seismic images and fault relations of the Santa Monica Thrust Fault, West Los Angeles, California: U.S. Geological Survey Open-File Report 01–111, 34 p., https://doi.org/10.3133/ofr01111.

Catchings, R.D., Goldman, M.R., Trench, D., Buga, M., Chan, J.H., Criley, C.J., and Strayer, L.M., 2017, Shallow-depth location and geometry of the Piedmont Reverse splay of the Hayward Fault, Oakland, California: U.S. Geological Survey Open-File Report 2016–1123, 22 p., https://doi.org/10.3133/ofr20161123.

Catchings, R.D., Rymer, M.J., Goldman, M.R., Prentice, C.S., and Sickler, R.R., 2013, Fine-scale delineation of the location of and relative ground shaking within the San Andreas Fault zone at San Andreas Lake, San Mateo County, California: U.S. Geological Survey Open-File Report 2013–1041, 53 p., https://doi.org/10.3133/ofr20131041.

Catchings, R.R., Rymer, M.J., Goldman, M.R., Sickler, R.R., and Criley, C.J., 2014, A method and example of seismically imaging near-surface fault zones in geologically complex areas using V_P, V_S, and their ratios: Bulletin of the Seismological Society of America, v. 104, no. 4, p. 1989–2006, https://doi.org/10.1785/0120130294.

Chan, J.H., Catchings, R.D., Goldman, M.R., and Criley, C.J., 2018a, V_{S30} at three strong-motion recording stations in Napa and Napa County, California—Main Street in downtown Napa, Napa fire station number 3, and Kreuzer Lane—Calculations determined from S-wave refraction tomography and multichannel analysis of surface waves (Rayleigh and Love): U.S. Geological Survey Open-File Report 2018–1161, 47 p., https://doi.org/10.3133/ofr20181161.

Chan, J.H., Catchings, R.D., Goldman, M.R., and Criley, C.J., 2018b, V_{S30} at three strong-motion recording stations in Napa and Solano Counties, California—Lovall Valley Road, Broadway Street and Sereno Drive in Vallejo, and Vallejo Fire Station—Calculations determined from S-wave refraction tomography and multichannel analysis of surface waves (Rayleigh and Love): U.S. Geological Survey Open-File Report 2018–1162, 62 p., https://doi.org/10.3133/ofr20181162.

Chan, J.H., Catchings, R.D., Goldman, M.R, Criley, C.J., and Sickler, R.R., 2021, High-resolution seismic data acquired at six Southern California seismic network (SCSN) recording stations in 2017: U.S. Geological Survey data release, https://doi.org/10.5066/P990O55F.

Garofalo, F., Foti, S., Hollender, F., Bard, P.Y., Cornou, C., Cox, B.R., Ohrnberger, M., Sicilia, D., Asten, M., Di Giulio, G., Forbriger, T., Guillier, B., Hayashi, K., Martin, A., Matsushima, S., Mercerat, D., Poggi, V., and Yamanaka, H., 2016a, InterPACIFIC project—Comparison of invasive and non-invasive methods for seismic site characterization—Part I—Intra-comparison of surface-wave methods: Soil Dynamics and Earthquake Engineering, v. 82, p. 222–240, https://doi.org/10.1016/j.soildyn.2015.12.010.

Garofalo, F., Foti, S., Hollender, F., Bard, P.Y., Cornou, C., Cox, B.R., Dechamp, A., Ohrnberger, M., Perron, V., Sicilia, D., Teague, D., and Vergniault, C., 2016b, InterPACIFIC project—Comparison of invasive and non-invasive methods for seismic site characterization—Part II—Inter-comparison between surface-wave and borehole methods: Soil Dynamics and Earthquake Engineering, v. 82, p. 241–254, https://doi.org/10.1016/j.soildyn.2015.12.009.

Hayashi, K., and Hikima, K., 2003, CMP analysis of multi-channel surface wave data and its application to near-surface s-wave velocity delineation, *in* Symposium on the Application of Geophysics to Engineering and Environmental Problems (SAGEEP), 15th, San Antonio, Tex., April 2003: Denver, Colo., SAGEEP, p. 1348–1355.

Hayashi, K., and Suzuki, H., 2004, CMP cross-correlation analysis of multi-channel surface-wave data: Exploration Geophysics, v. 35, no. 1, p. 7–13, https://doi.org/10.1071/EG04007.

Hole, J.A., 1992, Nonlinear high-resolution three-dimensional seismic travel time tomography: Journal of Geophysical Research, v. 97, no. B5, p. 6553–6562, https://doi.org/10.1029/92JB00235.

Holtzer, T.L., Padovani, A.C., Bennett, M.J., Noce, T.E., Tinsley, J.C., 2005, Mapping NEHRP V_{S30} site classes: Earthquake Spectra, v. 21, no. 2, p. 1–18, https://doi.org/10.1193/1.1895726.

Ivanov, J., Leitner, B., Shefchik, W., Shwenk, J.T., and Peterie, S.L., 2013, Evaluating hazards at salt cavern sites using multichannel analysis of surface waves: Leading Edge, v. 32, no. 3, p. 298–305, https://doi.org/10.1190/tle32030298.1.

Ivanov, J., Miller, R.D., Park, C.P., and Ryden, N., 2003, Seismic search for underground anomalies: Society of Exploration Geophysicists, SEG Technical Program Expanded Abstract 2003, p. 1223–1226.

Ivanov, J., Miller, R.D. and Tsoflias, G., 2008, Some practical aspects of MASW analysis and processing: Symposium on the Application of Geophysics to Engineering and Environmental Problems, v. 21, p. 1186–1198.

Ladak, S., Molnar, S., and Palmer, S., 2021, Multi-method site characterization to verify the hard rock (site class A) assumption at 25 seismograph stations across Eastern Canada: Earthquake Spectra, v. 37, no. 1, p. 1487–1515.

Miller, R.D., Xia, J., Park, C.B., and Ivanov, J., 1999, Using MASW to map bedrock in Olathe, Kansas: Kansas Geological Survey Open-File Report No. 99–9, 9 p.

Park, C., 2013, MASW for geotechnical site investigation: Leading Edge, v. 32, no. 6, p. 656–662, https://doi.org/10.1190/tle32060656.1.

Park, C., Miller, R., and Xia, J., 1999, Multichannel analysis of surface waves: Geophysics, v. 64, no. 3, p. 800–808, https://doi.org/10.1190/1.1444590.

Park, C., Miller, R., Xia, J., and Ivanov, J., 2007, Multichannel analysis of surface waves (MASW)—Active and passive methods: Leading Edge, v. 26, no. 1, p. 60–64, https://doi.org/10.1190/1.2431832.

Pujol, J., 2003, Elastic wave propagation and generation in seismology: Cambridge University Press, United Kingdom, https://doi.org/10.1017/CBO9780511610127.

Tatham, R.H., 1982, V_p/V_s and lithology: Geophysics, v. 47, p. 336–344, https://doi.org/10.1190/1.1441339.

Thomsen, L., 1990, Poisson was not a geophysicist!: Leading Edge, v. 9, no. 12, p. 27–29, https://doi.org/10.1190/1.1439706.

U.S. Geological Survey National Geospatial Program, 2009, The National Map-Orthimagery: U.S. Geological Survey, accessed March 1, 2022, at https://apps.nationalmap.gov/viewer/.

U.S. Geological Survey Earthquake Hazards Program, 2020, Quaternary fault and fold database for the United States: U.S. Geological Survey, accessed March 1, 2021, at https://www.usgs.gov/natural-hazards/.

Xia, J., Miller, R.D., and Park, C.B., 1999, Estimation of near-surface shear-wave velocity by inversion of Rayleigh waves: Geophysics, v. 64, no. 3, p. 691–700, https://doi.org/10.1190/1.1444578.

Xia, J., Miller, R., Park, C., and Ivanov, J., 2000, Construction of 2-D vertical shear wave velocity field by the multichannel analysis of surface wave technique, *in* Symposium on the application of geophysics to engineering and environmental problems 2000: Environment and Engineering Geophysical Society, Symposium on the Application of Geophysics to Engineering and Environmental Problems, p. 1197–1206, https://doi.org/10.4133/1.2922726.

Yong, A., Martin, A., Stokoe, K., and Diehl, J., 2013, ARRA-funded V_{S30} measurements using multi-technique approach at strong-motion stations in California and Central-Eastern United States: U.S. Geological Survey Open-File Report 2013–1102, 60 p., https://doi.org/10.3133/ofr20131102.

Zeng, C., Xia, J., Miller, R.D., Tsoflias, G.P., and Wang, Z., 2012, Numerical investigation of MASW applications in the presence of surface topography: Journal of Applied Geophysics, v. 84, p. 52–60, https://doi.org/10.1016/j.jappgeo.2012.06.004.

Appendix 1. Rayleigh- and Love-Wave Dispersion Curves Nearest to Strong-Motion Recording Station

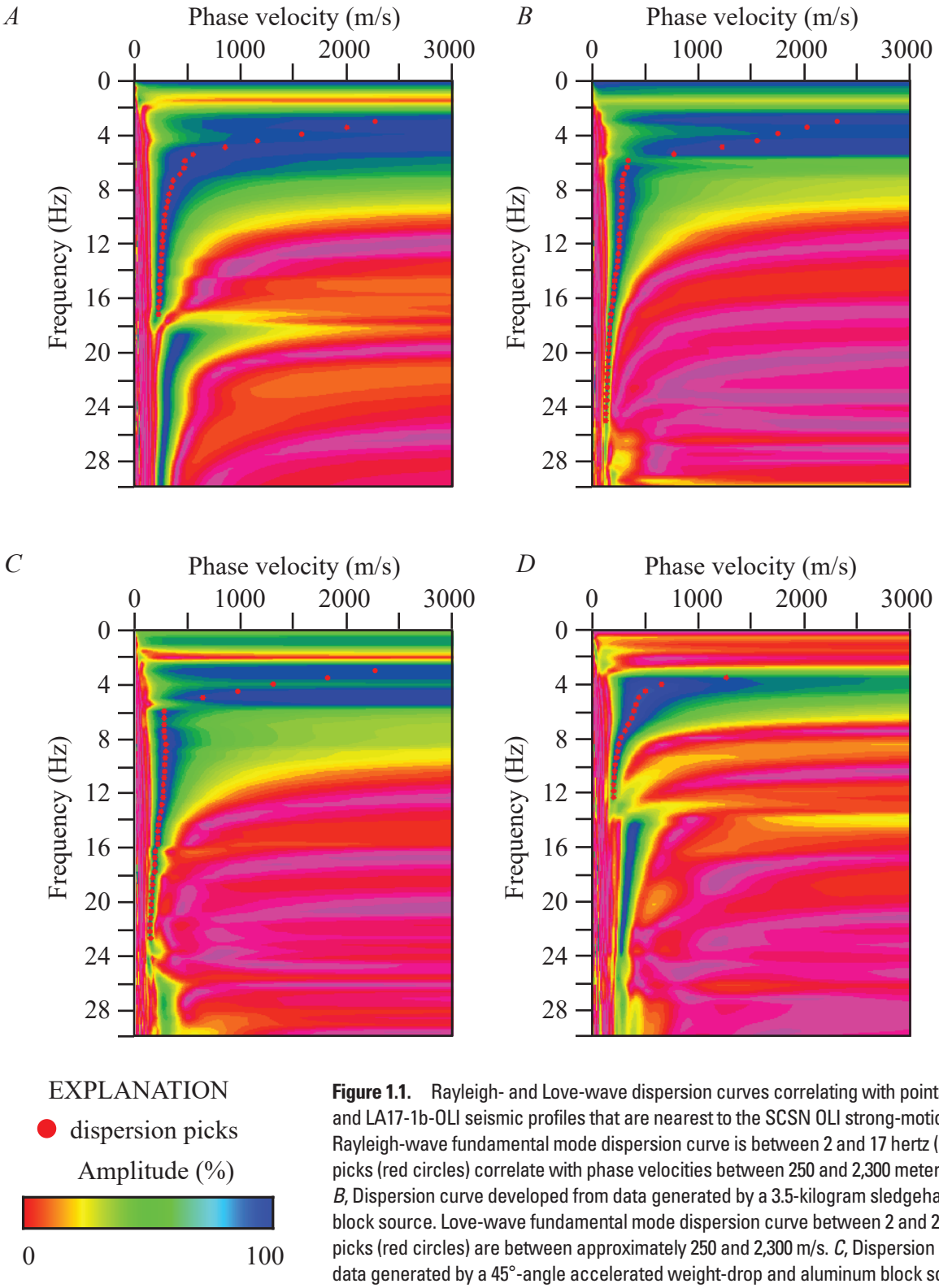

Figure 1.1. Rayleigh- and Love-wave dispersion curves correlating with points on our LA17-1-OLI and LA17-1b-OLI seismic profiles that are nearest to the SCSN OLI strong-motion station. *A*, The Rayleigh-wave fundamental mode dispersion curve is between 2 and 17 hertz (Hz). Dispersion curve picks (red circles) correlate with phase velocities between 250 and 2,300 meters per second (m/s). *B*, Dispersion curve developed from data generated by a 3.5-kilogram sledgehammer and aluminum block source. Love-wave fundamental mode dispersion curve between 2 and 26 Hz. Dispersion curve picks (red circles) are between approximately 250 and 2,300 m/s. *C*, Dispersion curve developed from data generated by a 45°-angle accelerated weight-drop and aluminum block source. Love-wave fundamental mode dispersion curve between 2 and 24 Hz. Dispersion curve picks (red circles) correlate with phase velocities between 250 and 2,300 m/s. *D*, A Rayleigh-wave fundamental mode dispersion curve for the LA17-1b-OLI seismic profile is distinct from higher modes between 3 and 12 Hz. Dispersion curve picks (red circles) correlate with phase velocities between approximately 250 and 1,400 m/s.

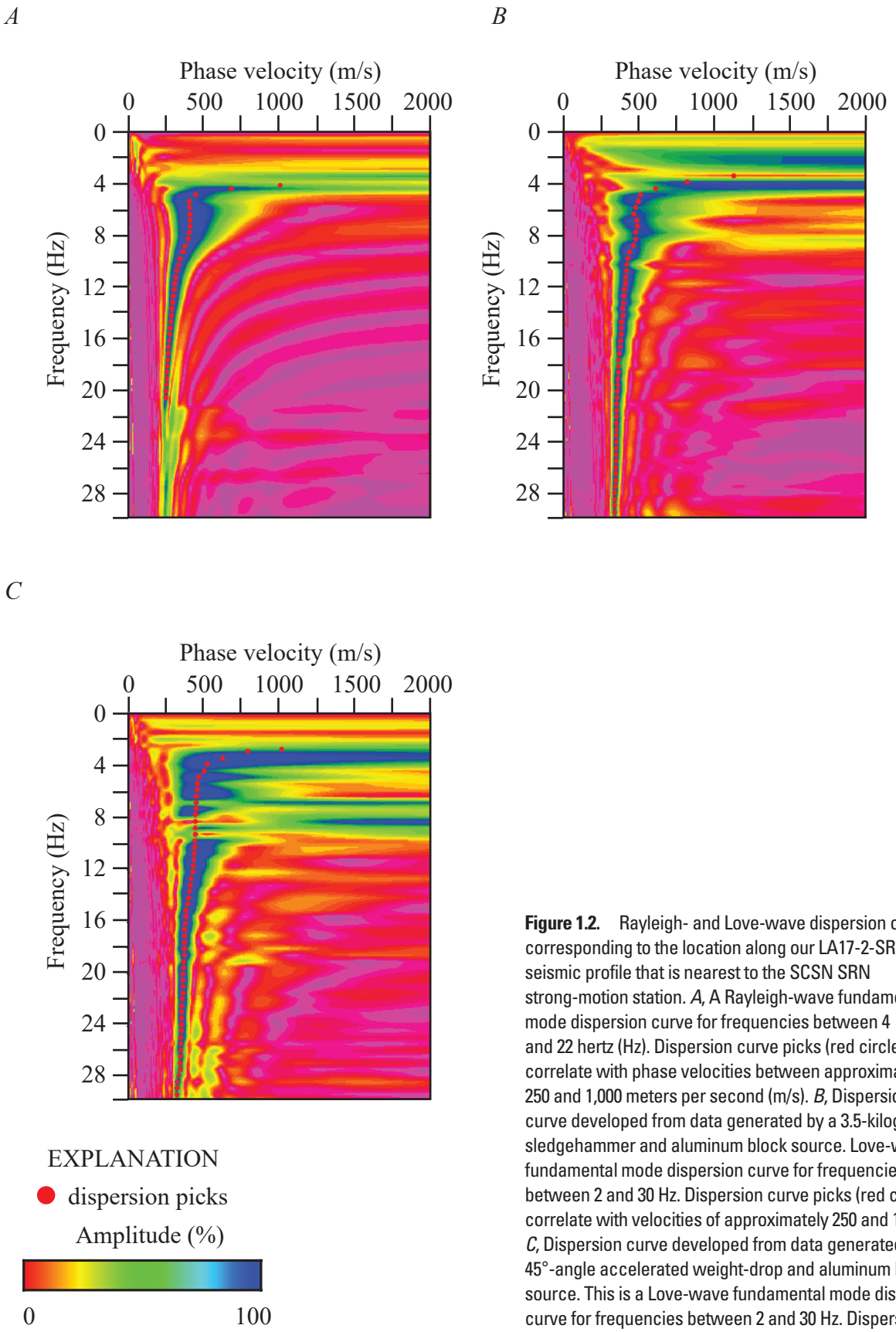

Figure 1.2. Rayleigh- and Love-wave dispersion curves corresponding to the location along our LA17-2-SRN seismic profile that is nearest to the SCSN SRN strong-motion station. *A*, A Rayleigh-wave fundamental mode dispersion curve for frequencies between 4 and 22 hertz (Hz). Dispersion curve picks (red circles) correlate with phase velocities between approximately 250 and 1,000 meters per second (m/s). *B*, Dispersion curve developed from data generated by a 3.5-kilogram sledgehammer and aluminum block source. Love-wave fundamental mode dispersion curve for frequencies between 2 and 30 Hz. Dispersion curve picks (red circles) correlate with velocities of approximately 250 and 1,200 m/s. *C*, Dispersion curve developed from data generated by a 45°-angle accelerated weight-drop and aluminum block source. This is a Love-wave fundamental mode dispersion curve for frequencies between 2 and 30 Hz. Dispersion curve picks (red circles) correlate with phase velocities between approximately 250 and 1,100 m/s.

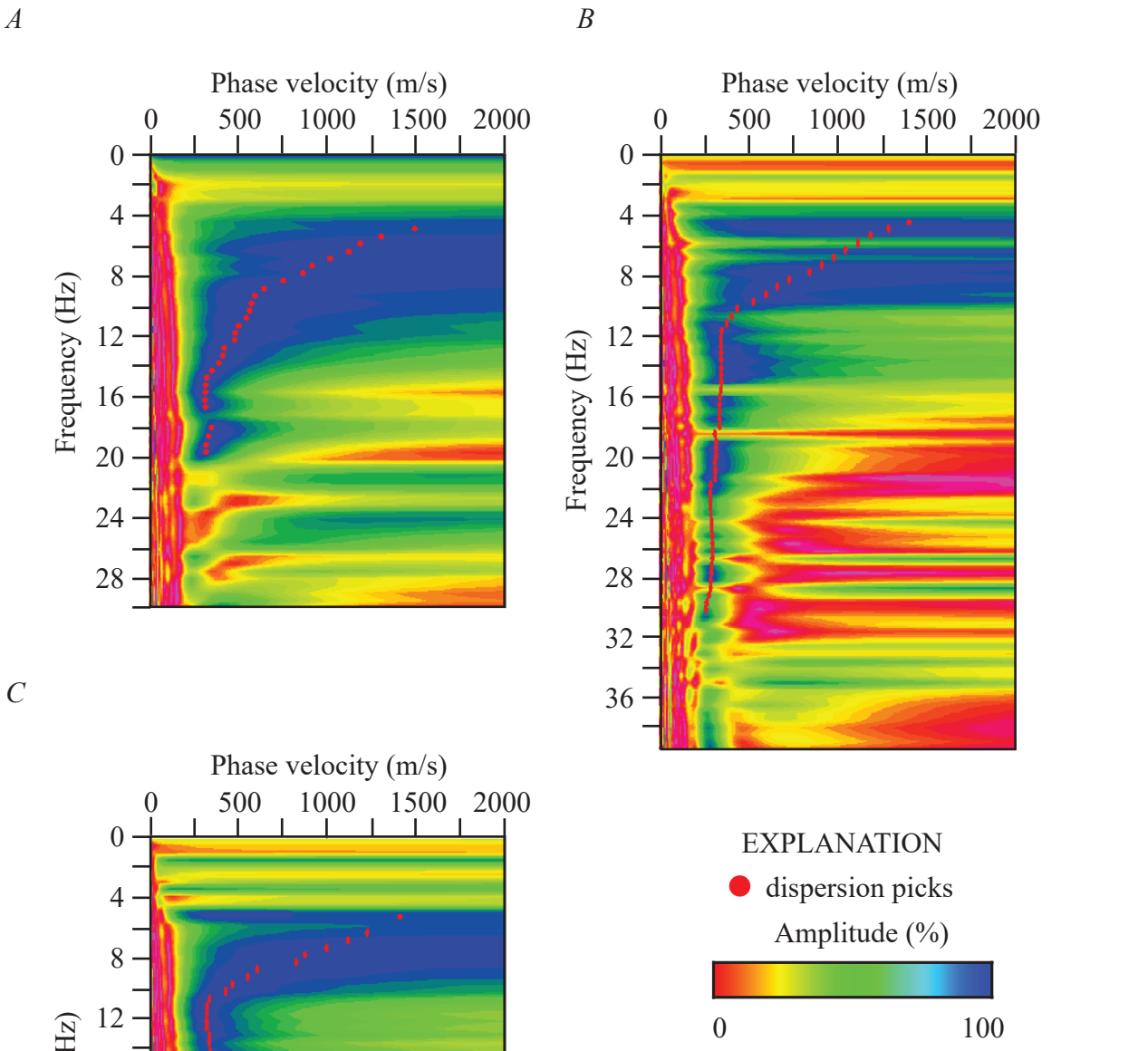

Figure 1.3. Rayleigh- and Love-wave dispersion curves corresponding to the location on our LA17-3-MUR seismic profile that is nearest to the SCSN MUR strong-motion station. *A*, Rayleigh-wave fundamental mode dispersion curve for frequencies between 4 and 20 hertz (Hz). Dispersion curve picks (red circles) correlate with phase velocities between 250 and 1,500 meters per second (m/s). *B*, Dispersion curve developed from data generated by a 3.5-kilogram sledgehammer and aluminum block source. Love-wave fundamental mode dispersion curve for frequencies between 4 and 32 Hz. Dispersion curve picks (red circles) correlate with phase velocities between 250 and 1,500 m/s. *C*, Dispersion curve developed from data generated by a 45°-angle accelerated weight-drop and aluminum block source. Love-wave fundamental mode dispersion curve for frequencies between 4 and 32 Hz. Dispersion curve picks (red circles) correlating with phase velocities between 250 and 1,500 m/s.

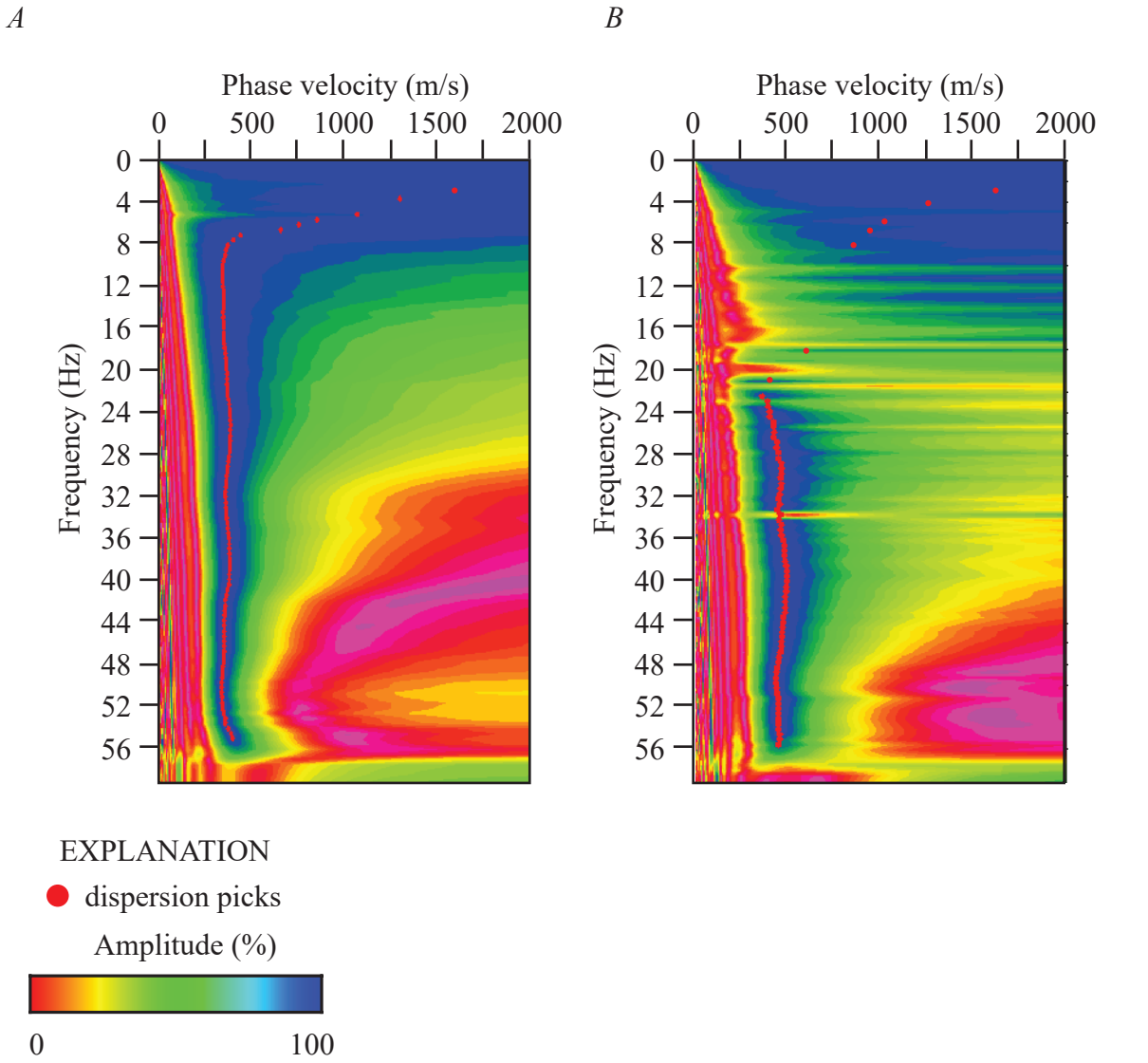

Figure 1.4. Rayleigh- and Love-wave dispersion curves corresponding to the location on our LA17-4-LCG seismic profile that is nearest to the SCSN LCG strong-motion station. *A*, Rayleigh-wave fundamental mode dispersion curve for frequencies between 2 and 56 hertz (Hz). Dispersion curve picks (red circles) correlating with phase velocities between 250 and 1,600 meters per second (m/s). *B*, Dispersion curve developed from data generated by a 3.5-kilogram sledgehammer and aluminum block source. The Love-wave fundamental mode dispersion curve for frequencies between 2 and 56 Hz. Dispersion curve picks (red circles) correlating with phase velocities between 250 and 1,600 m/s.

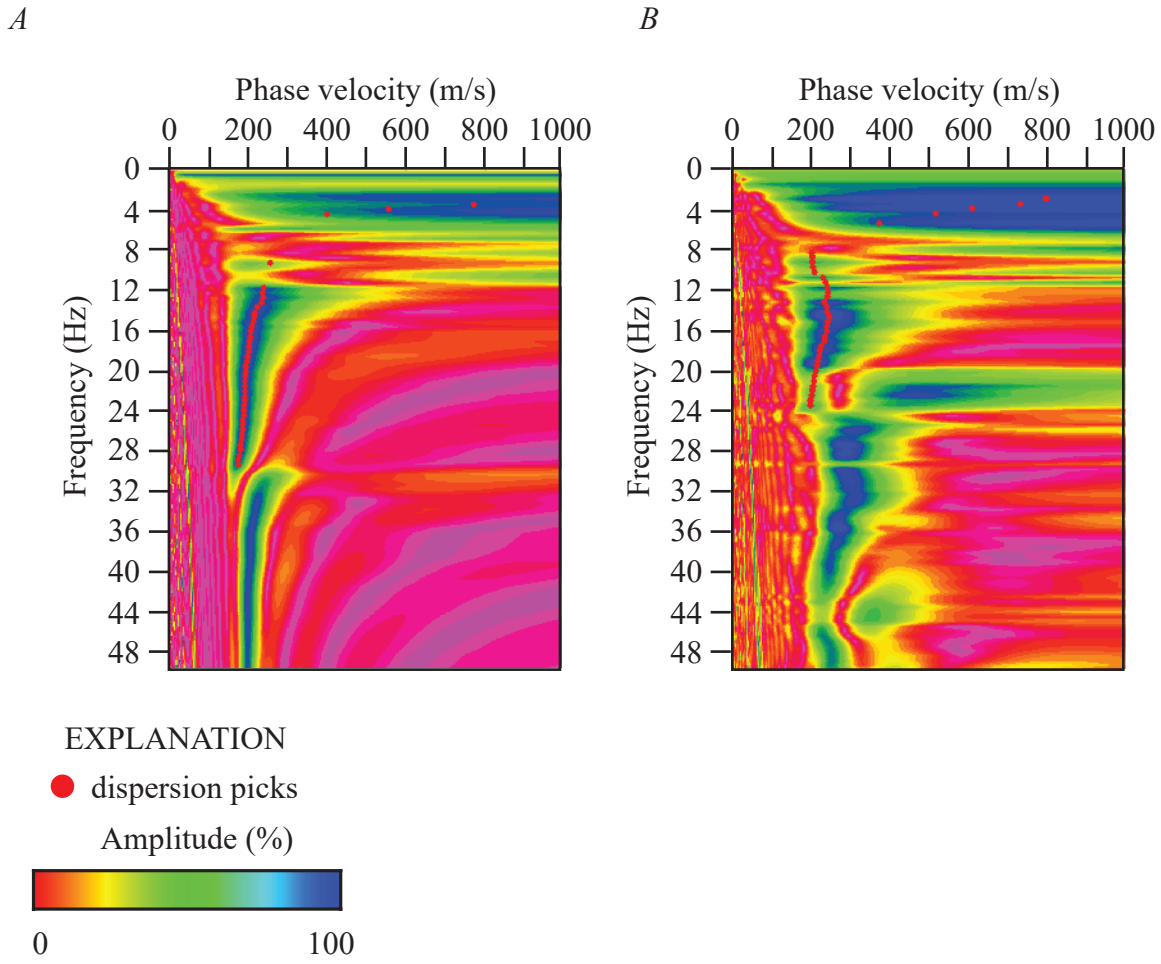

Figure 1.5. Rayleigh- and Love-wave dispersion curves corresponding to the location along our profile LA17-5-RUS seismic profile that is nearest to the SCSN RUS strong-motion station. *A*, Rayleigh-wave fundamental mode dispersion curve for frequencies between 2 and 32 hertz (Hz). Dispersion curve picks (red circles) correlating with phase velocities between 200 and 800 meters per second (m/s). *B*, Dispersion curve picks developed from data generated by a 3.5-kilogram sledgehammer and aluminum block source. Love-wave fundamental mode dispersion curve for frequencies between 2 and 24 Hz. Dispersion curve picks (red circles) correlate with phase velocities between 150 and 800 m/s.

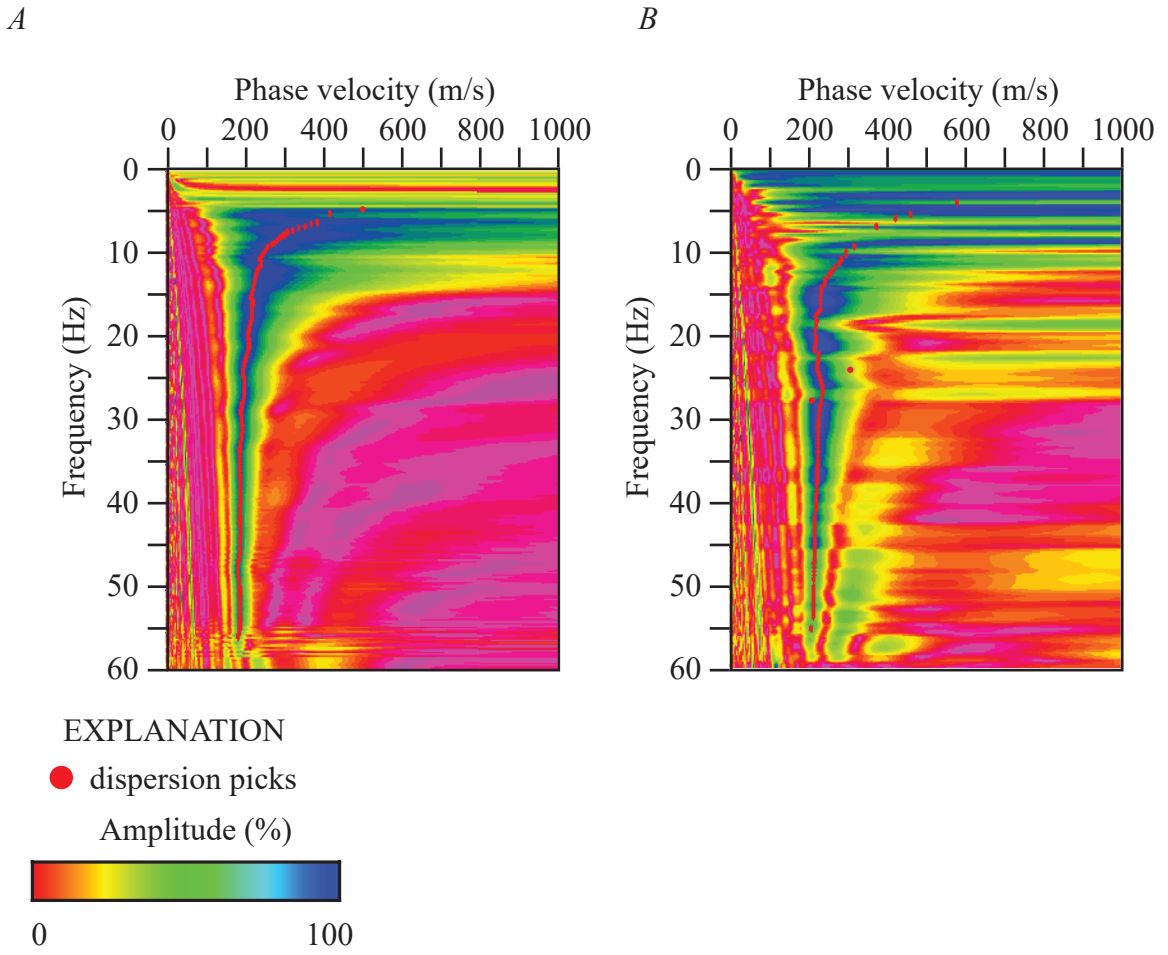

Figure 1.6. Rayleigh- and Love-wave dispersion curves corresponding to the location on our LA17-6-STC seismic profile that is nearest to the SCSN STC strong-motion station. *A*, Rayleigh-wave fundamental mode dispersion curve for frequencies between 4 and 60 hertz (Hz). Dispersion curve picks (red circles) correlate with phase velocities between 200 and 500 meters per second (m/s). *B*, Dispersion curve developed from data generated by a 3.5-kilogram sledgehammer and aluminum block source. Love-wave fundamental mode dispersion curve for frequencies between 3 and 55 Hz. Dispersion curve picks (red circles) correlate with phase velocities between 200 and 600 m/s.

Appendix 2. Rayleigh- and Love-Wave Fundamental mode Dispersion Curve Picks

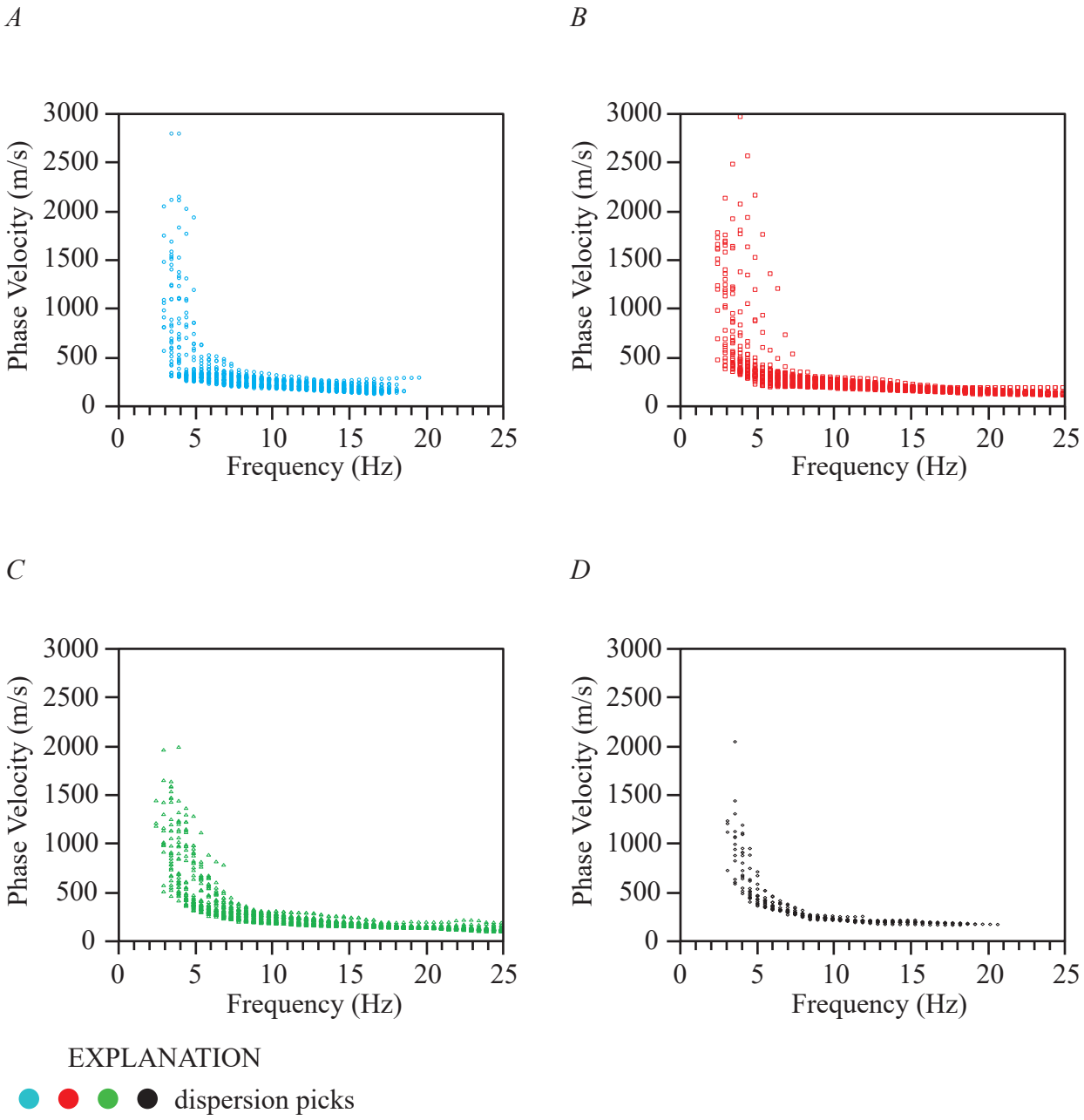

Figure 2.1. Rayleigh- and Love-wave fundamental mode dispersion curve picks for our LA17-1-OLI and LA17-1b-OLI seismic profiles. *A*, Rayleigh-wave fundamental mode dispersion curve picks correlate with frequencies between 3 and 20 hertz (Hz) and with phase velocities between 200 and 2,500 meters per second (m/s). *B*, Dispersion curves developed from data generated by a 3.5-kilogram sledgehammer and aluminum block source. Love-wave fundamental mode dispersion curve picks for frequencies between 2 and 25 Hz and phase velocities between 200 and 2,500 m/s. *C*, Dispersion curves developed from data generated by a 45°-angle accelerated weight-drop and aluminum block source. Love-wave fundamental mode dispersion curve picks for frequencies between 2 and 25 Hz and phase velocities between 200 and 2,000 m/s. *D*, Rayleigh-wave fundamental mode dispersion curve picks from data along the LA17-1b-OLI profile for frequencies 3 and 21 Hz and phase velocities between 200 and 1,500 m/s.

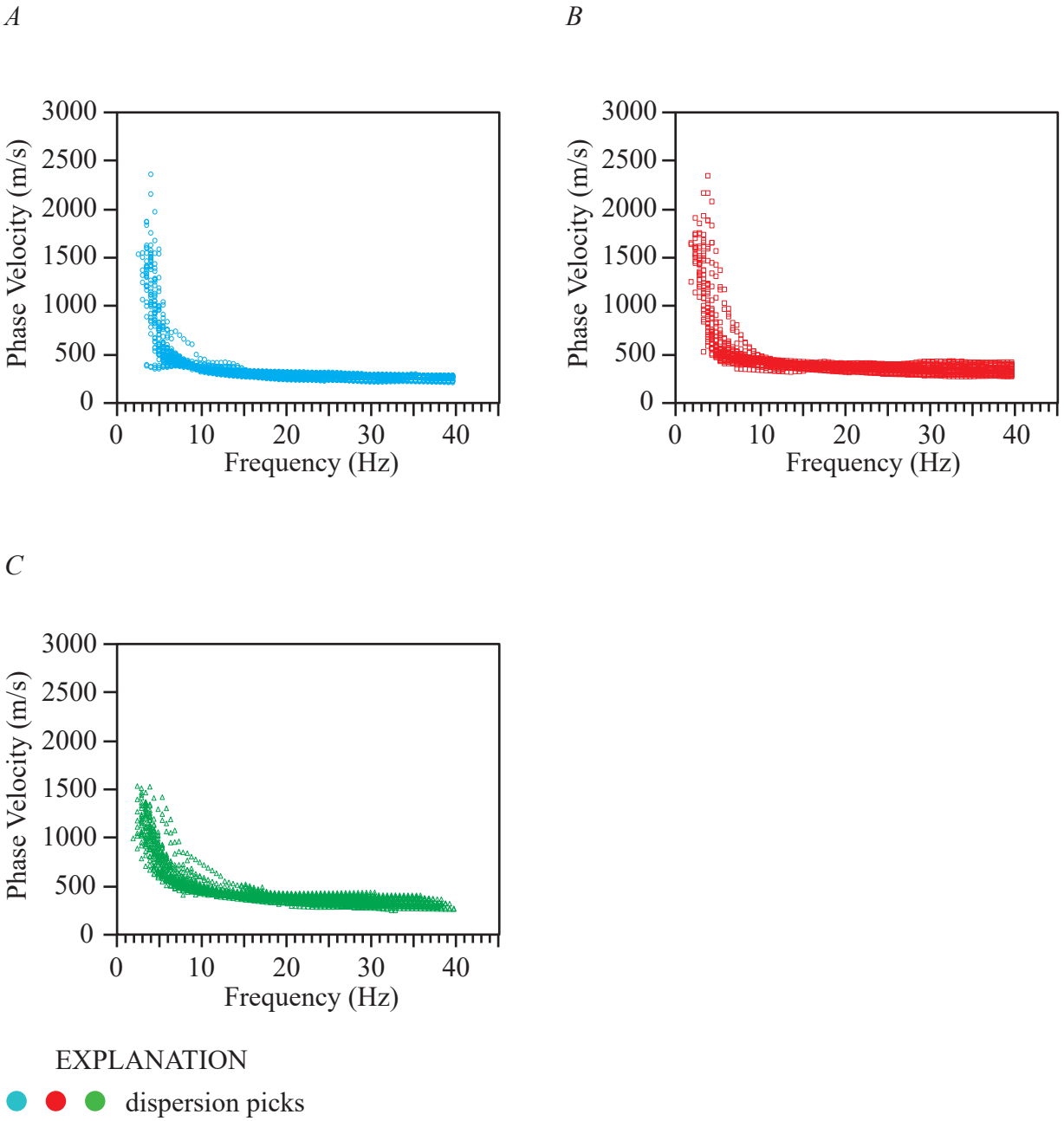

Figure 2.2. Rayleigh- and Love-wave fundamental mode dispersion curve picks for our LA17-2-SRN seismic profile. *A*, Rayleigh-wave fundamental mode dispersion curve picks correlate with frequencies between 2 and 40 hertz (Hz) and with phase velocities between 250 and 2,500 meters per second (m/s). *B*, Dispersion curves developed from data generated by a 3.5-kilogram sledgehammer and aluminum block source. Love-wave fundamental mode dispersion curve picks for frequencies between 1 and 40 Hz and phase velocities between 250 and 2,500 m/s. *C*, Dispersion curves developed from data generated by a 45°-angle accelerated weight-drop and aluminum block source. Love-wave fundamental mode dispersion curve picks for frequencies between 2 and 40 Hz and phase velocities between 250 and 1,600 m/s.

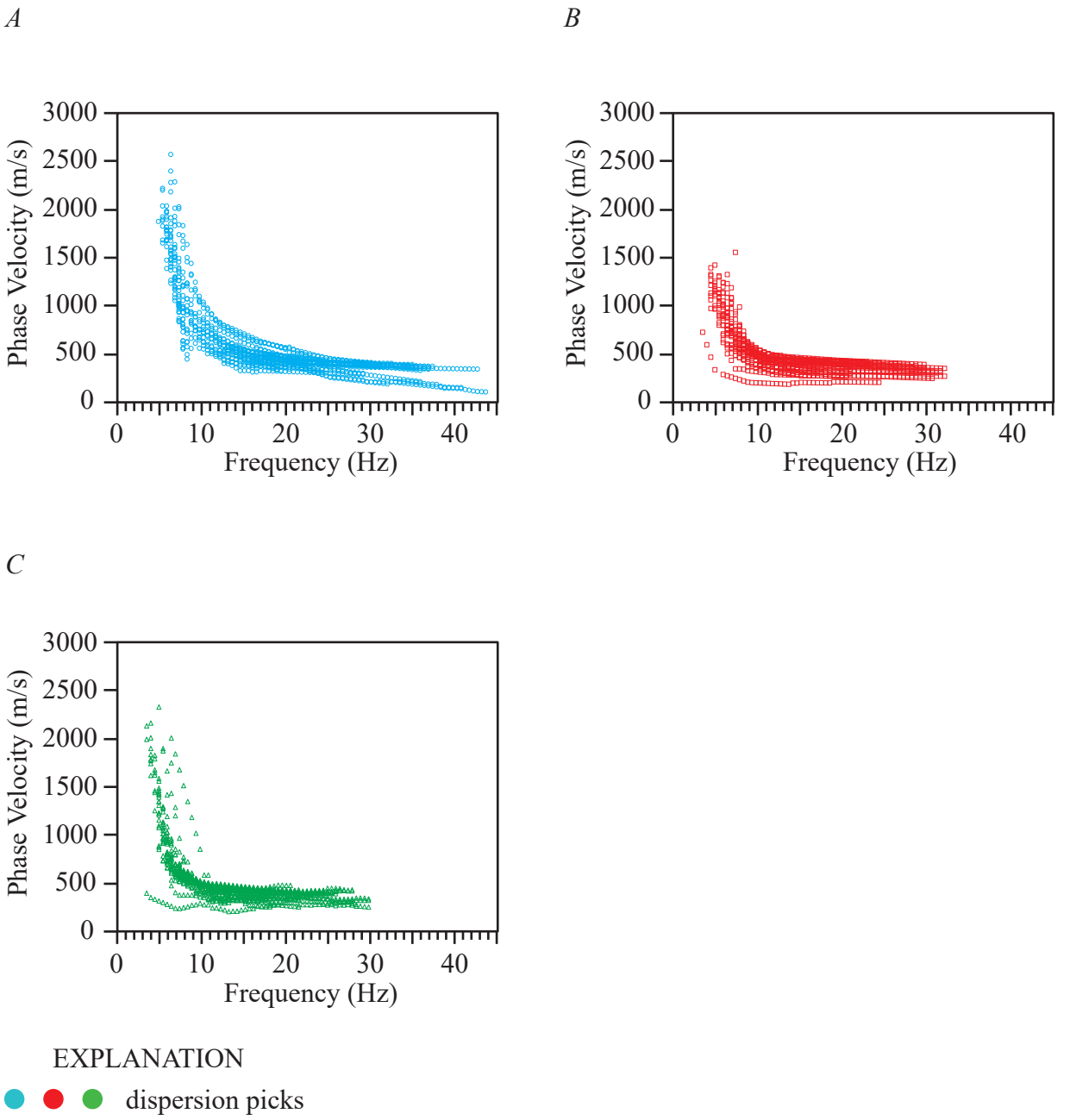

Figure 2.3. Rayleigh- and Love-wave fundamental mode dispersion curve picks for our LA17-3-MUR seismic profile. *A*, Rayleigh-wave fundamental mode dispersion curve picks correlate with frequencies between 4 and 45 hertz (Hz) and with phase velocities between 100 and 2,600 meters per second (m/s). *B*, Dispersion curves developed from data generated by a 3.5-kilogram sledgehammer and aluminum block source. Love-wave fundamental mode dispersion curve picks for frequencies between 3 and 33 Hz and phase velocities between 200 and 1,500 m/s. *C*, Dispersion curves developed from data generated by a 45°-angle accelerated weight-drop and aluminum block source. Love-wave fundamental mode dispersion curve picks for frequencies between 3 and 30 Hz and phase velocities between 200 and 2,500 m/s.

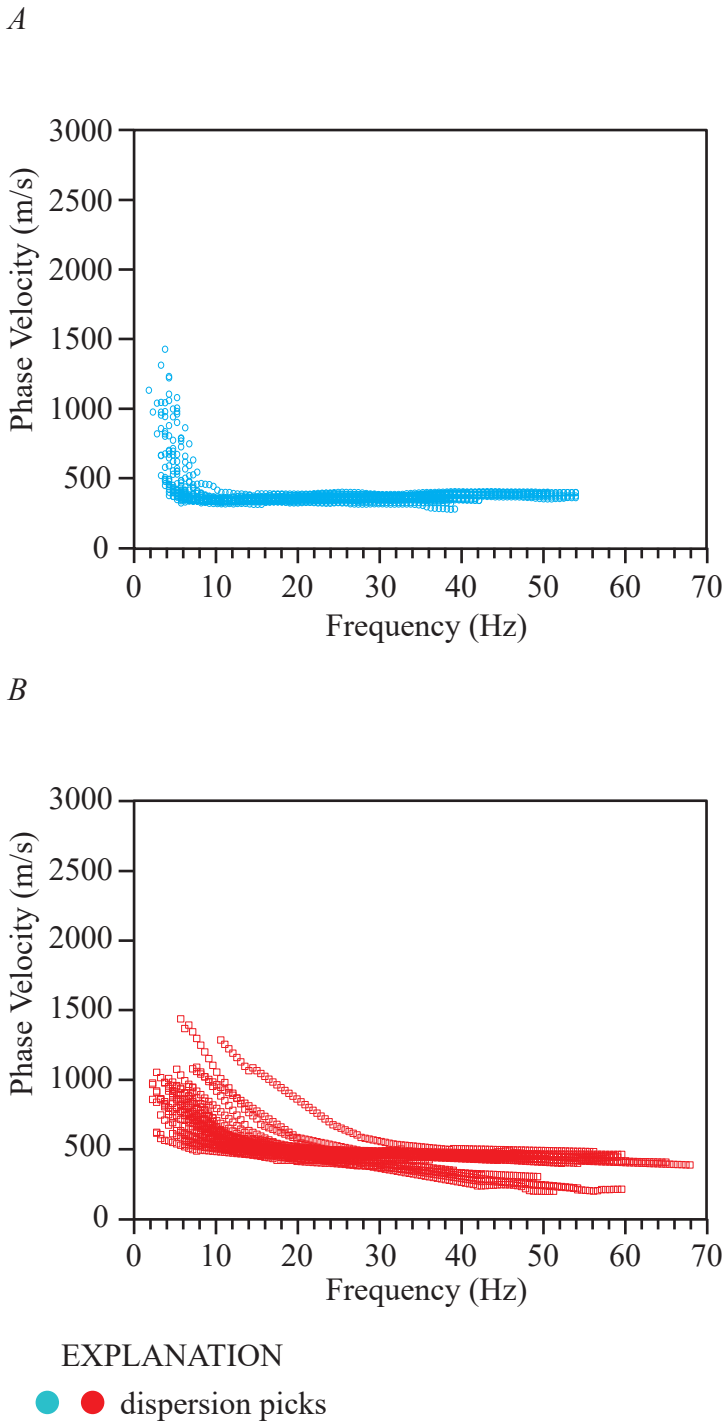

Figure 2.4. Rayleigh- and Love-wave fundamental mode dispersion curve picks for our LA17-4-LCG seismic profile. *A*, Rayleigh-wave fundamental mode dispersion curve picks correlate with frequencies between 2 and 56 hertz (Hz) and with phase velocities between 300 and 1,500 meters per second (m/s). *B*, Dispersion curves developed from data generated by a 3.5-kilogram sledgehammer and aluminum block source. Love-wave fundamental mode dispersion curve picks for frequencies between 2 and 70 Hz and phase velocities between 150 and 1,600 m/s.

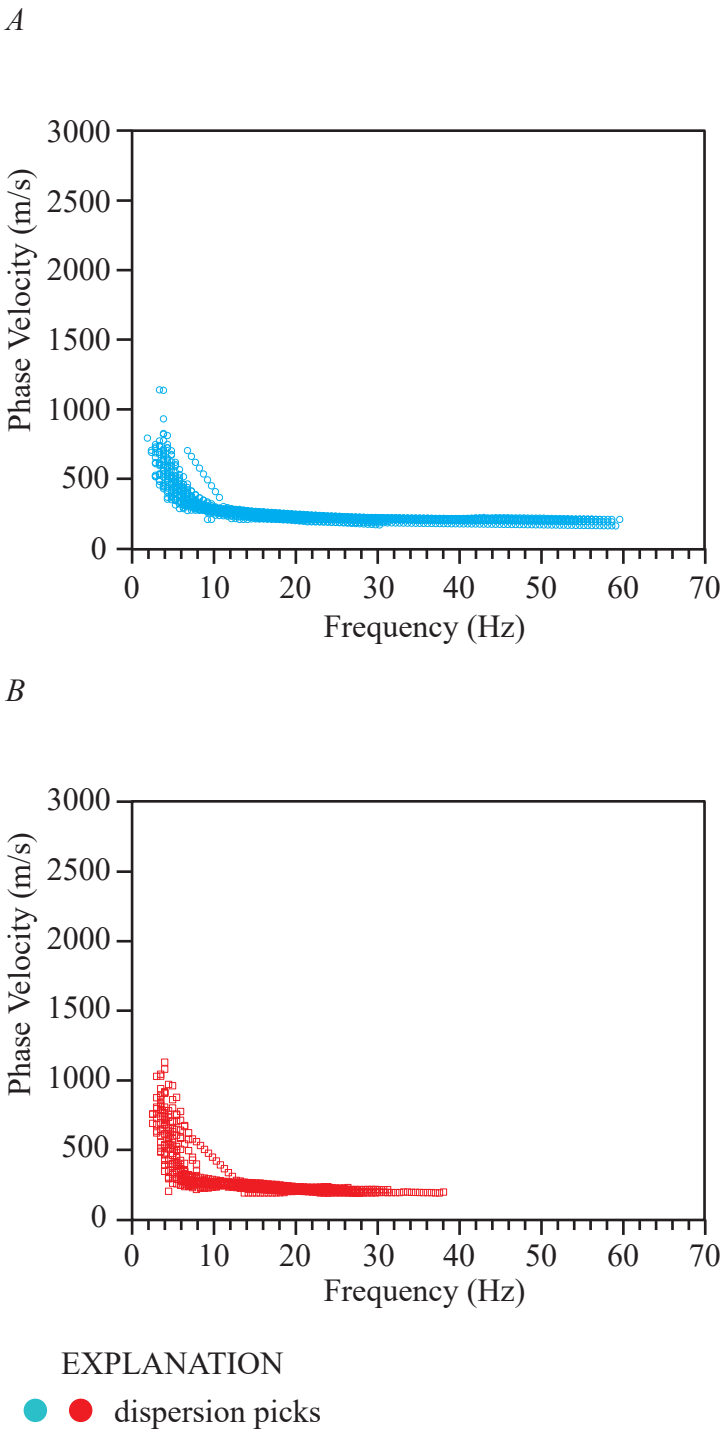

Figure 2.5. Rayleigh- and Love-wave fundamental mode dispersion curve picks for our LA17-5-RUS seismic profile. *A*, Rayleigh-wave fundamental mode dispersion curve picks correlate with frequencies between 2 and 60 hertz (Hz) and with phase velocities between 200 and 1,300 meters per second (m/s). *B*, Dispersion curves developed from data generated by a 3.5-kilogram sledgehammer and aluminum block source. Love-wave fundamental mode dispersion curve picks for frequencies between 2 and 40 Hz and phase velocities between 150 and 1,200 m/s.

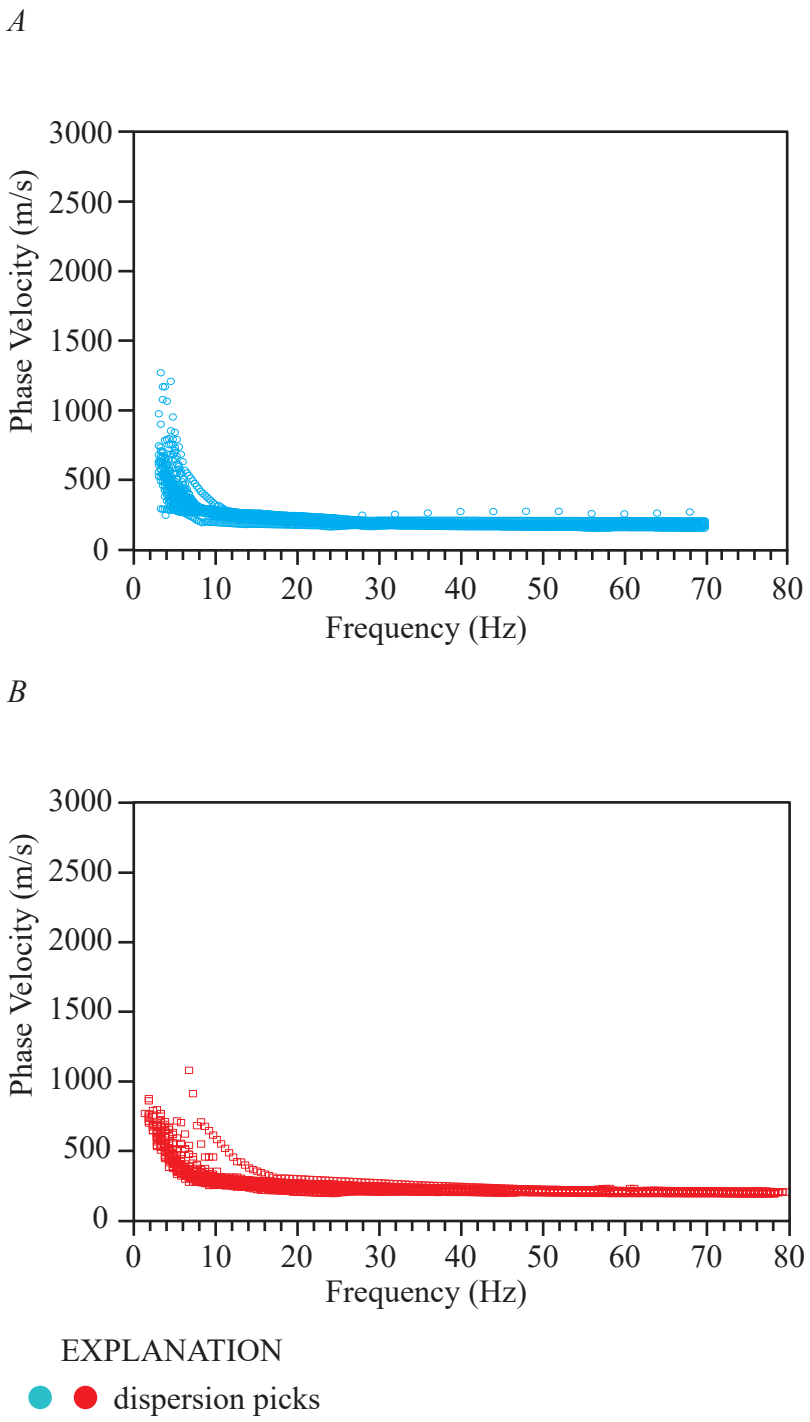

Figure 2.6. Rayleigh- and Love-wave fundamental mode dispersion curve picks for our LA17-6-STC seismic profile. *A*, Rayleigh-wave fundamental mode dispersion curve picks correlate with frequencies between 2 and 70 hertz (Hz) and with phase velocities between 150 and 1,400 meters per second (m/s). *B*, Dispersion curves developed from data generated by a 3.5-kilogram sledgehammer and aluminum block source. Love-wave fundamental mode dispersion curve picks for frequencies between 2 and 80 Hz and phase velocities between 150 and 1,300 m/s.

Appendix 3. Rayleigh- and Love-Wave 1-D Velocity Depth Profiles

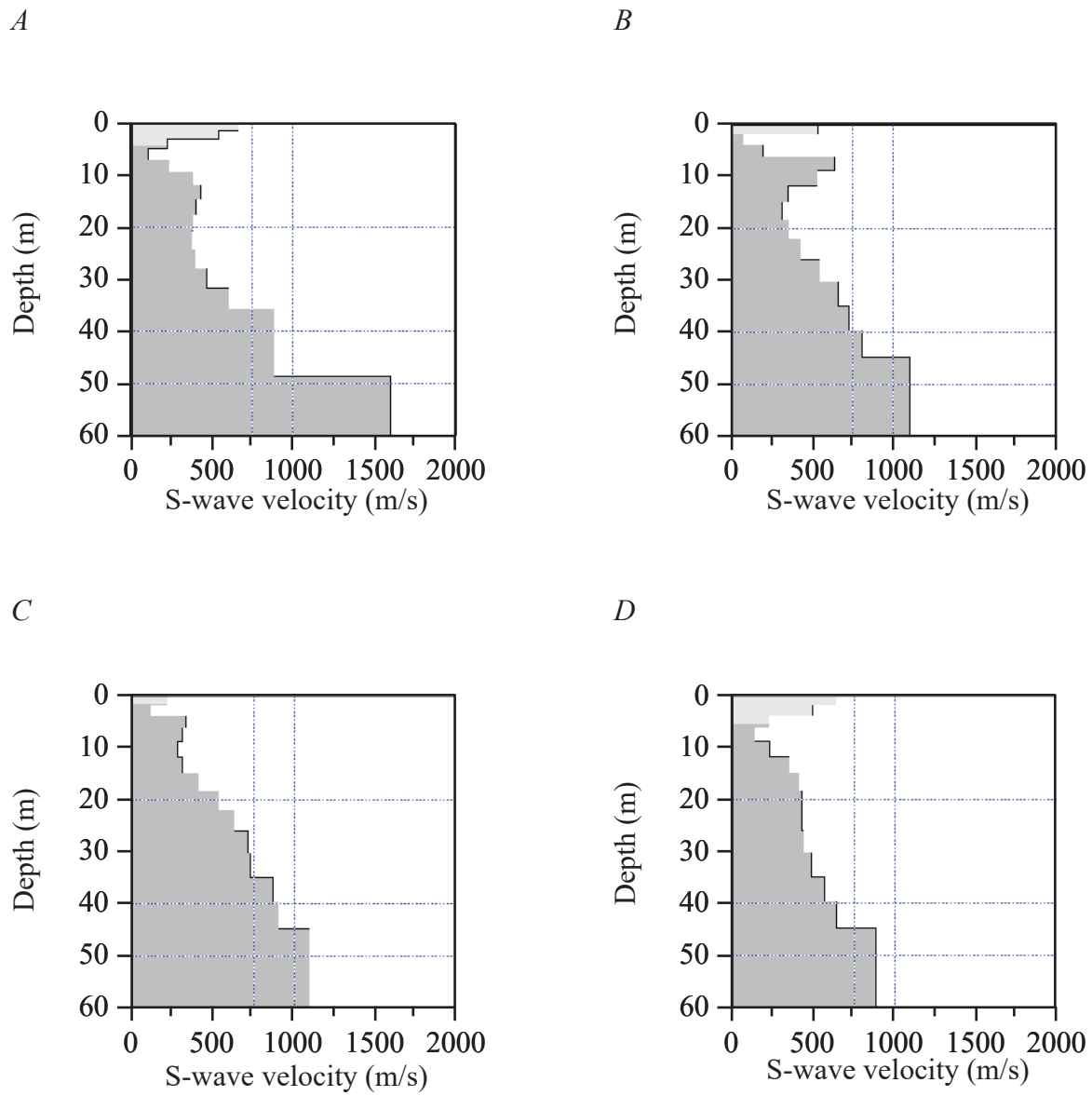

Figure 3.1. Rayleigh- and Love-wave 1-D depth-velocity profiles correlating with the location along our LA17-1-OLI and LA17-1b-OLI seismic profiles that is nearest to the SCSN OLI strong-motion station. *A*, Rayleigh-wave 1-D depth-velocity profile showing relatively high gradients below about 30 meters (m) depth. *B*, Seismic data generated by a 3.5-kilogram sledgehammer and aluminum block source. The Love-wave one-dimensional (1-D) depth-velocity profile shows weak positive gradient in shear-wave velocity (V_S) below approximately 10 m depth. *C*, Dispersion curve developed from data generated by a 45°-angle accelerated weight-drop and aluminum block source. The Love-wave 1-D depth-velocity profile shows weak positive gradient in V_S below 10 m depth. *D*, Rayleigh-wave 1-D depth-velocity profile for the LA17-1b-OLI seismic profile showing a weak positive gradient in V_S below approximately 8 m depth. Light grey areas at the near surface represent regions with few data points. (m/s, meters per second.)

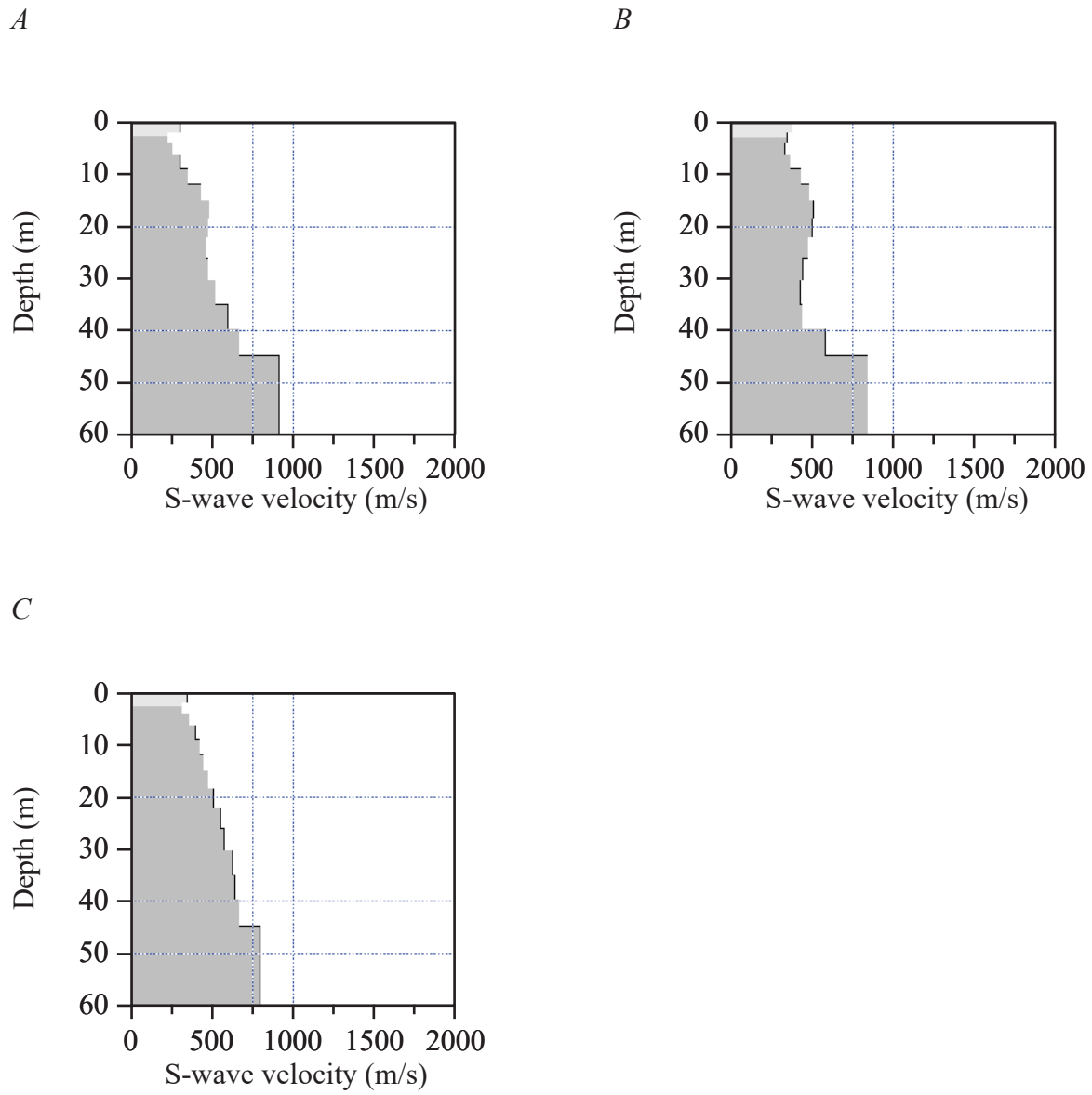

Figure 3.2. Rayleigh- and Love-wave one-dimensional (1-D) depth-velocity profiles correlating with the location along our LA17-2-SRN seismic profile that is nearest to the SCSN SRN strong-motion station. *A*, Rayleigh-wave 1-D depth-velocity profile shows positive gradient in shear-wave velocity (V_S) below approximately 2 meters (m) depth. *B*, Seismic data generated by a 3.5-kilogram sledgehammer and aluminum block source. The Love-wave 1-D depth-velocity profile shows weak positive gradient in V_S between approximately 2 and approximately 20 m depth, then weak negative gradient in V_S between approximately 20 and approximately 40 m depth. *C*, Seismic data generated by a 45°-angle accelerated weight-drop and aluminum block source. The Love-wave 1-D depth-velocity profile shows weak positive gradient in V_S below approximately 2 m depth. Light grey areas at the near surface represent regions with few data points. (m/s, meters per second.)

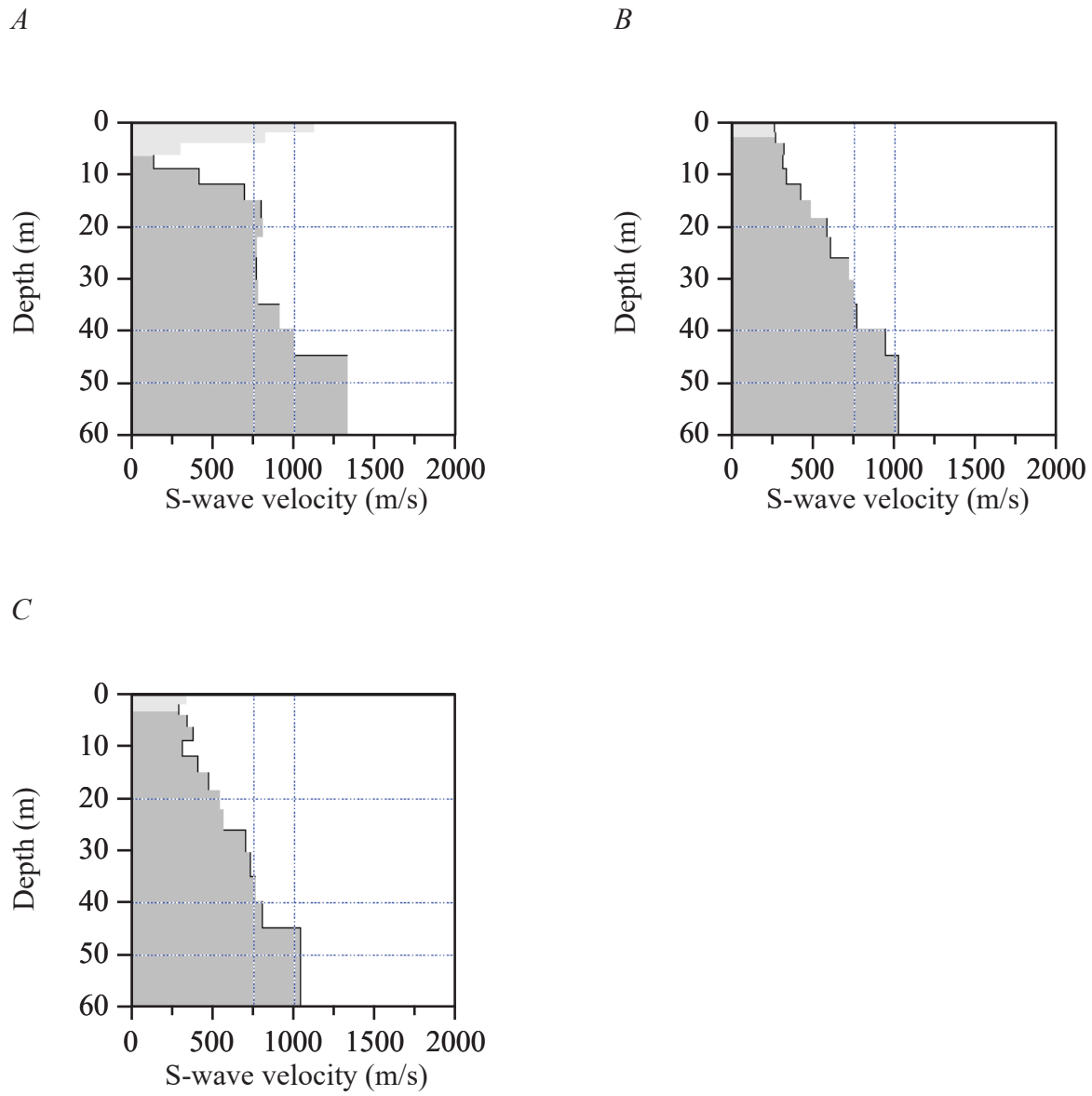

Figure 3.3. Rayleigh- and Love-wave one-dimensional (1-D) depth-velocity profiles correlating with the location along our LA17-3-MUR seismic profile that is nearest to the SCSN MUR strong-motion station. *A*, Rayleigh-wave 1-D depth-velocity profile showing positive gradient in shear-wave velocity (V_S) between approximately 8 and approximately 18 meters m depth and below approximately 36 m depth. *B*, Seismic data generated by a 3.5-kilogram sledgehammer and aluminum block source. The Love-wave 1-D depth-velocity profile shows weak positive gradient in V_S at all depths. *C*, Seismic data generated by a 45°-angle accelerated weight-drop and aluminum block source. The Love-wave 1-D depth-velocity profile shows weak positive gradient in V_S at all depths. Light grey areas at the near surface represent regions with few data points. (m/s, meters per second)

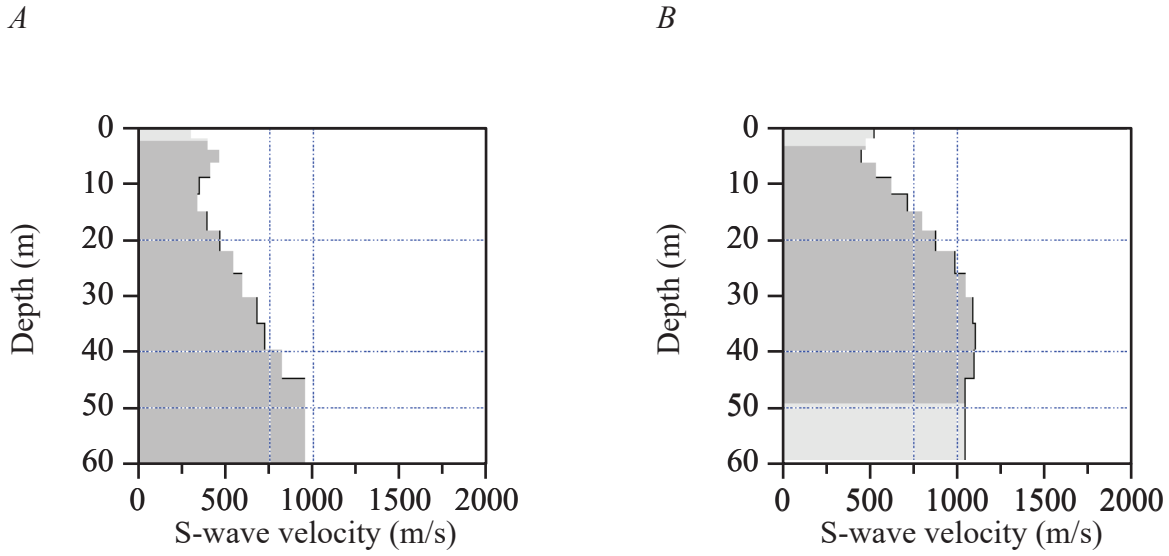

Figure 3.4. Rayleigh- and Love-wave one-dimensional (1-D) depth-velocity profile correlating with the location along our LA17-4-LCG seismic profile that is nearest to the SCSN LCG strong-motion station. *A*, Rayleigh-wave 1-D depth-velocity profile showing weak positive gradient in shear-wave velocity (V_S) below approximately 12 meters (m) depth. *B*, Seismic data generated by a 3.5-kilogram sledgehammer and aluminum block source. The Love-wave 1-D depth-velocity profile shows positive gradient in V_S between approximately 2 m and approximately 40 m depth. Light grey areas represent regions with few data points. (m/s, meters per second.)

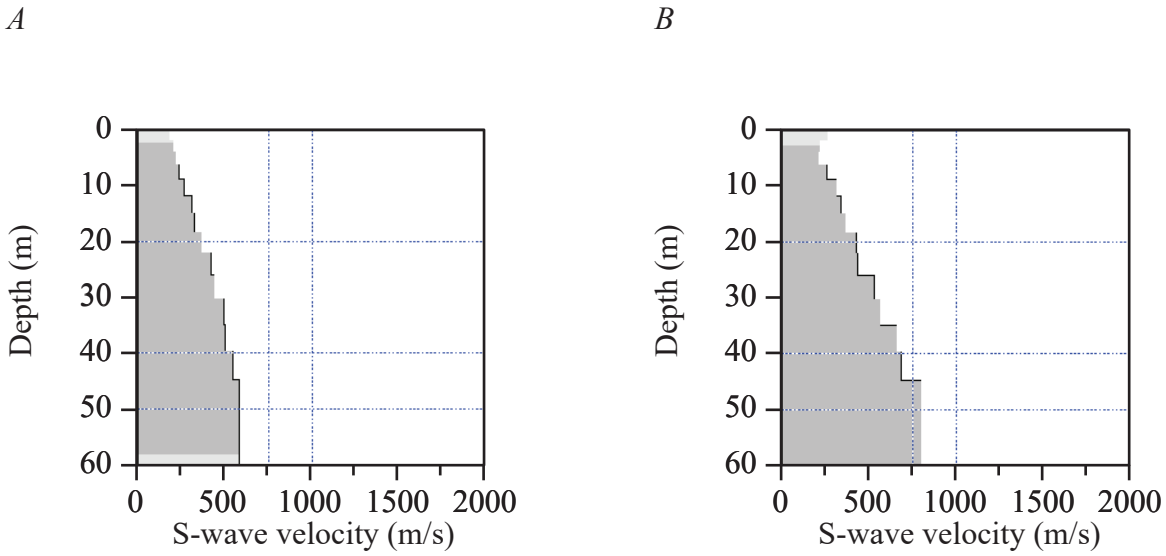

Figure 3.5. Rayleigh- and Love-wave one-dimensional (1-D) depth-velocity profiles correlating with the location along our LA17-5-RUS seismic profile that is nearest to the SCSN RUS strong-motion station. *A*, Rayleigh-wave 1-D depth-velocity profile showing weak positive gradient in shear-wave velocity (V_S) at all depths. *B*, Seismic data generated by a 3.5-kilogram sledgehammer and aluminum block source. The Love-wave 1-D depth-velocity profile shows weak positive gradient in V_S below approximately 2 m depth. Light grey areas represent regions with few data points. (m/s, meters per second.)

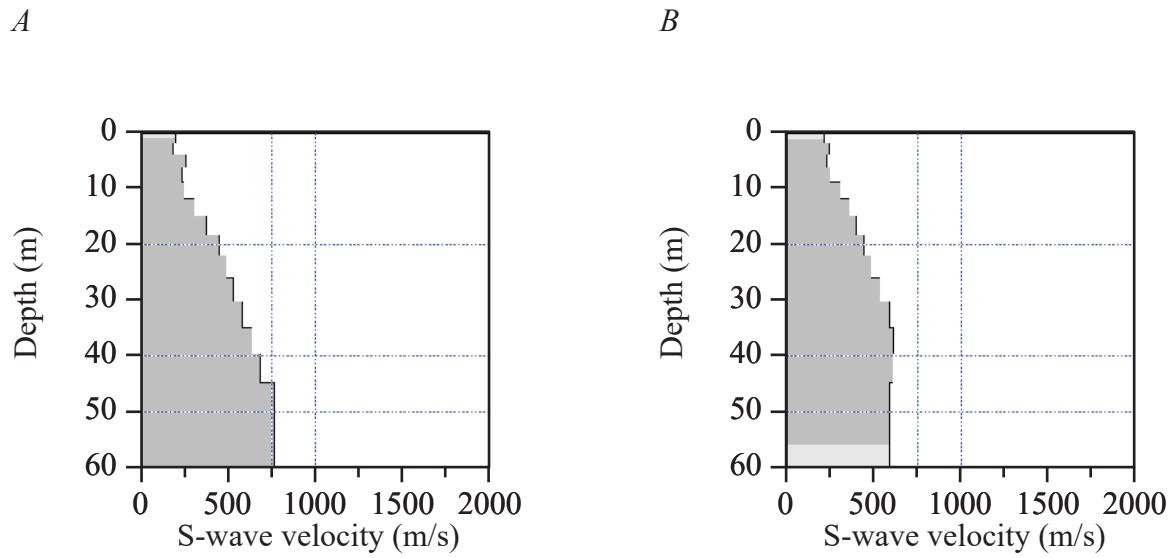

Figure 3.6. Rayleigh- and Love-wave one-dimensional (1-D) depth-velocity profiles correlating with the location along our LA17-6-STC seismic profile that is nearest to the SCSN STC strong-motion station. *A*, Rayleigh-wave 1-D depth-velocity profile shows weak positive gradient in shear-wave velocity (V_S) below approximately 8 meters (m) depth. *B*, Seismic data generated by a 3.5-kilogram sledgehammer and aluminum block source. The Love-wave 1-D depth-velocity profile shows weak positive gradient in V_S between approximately 2 m and approximately 40 m depth. Light grey areas represent regions with few data points. (m/s, meters per second)

Appendix 4. V_P/V_S Ratios Determined from P-wave and S-wave Refraction Tomography

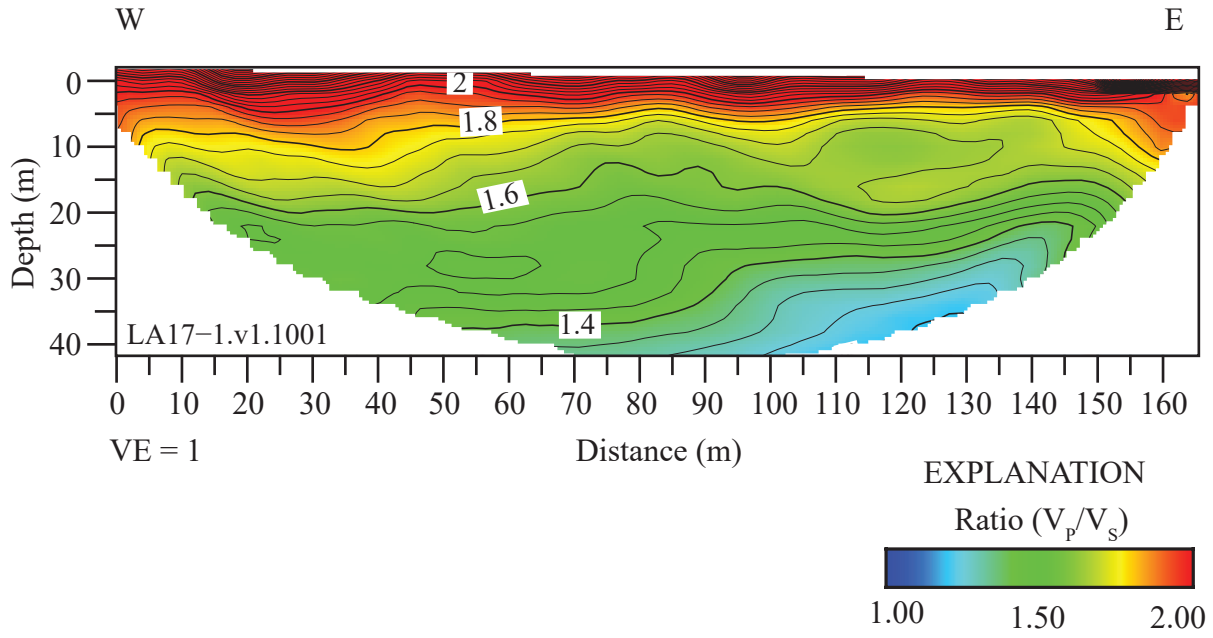

Figure 4.1. Two-dimensional tomography image of P- to S-wave velocity (V_P/V_S) ratios along the LA17-1-OLI seismic profile. V_P/V_S ratios range from about 1.2 to about 2.6 along the seismic profile. (W, west; E, east; m, meters)

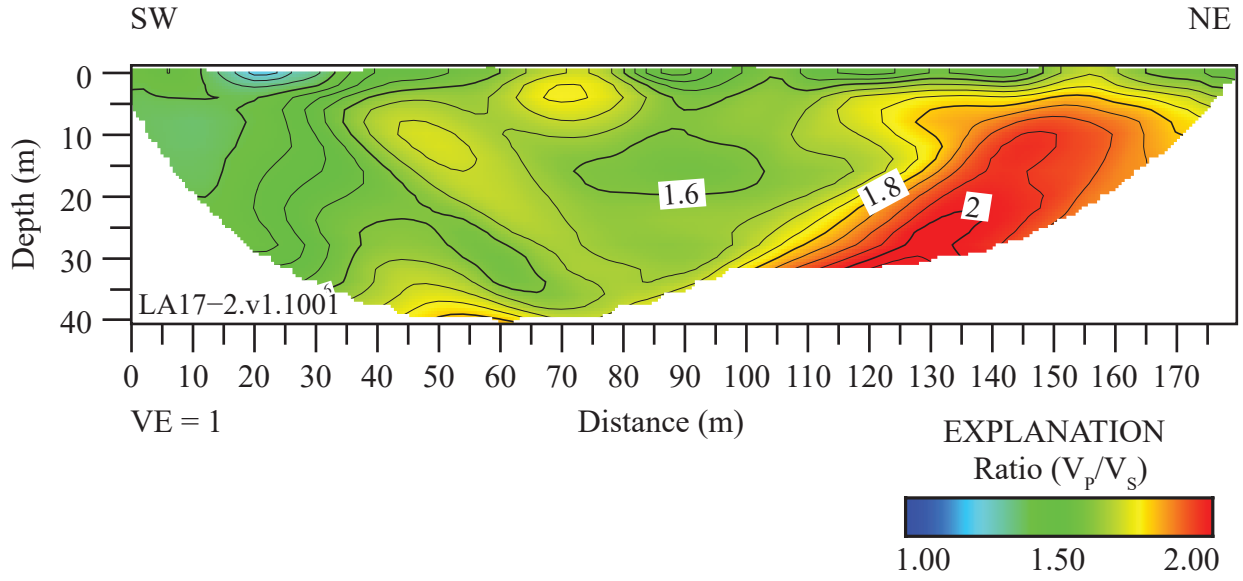

Figure 4.2. Two-dimensional tomography image of P- to S-wave velocity (V_P/V_S) ratios along LA17-2-SRN seismic profile. V_P/V_S ratios range from about 1.2 to about 2 along the seismic profile; the highest (approximately 2) V_P/V_S ratio coincides with the mapped location of Peralta Hills Fault. (SW, southwest; NE, northeast; m, meters.)

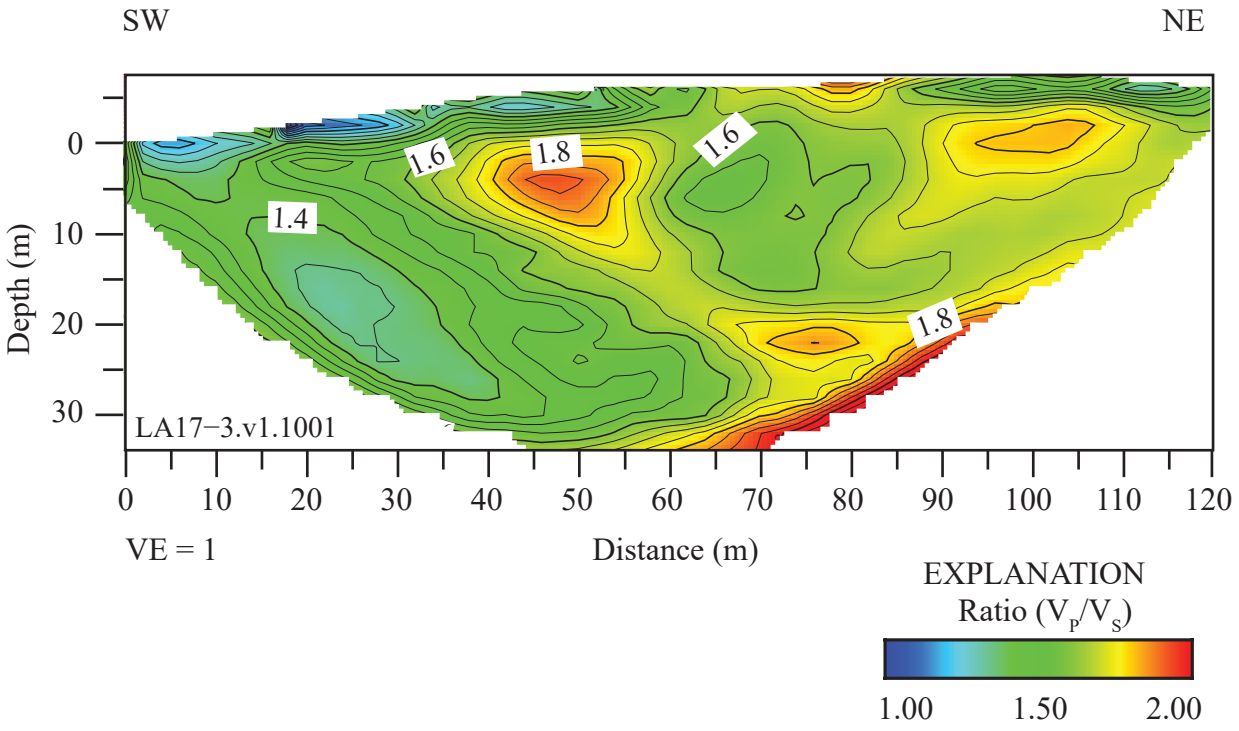

Figure 4.3. Two-dimensional tomography image of P- to S-wave velocity (V_P/V_S) ratios along LA17-3-MUR seismic profile. V_P/V_S ratios range from about 1 to about 2 along the seismic profile. (SW, southwest; NE, northeast; m, meters)

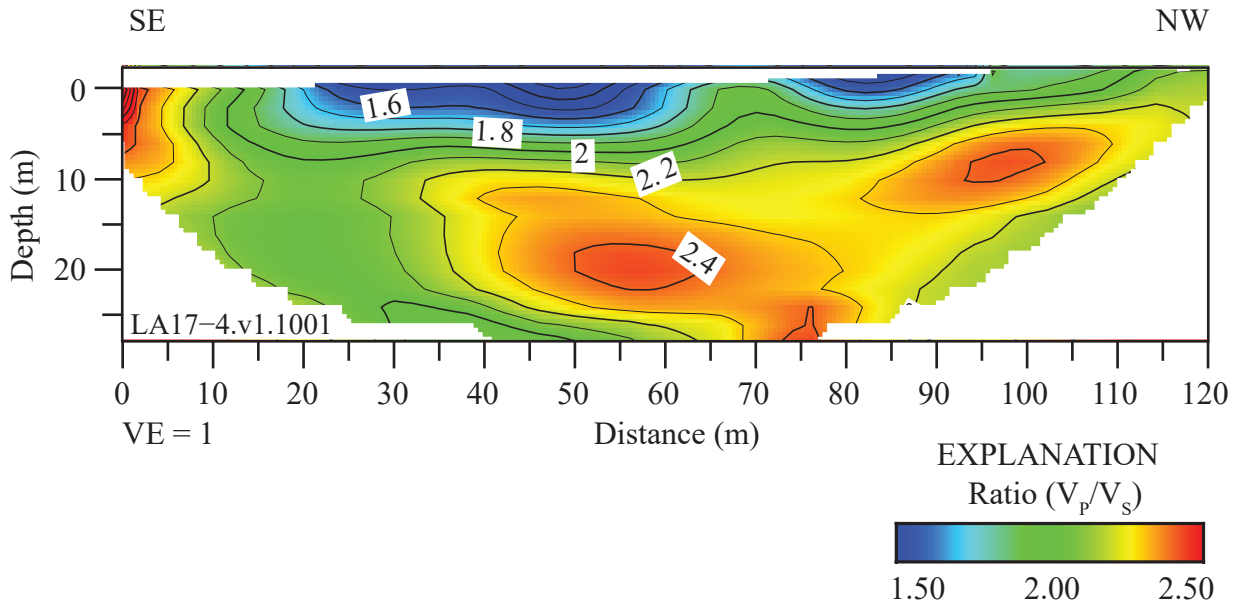

Figure 4.4. Two-dimensional tomography image of P- to S-wave velocity (V_P/V_S) ratios along LA17-4-LCG seismic profile. V_P/V_S ratios range from about 1.4 to about 2.6 along the seismic profile. (SE, southeast; NW, northwest; m, meters.)

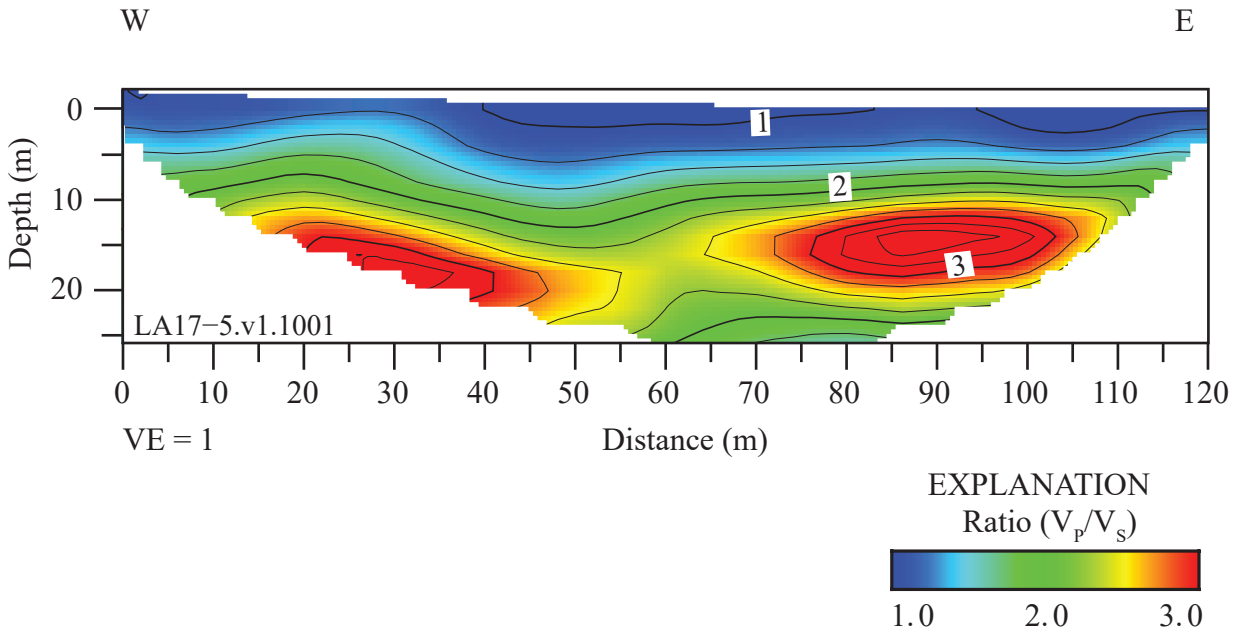

Figure 4.5. Two-dimensional tomography image of P- to S-wave velocity (V_P/V_S) ratios along LA17-5-RUS seismic profile. V_P/V_S ratios range from about 1 to about 3.5 along the seismic profile. (W, west; E, east; m, meters.)

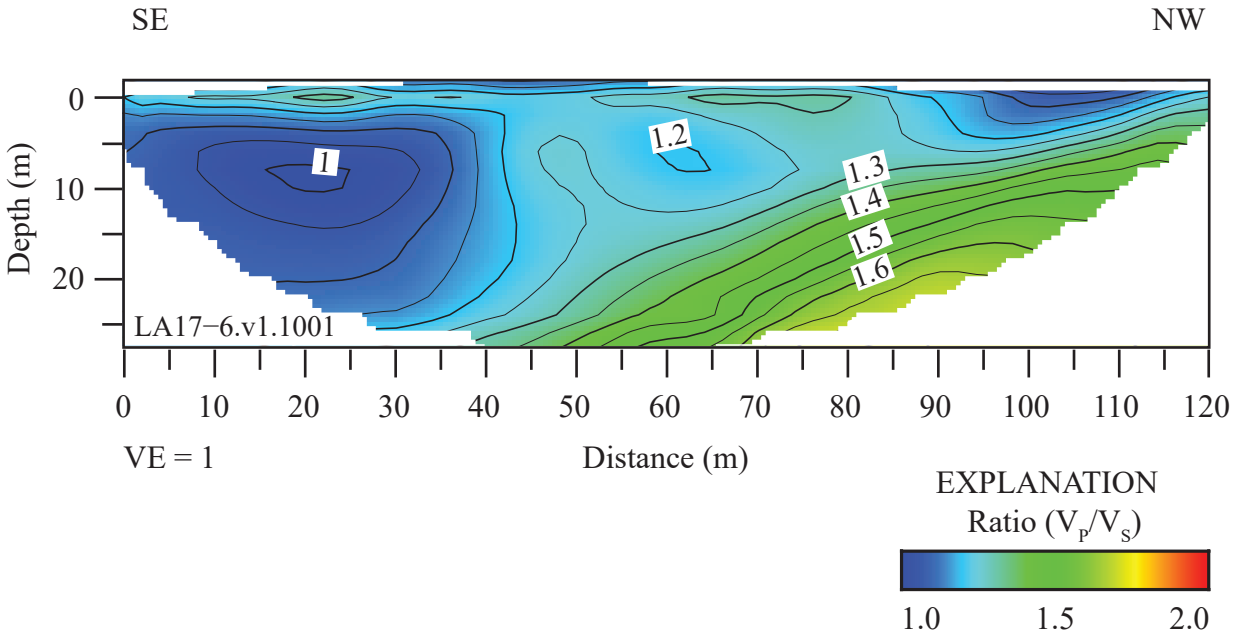

Figure 4.6. Two-dimensional tomography image of P- to S-wave velocity (V_P/V_S) ratio along LA17-6-STC seismic profile. V_P/V_S ratios range from about 1 to about 1.6 along the seismic profile. (SE, southeast; NW, northwest; m, meters.)

Appendix 5. Poisson's Ratios Determined from P-wave and S-wave Refraction Tomography

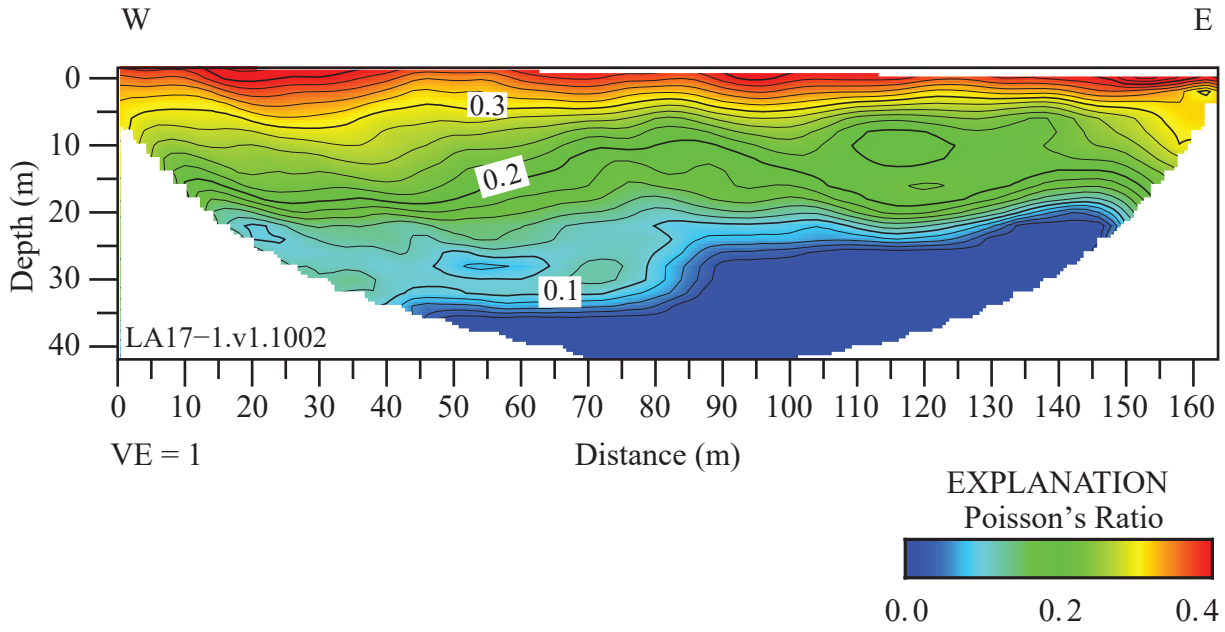

Figure 5.1. Two-dimensional tomography image of Poisson's ratios along the LA17-1-OLI seismic profile, derived from P- and S-wave tomography. Poisson's ratios are highest (approximately 0.4) at the upper approximately 2 meters (m) of the subsurface. (SE, southeast; NW, northwest)

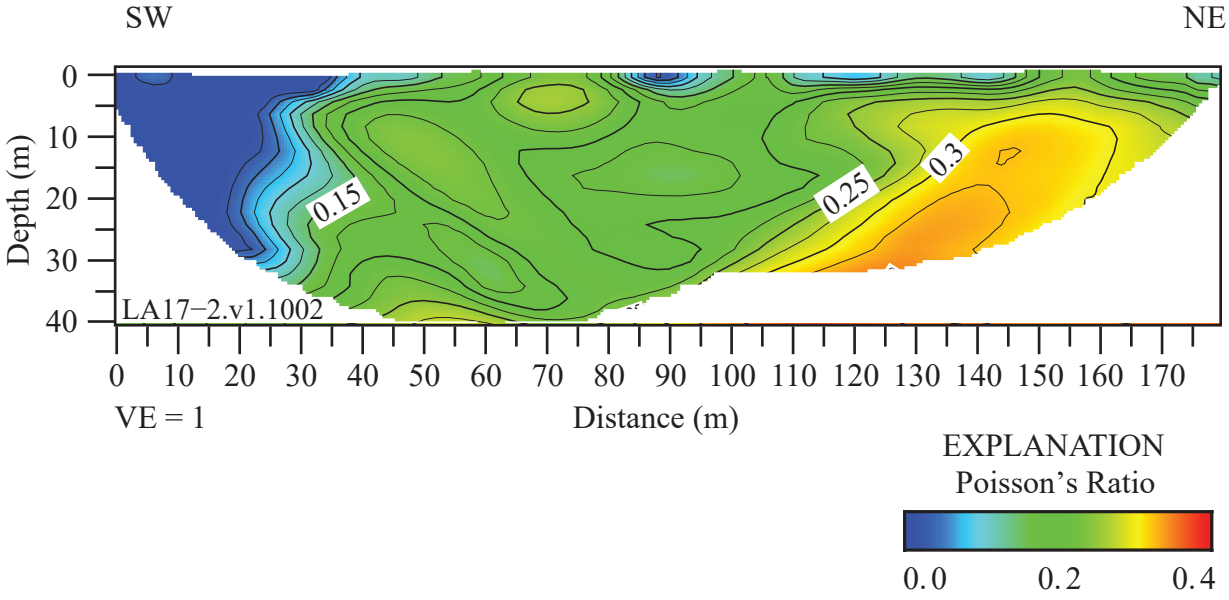

Figure 5.2. Two-dimensional tomography image of Poisson's ratios along the LA17-2-SRN seismic profile, derived from P- and S-wave tomography. Highest Poisson's ratios (approximately 0.3) coincide with the mapped location of Peralta Hills Fault, between approximately 110 and 155 meters (m) distance. (SW, southwest; NE, northeast.)

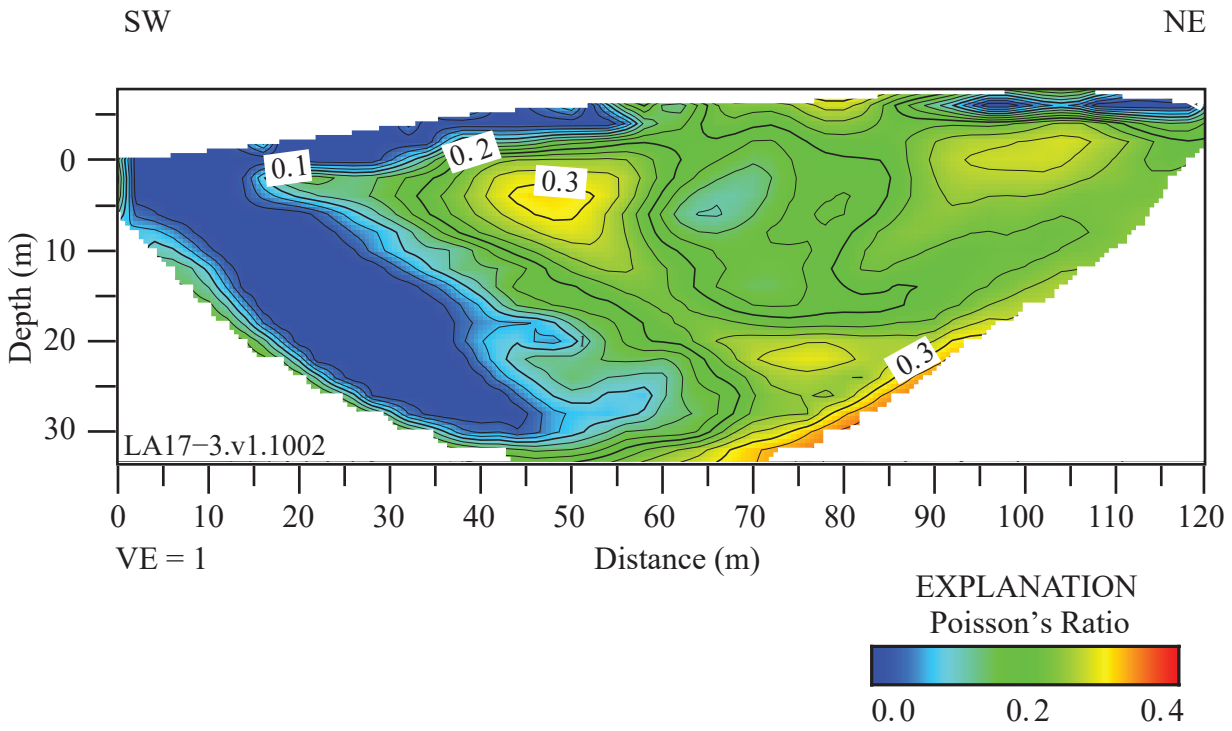

Figure 5.3. Two-dimensional tomography image of Poisson's ratios along the LA17-3-MUR seismic profile, derived from P- and S-wave tomography. Poisson's ratios are highest (approximately 3) at discrete locations across the profile. (SW, southwest; NE, northeast; m, meters)

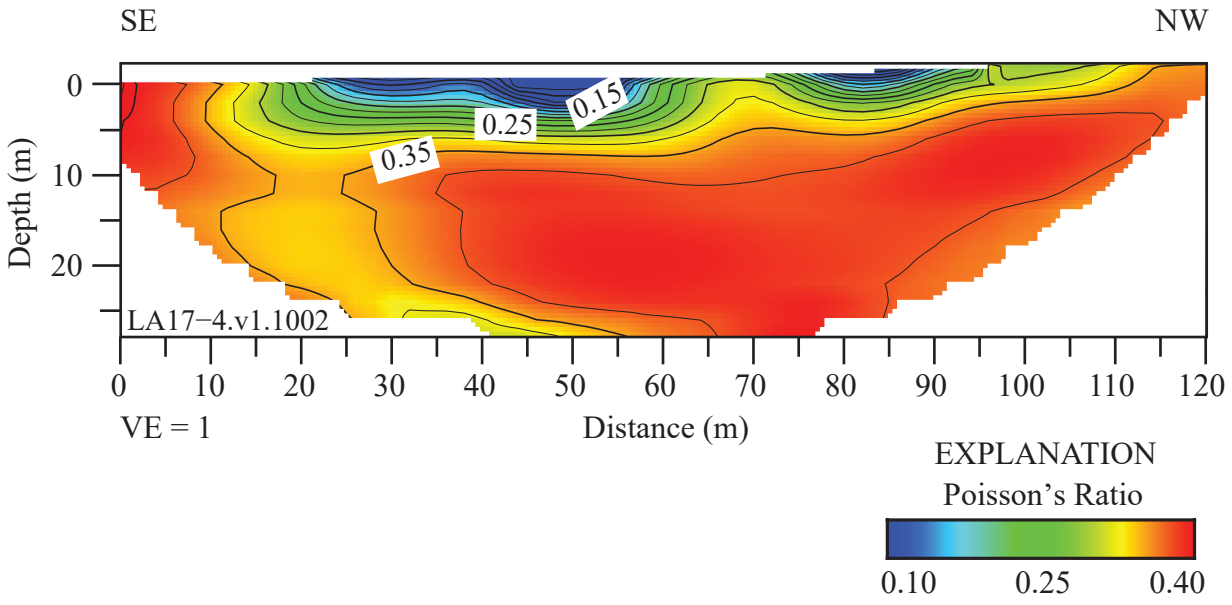

Figure 5.4. Two-dimensional tomography image of Poisson's along the LA17-4-LCG seismic profile, derived from P- and S-wave tomography. Poisson's ratios are highest (approximately 0.35) at depths below approximately 5 meters (m). (SE, southeast; NW, northwest)

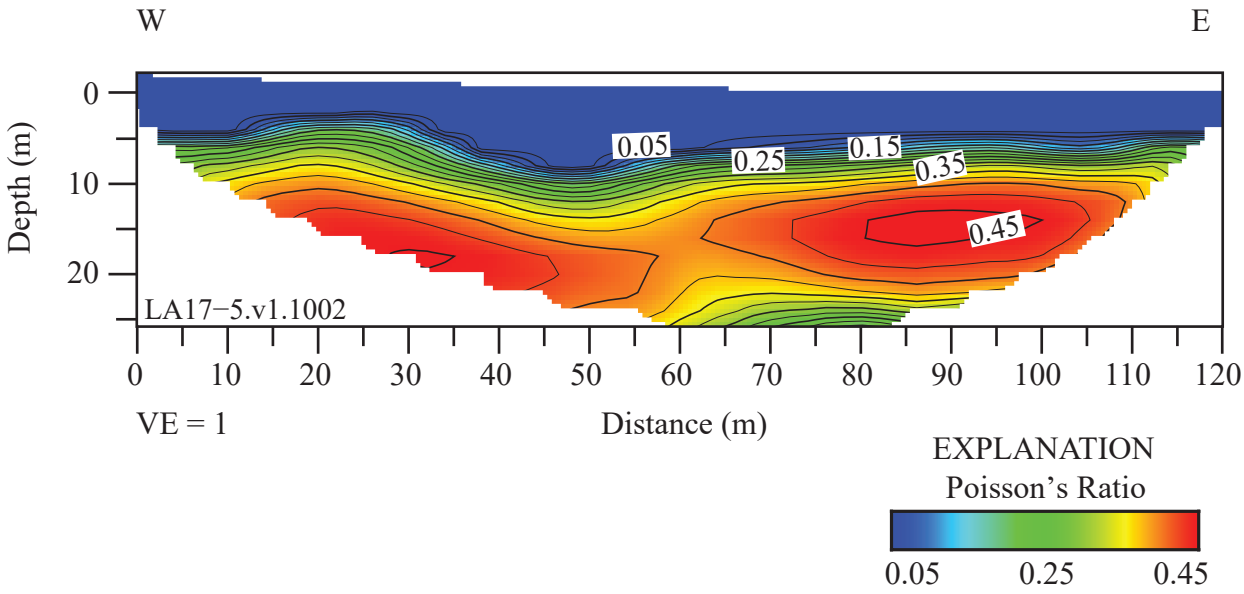

Figure 5.5. Two-dimensional tomography image of Poisson's ratios along the LA17-5-RUS seismic profile, derived from P- and S-wave tomography. Poisson's ratios are highest (approximately 0.4) at depths below approximately 15 meters (m). (W, west; E, east.)

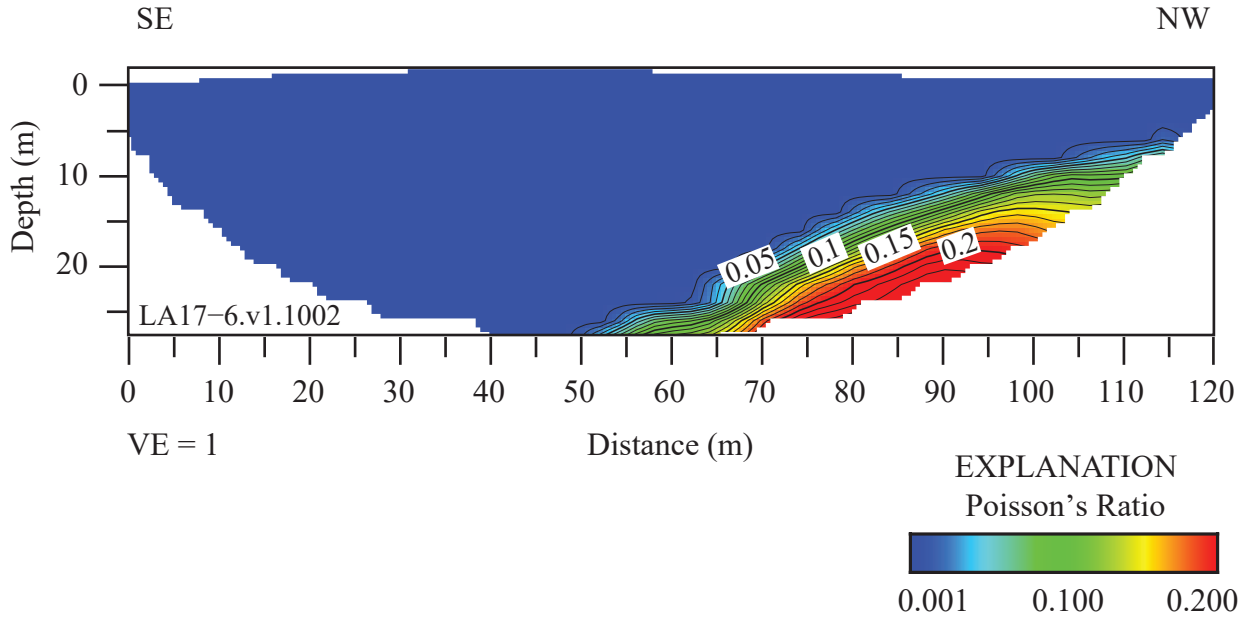

Figure 5.6. Two-dimensional tomography image of Poisson's ratios along the LA17-6-STC seismic profile, derived from P- and S-wave tomography. Poisson's ratios are highest (0.2) at depths below approximately 20 meters (m) in the northwest end of the seismic profile. (SE, southeast; NW, northwest)

Publishing support provided by the Moffett Field Publishing Service Center
Manuscript approved for publication February 22, 2024
Layout by Cory Hurd

ISSN 2331-1258 (online)
https://doi.org/10.3133/ofr20241016